

PETRO VIETNAM JOURNAL



An Official Publication of the Vietnam National Oil and Gas Group Vol. 6 - 2021

ISSN 2615-9902

PETROVIETNAM Vol. 6 - 2021





EDITOR-IN-CHIEF

Dr. Le Xuan Huyen

DEPUTY EDITOR-IN-CHIEF

Dr. Le Manh Hung

Dr. Phan Ngoc Trung

EDITORIAL BOARD MEMBERS

Dr. Trinh Xuan Cuong

Dr. Nguyen Anh Duc

MSc. Vu Dao Minh

M.A. Tran Thai Ninh

MSc. Duong Manh Son

MSc. Le Ngoc Son

Assoc. Prof. Dr. Le Van Sy

Eng. Le Hong Thai

M.A. Bui Minh Tien

MSc. Nguyen Van Tuan

MSc. Pham Xuan Trung

Dr. Tran Quoc Viet

SECRETARY

MSc. Le Van Khoa

M.A. Nguyen Thi Viet Ha

DESIGNED BY

Le Hong Van

MANAGEMENT

Vietnam Petroleum Institute

CONTACT ADDRESS

Floor M2, VPI Tower, Trung Kinh street, Yen Hoa ward, Cau Giay district, Ha Noi

*Tel: (+84-24) 37727108 * Fax: (+84-24) 37727107 * Email: tcdk@pvn.vn/pvj@pvn.vn*

Mobile: (+84)982288671

Cover photo: Ha Long bay, Vietnam. Photo: Freepik



PETROLEUM EXPLORATION & PRODUCTION

PETROVIETNAM JOURNAL
Volume 6 (2021), pp. 4 - 17
ISSN 2615-9902

PETROVIETNAM
JOURNAL

SCREENING SELECTION OF ENHANCED OIL RECOVERY METHODS BASED ON ANALYTICS OF WORLDWIDE OILFIELD DATA WITH REFERENCE TO OFFSHORE OIL FIELDS IN VIETNAM

Dean Huy Hien, Hoang Long, Pham Quy Ngoc
Vietnam Petroleum Institute
Email: hienhd@vpi.gov.vn
<https://doi.org/10.47992/PPEJ.2021.06-01>

Summary

Selecting a proper enhanced oil recovery (EOR) method for a prospective reservoir is a key factor for successful application of EOR techniques. Reservoir engineers usually refer to screening guidelines to identify potential EOR processes for a given reservoir. However, these guidelines are often too general. In this study, we develop an advanced EOR screening technique based on the statistical analyses with bootstrap in combination with some initial deep learning analyses to select the most suitable EOR method for a given mature oil field. At first, a database and the screening guidelines were established by compiling the information of 1,098 EOR projects from various publications in different languages, including Oil and Gas Journal (OGJ) biannual EOR surveys, SPE publications, DOI reports, and Chinese publications, etc. Bootstrap was used to detect the special cases for each reservoir/fluid property and to present the graphical screening results. A case study was used to demonstrate that with a simple input of reservoir/fluid information, the proposed procedure could effectively give recommendations for EOR method selection. With the inputs (reservoir and fluid properties) from Vietnam offshore oil fields, the EOR methods recommended by this study are mostly chemical, including polymer and surfactant injection.

Key words: Enhanced oil recovery (EOR), database, statistical analysis, deep learning.

1. Introduction

The life of an oil and gas reservoir goes through different production stages, namely primary, secondary, and tertiary recovery. Primary recovery is carried out by naturally initial reservoir drive energy such as rock and fluid expansion, solution gas, water influx, gas cap or gravity drainage. Secondary recovery requires the injection of external fluid (water or gas) mainly for the purpose of pressure maintenance and volumetric sweep efficiency. The tertiary stage refers to recovery by injection of more special fluids such as chemical, miscible gases or thermal energy after the secondary.

EOR is an essential technique for extending the lifetime of reservoirs, especially for mature oil fields where productivity has declined or the reservoir pressure rapidly reduces. EOR may include physical, mechanical and chemical processes, such as infill drilling, waterflooding,

gas and/or chemical injection. There are more than 20 EOR techniques which are classified as thermal (steam flooding, in-situ combustion) and nonthermal methods including chemical (polymer, surfactant, polymer/surfactant and miscible hydrocarbon gas, CO₂, and nitrogen injection) [1].

Generally, by applying various EOR technologies to different oil fields, crude oil production from a reservoir could be increased up to 30%. Therefore, EOR technologies are important in the oil industry and have been used worldwide [2]. The main mechanism of EOR is to inject into the reservoir an agent to improve the oil displacement efficiency by modifying the reservoir rock and fluid properties such as interfacial tension, capillary pressure, viscosity, density, and mobility ratio. EOR selection is a complex process depending on reservoir characterization, technology availability and economical confirmation to find the most appropriate method for further reservoir simulation, economic evaluation and field planning. In 1978, the first EOR screening studies were presented by Brashear and Kuskras [3], using

4

PETROLEUM EXPLORATION & PRODUCTION

PETROVIETNAM JOURNAL
Volume 6 (2021), pp. 18 - 36
ISSN 2615-9902

PETROVIETNAM
JOURNAL

INTERPRETATION OF INTERWELL CONNECTIVITY TESTS IN A WATERFLOOD SYSTEM

Dirah Viet Anh, Opshar Tiab
Petroleum Exploration Production Corporation
University of Oklahoma
Email: anh@pepc.com.vn, dtiab@ou.edu
<https://doi.org/10.47992/PPEJ.2021.06-02>

Summary

This study is an extension of a novel technique to determine interwell connectivity in a reservoir based on fluctuations of bottom hole pressure of both injectors and producers in a waterflood system. The technique uses a constrained multivariate linear regression analysis to obtain information about permeability trends, channels, and barriers. Some of the advantages of this new technique are simplified one-step calculation of interwell connectivity coefficients, small number of data points and flexible testing plan. However, the previous study did not provide either in-depth understanding or any relationship between the interwell connectivity coefficients and other reservoir parameters.

This paper presents a mathematical model for bottom hole pressure responses of injectors and producers in a waterflood system. The model is based on available solutions for fully penetrating vertical wells in a closed rectangular reservoir. It then used to calculate interwell relative permeability, average reservoir pressure change and total reservoir pore volume using data from the interwell connectivity test described in the previous study. Reservoir compartmentalization can be inferred from the results. Cases where producers as signal wells, injectors as response wells and shut-in wells as response wells are also presented. Summary of results for these cases are provided. Reservoir behaviour and effects of skin factors are also discussed in this study.

Some of the conclusions drawn from this study are: (1) The mathematical model works well with interwell connectivity coefficients to quantify reservoir parameters; (2) The procedure provides in-depth understanding of the multi-well system with water injection in the presence of heterogeneity; (3) Injectors and producers have the same effect in terms of calculating interwell connectivity and thus, their roles can be interchanged. This study provides flexibility and understanding to the method of inferring interwell connectivity from bottom-hole pressure fluctuations. Interwell connectivity tests allow us to quantify accurately various reservoir properties in order to optimize reservoir performance.

Different synthetic reservoir models were analyzed including homogeneous, anisotropic reservoirs, reservoirs with high permeability channel, partially sealing fault and sealing fault. The results are presented in detail in the paper. A step-by-step procedure, charts, tables, and derivations are included in the paper.

Key words: Interwell connectivity, multi-well testing, waterflood system, well test analysis, reservoir characterization.

1. Introduction

The previous study carried out by Dirah and Tiab has introduced a new technique to infer interwell connectivity from bottom-hole pressure fluctuations in a waterflood system. The technique was proven to yield good results based on numerical simulation models of various cases of heterogeneity [1].

In this study, an analytical model for multi-well system with water injection was derived for the technique. The model is based on an available solution for a fully penetrating vertical well in a closed rectangular multi-well system and uses the principle of superposition in space. Based on

18

SCIENTIFIC RESEARCH



PETROLEUM EXPLORATION & PRODUCTION

4. Screening selection of enhanced oil recovery methods based on analytics of worldwide oilfield data with reference to offshore oil fields in Vietnam

18. Interpretation of interwell connectivity tests in a waterflood system

37. Transport of oil/water partitioning components during water injection



PETROLEUM ECONOMICS & MANAGEMENT

43. Comparative analysis of financial assurance instruments for offshore oil decommissioning and mine restoration

55. An overview of the gasohol market in Vietnam, the next direction?

PETROVIETNAM

PETROVIETNAM JOURNAL
Volume 6 (2021), pp. 63 - 69
ISSN 26145-9902

PETROVIETNAM JOURNAL

A BREAKTHROUGH IN 3D SEISMIC INTERPRETATION

Nguyen Tuan Thinh*, Ha Quang Mai*
Egis Australia Pty Ltd,
Petrovietnam Exploration and Production Corporation (PVEP)
Email: ent.egip@petrovietnam.vn

Summary

Accompanying the advancement of computer science and technologies, new techniques have been introduced to optimise the seismic interpretation workflow. In this study, we apply the 'Global seismic interpretation method', developed by Fougere et al. [1]. A 3D Relative Geologic Time (RGT) model was obtained directly from the 3D seismic volume which is the outcome of this method. Given the fact that in the 3D RGT model, the geologic time is continuous, a relative geologic age can be interpolated and assigned to every voxel of the seismic volume.

The dataset used in this study is the Maui 3D seismic volume from Taranaki basin, offshore New Zealand. A stack of 400 continuous stratigraphic horizons is produced from the Maui RGT model, even for complex areas where classical methods failed to achieve or would take a long time to complete. Integrated with seismic attribute mappings such as RMS amplitude and/or spectral decomposition, the horizon stack enables to navigate the seismic volume in stratigraphic order. Thus, the result enhances the identification of geological elements, stratigraphic insights, and paleo-depositional environments in greater detail for stratigraphic reservoir detection and characterisation. The novel methodology indicates a new way to conduct seismic interpretation, utilises all the information in the 3D seismic data, hence greatly reduces the exploration time cycle.

Key words: Seismic interpretation, seismic attributes, geologic time model, subsurface imaging, Taranaki basin.

1. Introduction

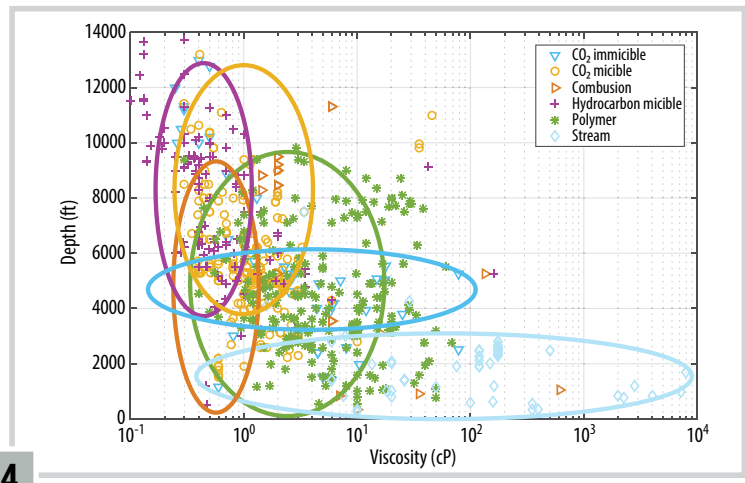
In the last few decades, seismic interpretation techniques have been rapidly developed for detailed reservoir delineation and characterisation. The traditional approach is generally an intensively time-consuming process that is heavily reliant on manually picking or auto-tracking of single horizons within the seismic volume. The tool allows tracking only one horizon at a time and is limited to areas with clear seismic signals or relatively simple geological structures.

Interpretation workflow with greater confidence and accuracy. Continuous chronostratigraphic surfaces can be generated at every sample of the seismic data, enabling to overcome the limitation of seismic polarity changes. In this study, we have applied this advanced seismic interpretation method and its associated attributes for enhancing subsurface imaging, reservoir delineation and characterisation for the Maui 3D seismic volume from Taranaki basin, offshore New Zealand.

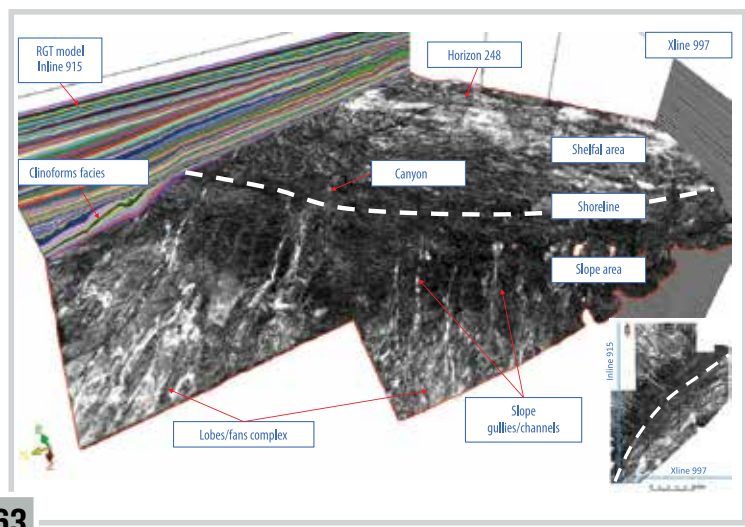
2. Regional geological settings

Extending 100,000 km² along the western margin and filled with 10 km thick Cretaceous - Cenozoic sediments, the Taranaki basin is the largest offshore sedimentary basin in New Zealand (Figure 1). Filling started from the Late Cretaceous and completely ended in the Paleocene, along with a rapid deposition within graben areas accompanied by high heat flow. During the Paleocene - Eocene period, a passive margin developed over the entire sub-continent; a slow subsidence rate allowed sediments to accumulate

PETROVIETNAM JOURNAL VOL. 6 (2021) 63



4



63



PETROLEUM TECHNOLOGIES

63. A breakthrough in 3D seismic interpretation

SCREENING SELECTION OF ENHANCED OIL RECOVERY METHODS BASED ON ANALYTICS OF WORLDWIDE OILFIELD DATA WITH REFERENCE TO OFFSHORE OIL FIELDS IN VIETNAM

Doan Huy Hien, Hoang Long, Pham Quy Ngoc

Vietnam Petroleum Institute

Email: hiendh@vpi.pvn.vn

<https://doi.org/10.47800/PVJ.2021.06-01>

Summary

Selecting a proper enhanced oil recovery (EOR) method for a prospective reservoir is a key factor for successful application of EOR techniques. Reservoir engineers usually refer to screening guidelines to identify potential EOR processes for a given reservoir. However, these guidelines are often too general. In this study, we develop an advanced EOR screening technique based on the statistical analyses with boxplot in combination with some initial deep learning analyses to select the most suitable EOR method for a given mature oil field. At first, a database and the screening guidelines were established by compiling the information of 1,098 EOR projects from various publications in different languages, including Oil and Gas Journal (OGJ) biannual EOR surveys, SPE publications, DOE reports, and Chinese publications, etc. Boxplots were used to detect the special cases for each reservoir/fluid property and to present the graphical screening results. A case study was used to demonstrate that with a simple input of reservoir/fluid information, the proposed procedure could effectively give recommendations for EOR method selection. With the inputs (reservoir and fluid properties) from Vietnam offshore oil fields, the EOR methods recommended by this study are mostly chemical, including polymer and surfactant injection.

Key words: Enhanced oil recovery (EOR), database, statistical analyses, deep learning.

1. Introduction

The life of an oil and gas reservoir goes through different production stages, namely primary, secondary, and tertiary recovery. Primary recovery is carried out by naturally initial reservoir drive energy such as rock and fluid expansion, solution gas, water influx, gas cap or gravity drainage. Secondary recovery requires the injection of external fluid (water or gas) mainly for the purpose of pressure maintenance and volumetric sweep efficiency. The tertiary stage refers to recovery by injection of more special fluids such as chemical, miscible gases or thermal energy after the secondary.

EOR is an essential technique for extending the lifetime of reservoirs, especially for mature oil fields where productivity has declined or the reservoir pressure rapidly reduces. EOR may include physical, mechanical and chemical processes, such as infill drilling, waterflooding,

gas and/or chemical injection. There are more than 20 EOR techniques which are classified as thermal (steam flooding, in-situ combustion) and nonthermal methods including chemical (polymer, surfactant, polymer/surfactant) and miscible (hydrocarbon gas, CO₂, and nitrogen injection) [1].

Generally, by applying various EOR technologies to different oil fields, crude oil production from a reservoir could be increased up to 30%. Therefore, EOR technologies are important in the oil industry and have been used worldwide [2]. The main mechanism of EOR is to inject into the reservoir an agent to improve the oil displacement efficiency by modifying the reservoir rock and fluid properties such as interfacial tension, capillary pressure, viscosity, density, and mobility ratio. EOR selection is a complex process depending on reservoir characterisation, technology availability and economical confirmation to find the most appropriate method for further reservoir simulation, economic evaluation and field planning. In 1978, the first EOR screening studies were presented by Brashear and Kuuskraa [3], using



Date of receipt: 27/10/2020. Date of review and editing: 27/10/2020 - 18/3/2021.
Date of approval: 11/6/2021.

200 pilot projects in the USA. After that, especially since the late 1990s, EOR screening criteria for broader EOR processes have been discussed by more researchers, and more methodologies have been developed. By far, EOR screening could be classified as conventional and advanced methods.

The conventional EOR screening is based on statistical methods, which generally use ranges or intervals of reservoir/fluid properties to filter out the applicable EOR technologies. Look-up tables coming from the statistical analysis of the existing EOR projects are provided with different property intervals for each EOR method. One well-known EOR screening guideline was proposed by Taber et al. in 1997 [4], which provides screening criteria (known as Taber's tables) based on the EOR projects conducted from 1974 to 1996 [4, 5]. The screening method used six important parameters that were considered in suitable ranges, including oil gravity, oil viscosity, oil saturation, average permeability, depth, and temperature. Similarly, Al-Adasani and Bai updated the Taber's screening guidelines by adding data from 1998 to 2010 [6]. Miscible and immiscible flooding were distinguished for all gas injection technologies, and the porosity guidelines were newly added in their work [6]. Even though both Taber and Al-Adasani provide useful guidelines for each EOR technique, updating screening

guidelines along with the dramatic increase of EOR projects is crucial since the conventional screening guidelines were constructed based on existing projects and experts' knowledge. Therefore, it is necessary to update the screening guidelines with projects conducted since 2010.

The advanced EOR screening method uses modern AI algorithms to process the available EOR project data for EOR selection based on similarity. The similarity here is understood as either physical distance (Euclidian, Manhattan, Jaccard, etc.) or probability distance. The application of AI algorithms in EOR selection is promising because it is capable of recommending a proper selection for EOR method by capturing the small patterns in the implementation of EOR techniques, revealing the relationships among the reservoir/fluids properties and predicting the physical properties for EOR. Alvarado et al. [7] proposed a methodology by utilising the machine learning algorithm (the combination of different clustering algorithms and expert systems) to draw the rules for EOR screening. Six clusters were classified based on the dataset, and each cluster has its own rules for application. Siena et al. [8] developed a methodology for target reservoirs analogy by applying the Bayesian hierarchical clustering algorithm.

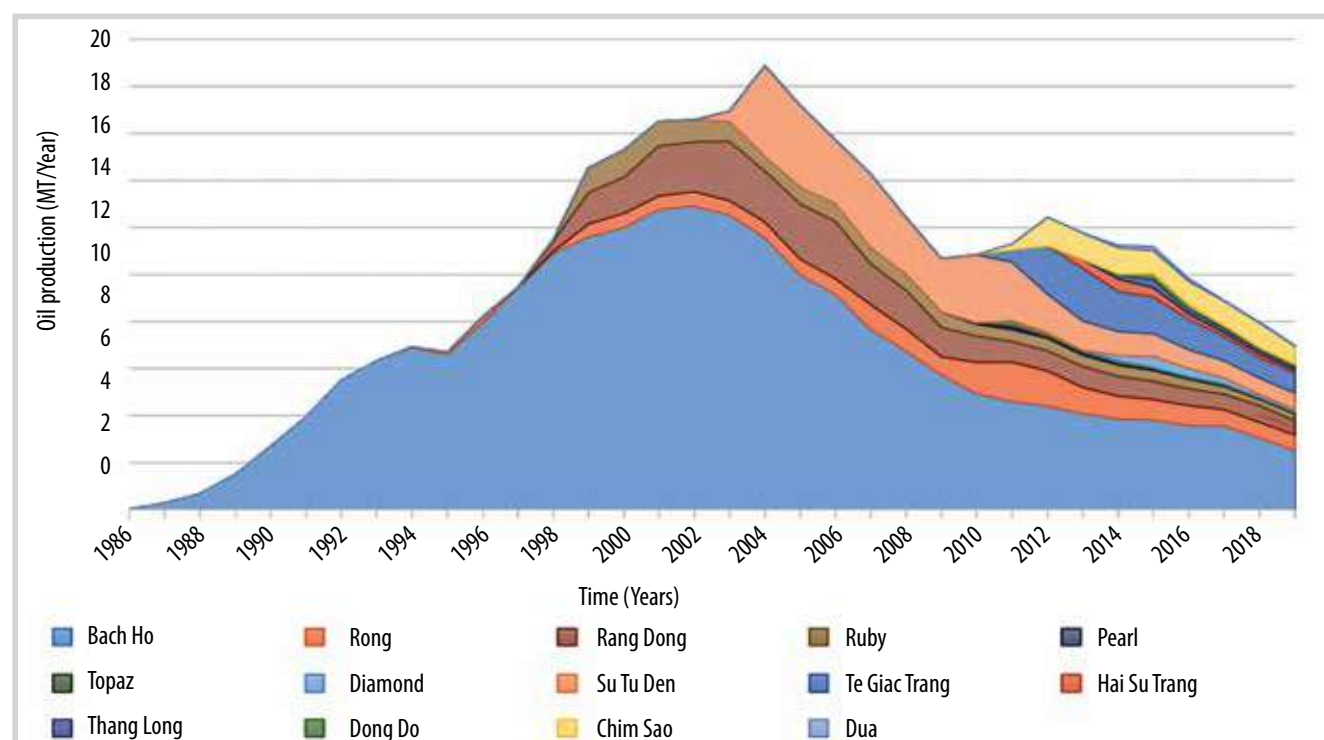


Figure 1. Production curve of many oil fields showing the declining period.

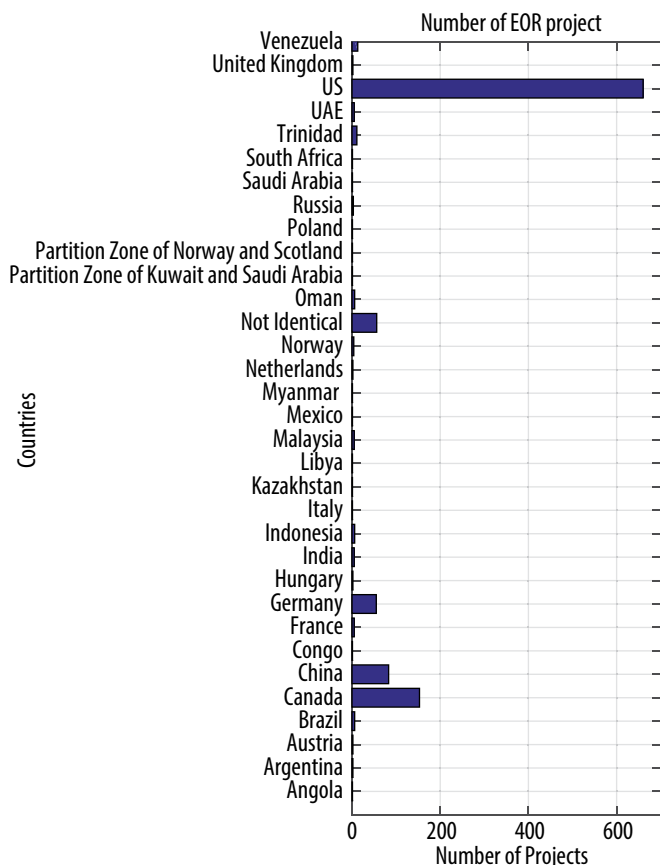


Figure 2. Number of EOR projects of each countries.

The application of artificial intelligence (AI) in screening reservoir candidates for EOR was first published by Guerillot [9]. Subsequently, several works have been published to improve the quality and accuracy of the models. These models are based on fuzzy-logic (FL) and expert system approach [10, 11] artificial neural network (ANN) [12] least square support vector machine (LSSVM), and very recently, the combination of both fuzzy-logic (FL) and neuro-fuzzy (NF) [13, 14]. These works and others recently published in literature on screening techniques are summarised in [14].

A quick overview of mature hydrocarbon fields in Vietnam showed that many oil fields are in declining phase as shown in Figure 1 and can be classified as mature or near mature fields which need the application of IRO/EOR to sustain their production. Consequently, it is crucial to find a proper EOR method for further field development.

The objective of this study is to find the most appropriate EOR method for a mature oil field offshore Vietnam based on the available EOR projects worldwide. The scopes of study include: i) collect data

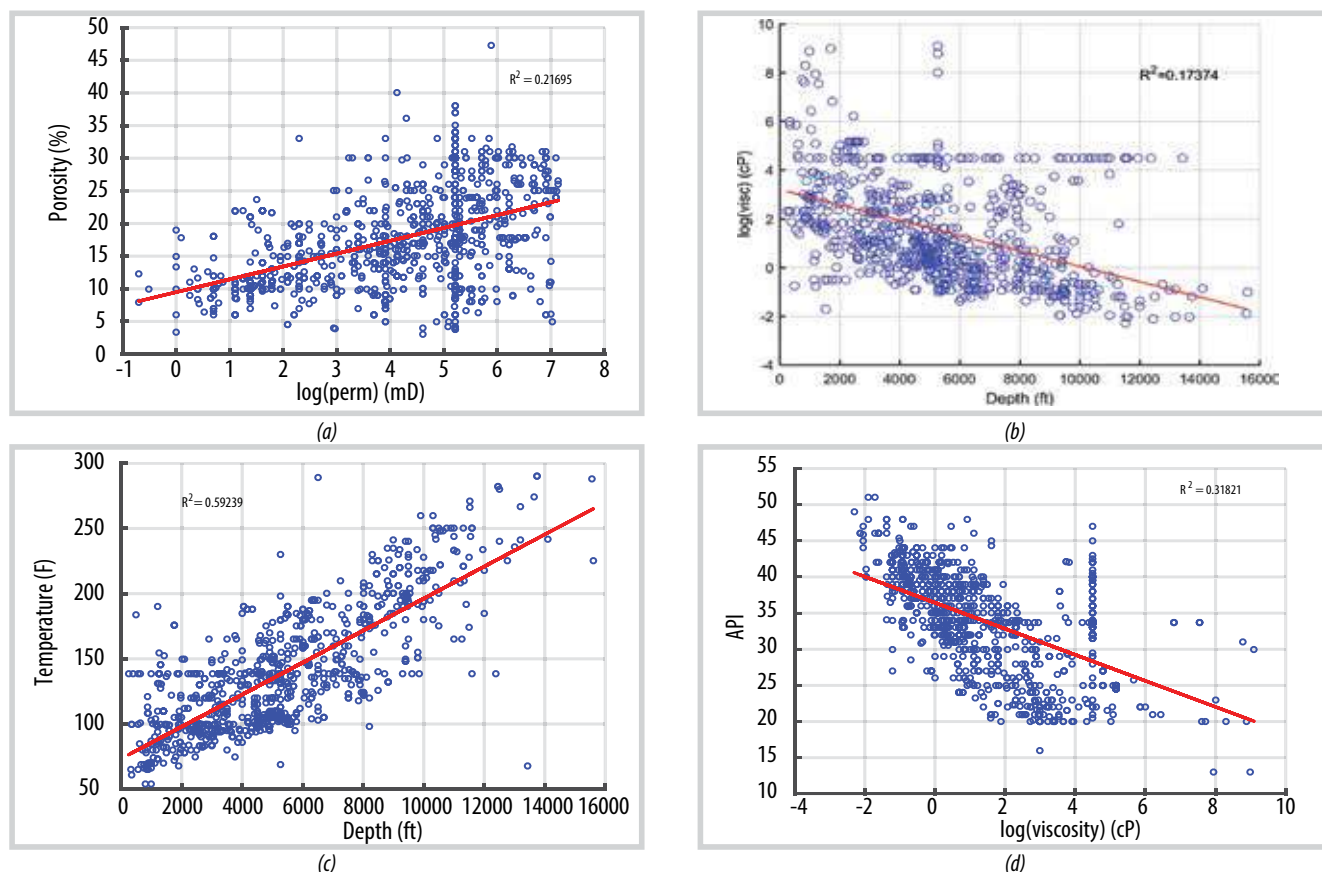


Figure 3. Relationship of oil fields parameters: a) Porosity and permeability; b) Depth and viscosity; c) Depth and temperature and d) API and viscosity.

of EOR projects all over the world; ii) statistically analyse the collected data; and iii) develop the statistical and machine learning approaches to get the most suitable EOR method for the offshore Vietnam oil field.

2. Data preparation and preprocessing

For EOR screening, it is required to get as much as possible information of the EOR projects worldwide to create an EOR database for later analyses. Establishing an EOR database is a great challenge because data are scattered and reported in a variety of documentation forms and languages. In this research, the EOR data were collected from the most updated EOR projects published biyearly by the Oil and Gas Journal, in a similar format used by many other researchers such as [2, 15 - 19]. This dataset is summarised in table style and collected from 33 countries, mainly from USA and Canada (more than 840 projects, equivalent to 76%) as seen in Figure 2. In fact, many countries have only one EOR project published. The dataset covering porosity, permeability, initial water saturation, reservoir depth, reservoir area, oil viscosity, and temperature will be used as an input for analyses and interpretation.

Pre-processing the collected data is necessary as the data of many EOR projects is missing or reported in a range of values, e.g. the porosity can be reported as a range of 10 - 22% instead of an exact value. For this kind of data, the average value will be calculated and used. Similarly, the missing data will be interpolated by linear correlation between two close parameters such as porosity and logarithm of permeability, viscosity and specific gravity (API), temperature and depth, or depth and viscosity. These linear correlations are shown in Figures 3a-d respectively, which will be used as a function to

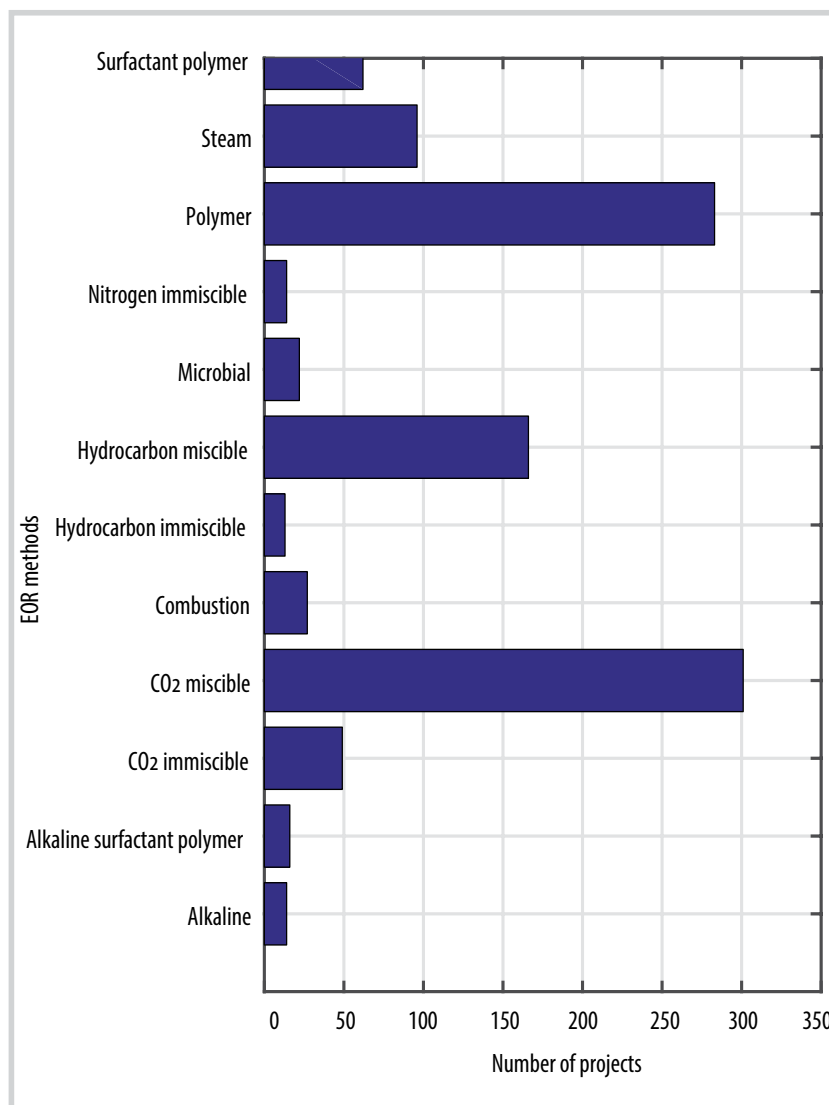


Figure 4. Number of EOR projects used for data analyses.

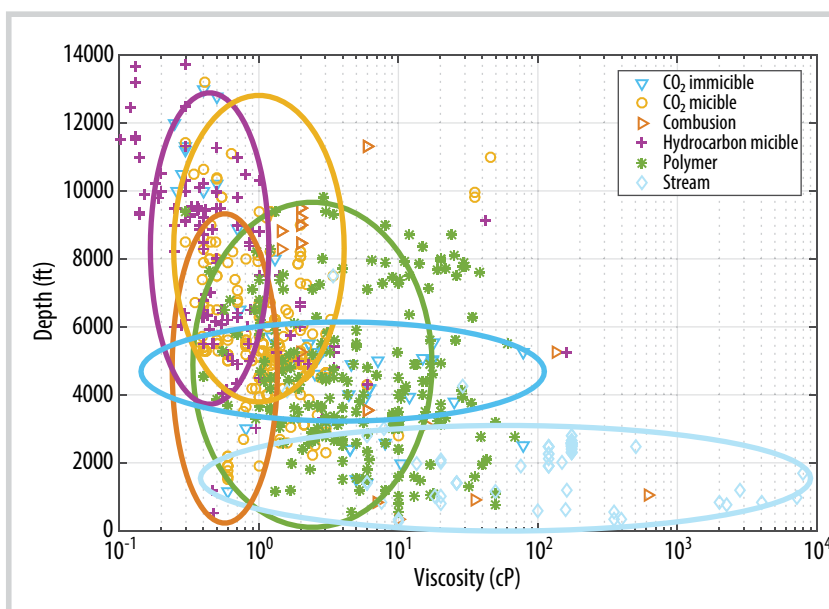


Figure 5. Modified conventional screening guidelines by Taber et al. [4, 5].

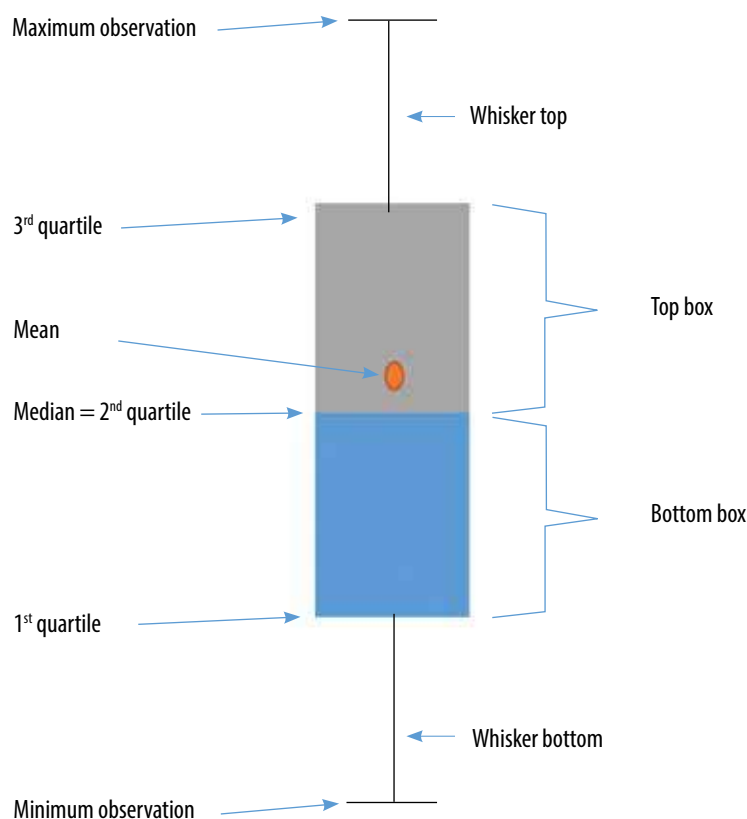
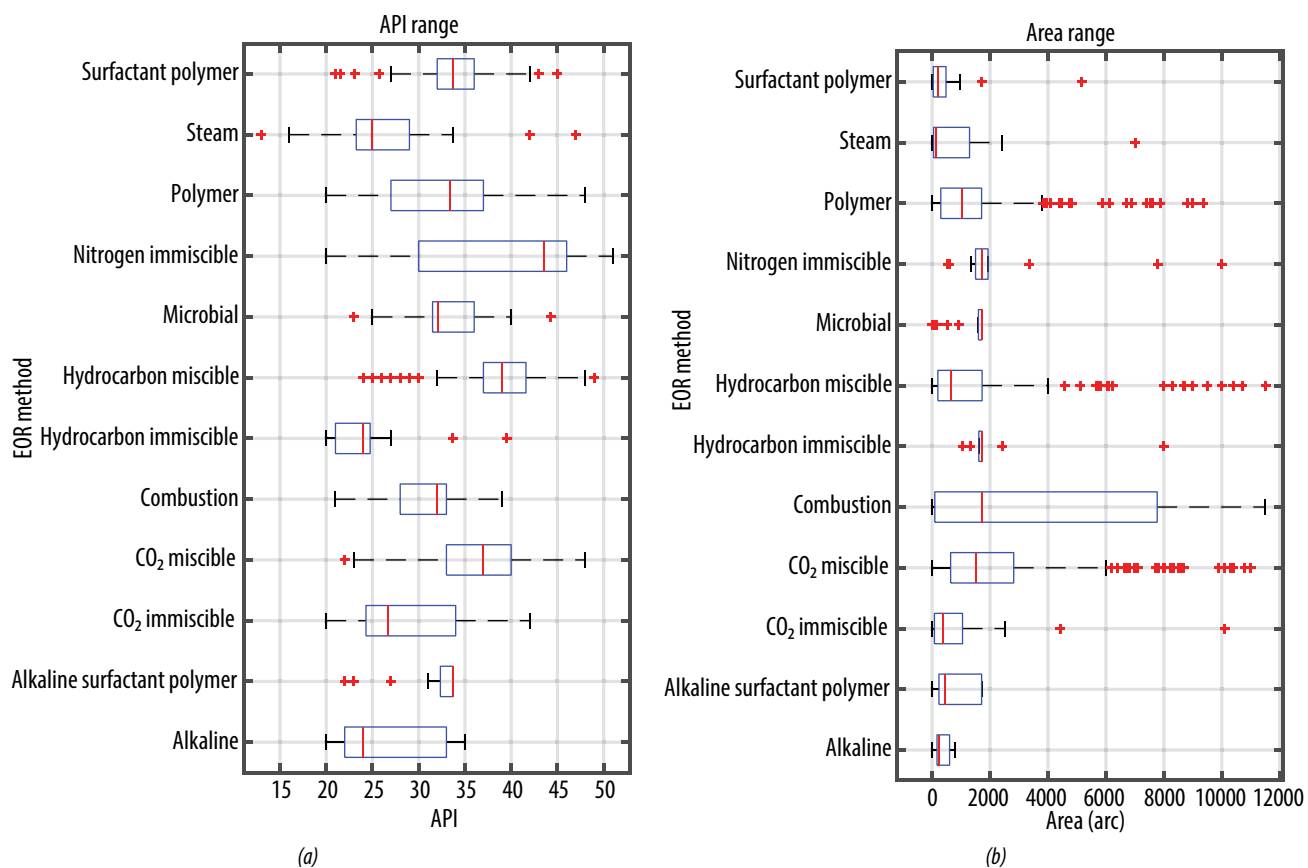
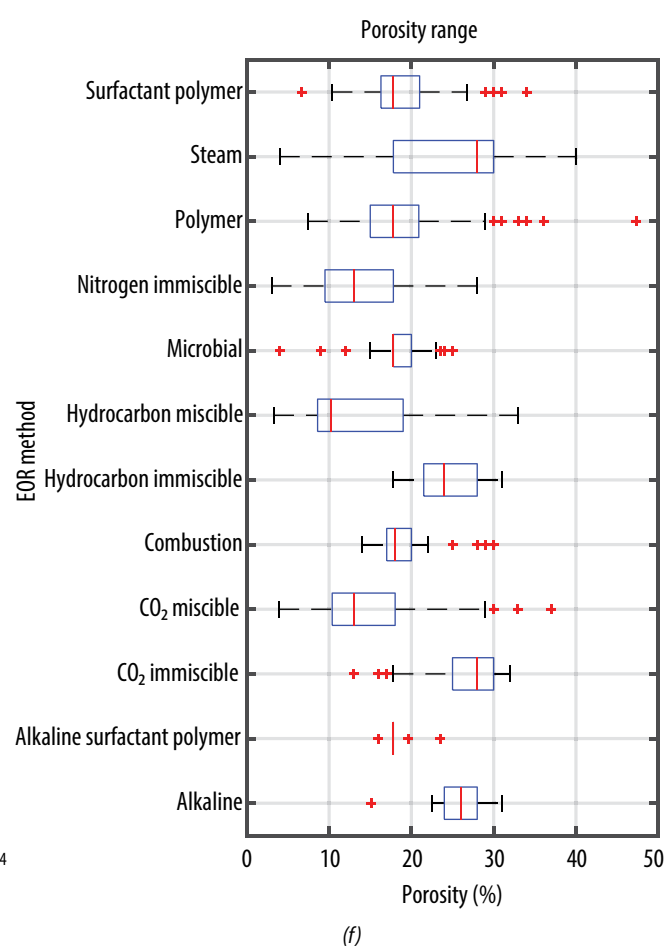
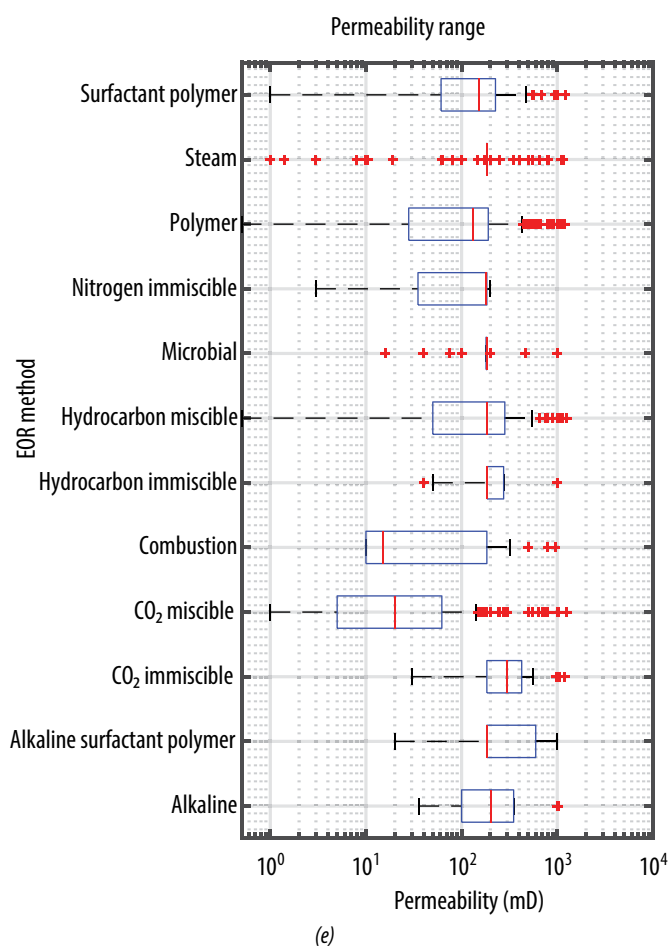
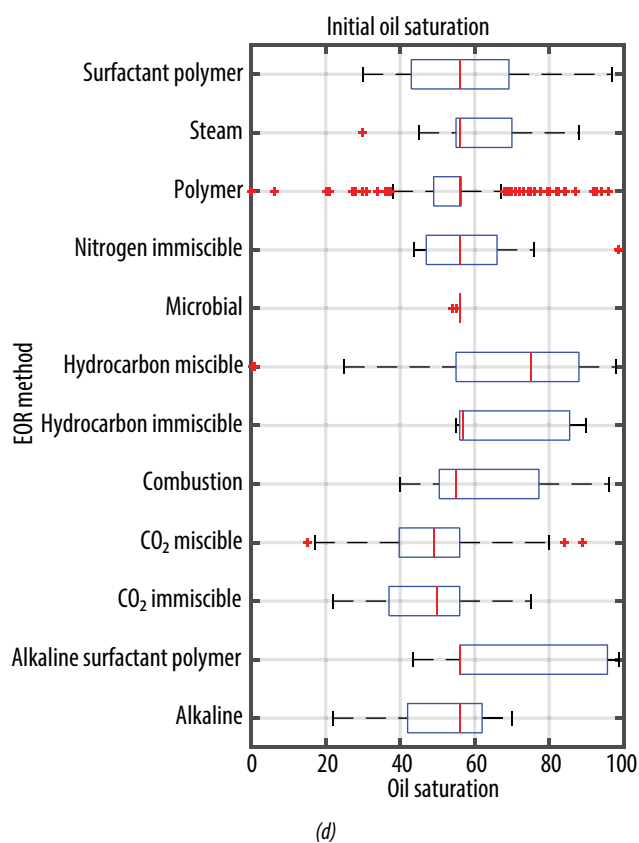
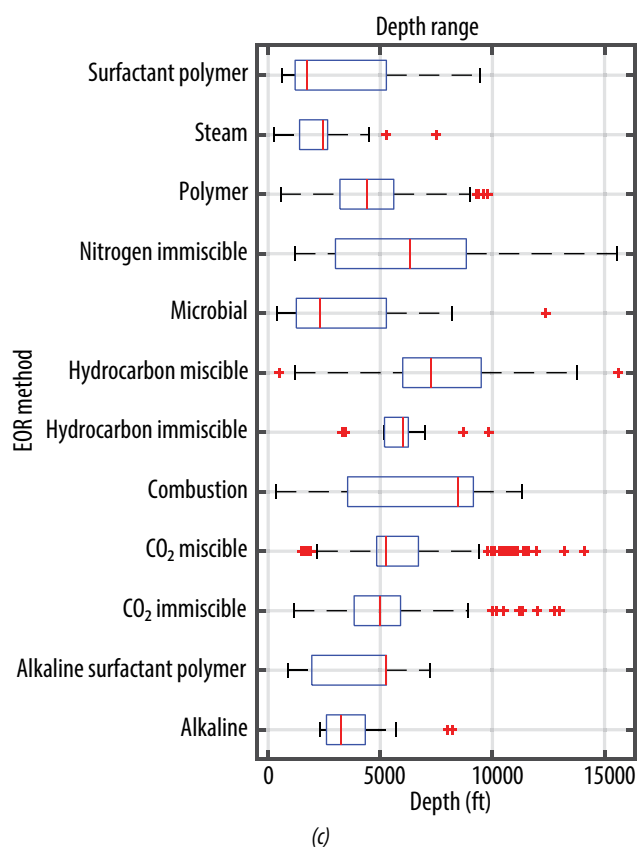


Figure 6. Schematic of boxplot.

recover and fill up the missing data. For some parameters that do not have any relationship or very loose relationship with the other parameters such as initial oil saturation and area, the filling up method will be the mean values of these available data. For the few data that are out of physical ranges or linear range, they are also corrected. Additionally, the oils produced offshore Vietnam are light oils with API from 30 to 40 and viscosity from 0.8 to 4 cP. Thus, the thermal EOR method will not be appropriate as it is more suitable for heavy and high viscosity oils. It is worth noting that the data filter needs to be applied for the collected data to make them more diverse, compared to other papers such as the one by Zhang [2]. In this particular data set, we filter out all the data with viscosity higher than 10,000 cP. The number of EOR projects is shown in Figure 4, where the majority are CO₂ miscible projects while the rest are other thermal projects such as steam or combustion.





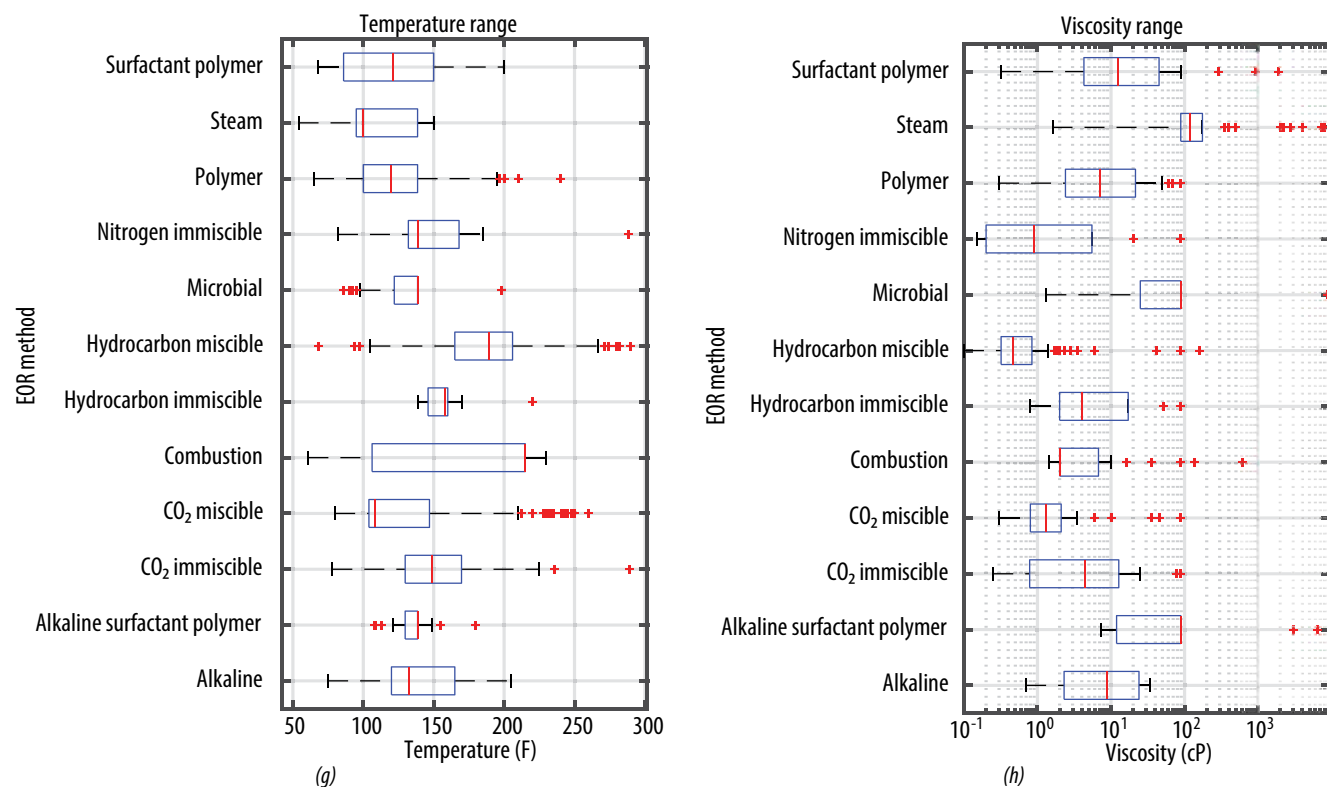


Figure 7. Boxplot analyses of reservoir and fluid properties of EOR projects.

Table 1. Statistical summarisation of porosity (%) from collected EOR projects

EOR method	Min.	Max.	q25	Mean	q75
Alkaline	15.10	31.00	24.00	26.00	28.00
Alkaline surfactant polymer	16.00	23.50	17.81	17.81	17.81
CO ₂ immiscible	13.00	32.00	25.00	28.00	30.00
CO ₂ miscible	3.93	37.00	10.00	12.00	18.00
Combustion	14.00	29.00	17.00	18.00	20.00
Hydrocarbon immiscible	20.00	31.00	22.00	24.00	28.00
Hydrocarbon miscible	4.25	33.00	8.60	10.15	20.00
Microbial	12.00	24.00	17.20	19.00	20.00
Nitrogen immiscible	3.00	28.00	6.65	11.95	16.50
Polymer	7.40	47.30	14.38	17.45	21.53
Steam	4.00	40.00	24.75	30.00	30.00
Surfactant polymer	10.40	34.00	15.70	19.00	21.60

Table 2. Statistical summarisation of permeability (mD) from collected EOR projects

EOR method	Min.	Max.	q25	Mean	q75
Alkaline	36.00	1025.00	100.00	201.84	350.00
Alkaline surfactant polymer	60.00	1000.00	501.00	601.50	676.00
CO ₂ immiscible	30.00	1200.00	179.34	275.00	450.00
CO ₂ miscible	1.00	1255.00	4.01	11.00	50.05
Combustion	10.00	958.00	10.00	10.00	147.17
Hydrocarbon immiscible	40.00	1000.00	183.68	183.68	275.00
Hydrocarbon miscible	0.50	1250.00	50.00	183.68	300.00
Microbial	16.00	465.00	120.38	183.68	200.00
Nitrogen immiscible	3.00	200.00	19.75	137.50	183.68
Polymer	0.50	1200.00	22.75	95.30	200.00
Steam	1.00	1150.00	168.00	183.68	183.68
Surfactant polymer	1.00	1218.00	50.00	115.00	197.00

Table 3. Statistical summarisation of depth (ft) from collected EOR projects

EOR method	Min.	Max.	q25	Mean	q75
Alkaline	2300.00	8200.00	2600.00	3250.00	4330.00
Alkaline surfactant polymer	870.00	5300.00	875.00	886.50	5279.45
CO ₂ immiscible	1400.00	13000.00	3975.00	5279.45	7254.25
CO ₂ miscible	1900.00	14100.00	4900.00	5279.45	6000.00
Combustion	347.50	11300.00	3550.00	8450.00	9050.00
Hydrocarbon immiscible	3300.00	8700.00	5162.50	6000.00	6000.00
Hydrocarbon miscible	500.00	15600.00	6000.00	6750.00	9432.00
Microbial	400.00	5740.00	1390.13	1970.00	4534.59
Nitrogen immiscible	1200.00	15565.00	4939.72	8092.50	10167.50
Polymer	550.00	9800.00	3000.00	4400.00	5802.25
Steam	250.00	7500.00	1400.00	2350.00	2600.00
Surfactant polymer	650.00	9460.00	1074.00	1900.00	5279.45

Table 4. Statistical summarisation of area (arc) from collected EOR projects

EOR method	Min.	Max.	q25	Mean	q75
Alkaline	1.00	800.00	170.00	228.50	604.00
Alkaline surfactant polymer	1.00	1708.63	236.44	450.78	1708.63
CO ₂ immiscible	5.00	10104.00	81.00	380.00	1050.75
CO ₂ miscible	5.00	11000.00	640.00	1500.00	2817.50
Combustion	6.00	11500.00	94.25	1708.63	7770.00
Hydrocarbon immiscible	1052.00	8000.00	1612.72	1708.63	1708.63
Hydrocarbon miscible	12.20	11520.00	200.00	640.00	1726.00
Microbial	10.00	1708.63	1600.00	1708.63	1708.63
Nitrogen immiscible	540.00	10000.00	1500.00	1708.63	1931.00
Polymer	2.50	9360.00	300.00	1024.00	1708.63
Steam	9.00	7020.00	51.50	133.50	1292.50
Surfactant polymer	1.00	5161.00	40.00	199.50	480.00

Table 5. Statistical summarisation of oil saturation (%) from collected EOR projects

EOR method	Min.	Max.	q25	Mean	q75
Alkaline	22.00	70.00	42.00	55.99	62.00
Alkaline surfactant polymer	43.50	98.70	55.99	55.99	95.65
CO ₂ immiscible	22.00	75.00	37.00	50.00	55.99
CO ₂ miscible	15.00	89.00	39.75	49.00	55.99
Combustion	40.00	96.00	50.50	55.00	77.25
Hydrocarbon immiscible	55.00	90.00	55.99	57.00	85.50
Hydrocarbon miscible	0.40	98.00	55.00	75.00	88.00
Microbial	54.00	55.99	55.99	55.99	55.99
Nitrogen immiscible	43.80	98.50	47.00	55.99	66.00
Polymer	0.00	95.90	49.00	55.99	56.38
Steam	30.00	88.00	55.00	55.99	70.00
Surfactant polymer	30.00	96.90	43.00	55.99	69.20

3. Conventional EOR screening method

Following the method presented in Zhang et al., [2], Figure 5 illustrates a modified graphical screening guideline that was created by Taber et al. [4, 5] for depth and viscosity. Regions enclosed within the ellipses represent the applicable ranges for each EOR technique.

Here we can see that the thermal method can only be applied for the shallow reservoirs with a very high range of viscosity, while the viscosity for application of polymer EOR is less than 100 cP. Similarly, the gas injection method (hydrocarbon and CO₂ miscible) should be applied for deep reservoirs with low viscosity (less than 3 cP).

Table 6. Statistical summarisation of oil viscosity (cP) from collected EOR projects

EOR method	Min.	Max.	q25	Mean	q75
Alkaline	0.70	34.00	2.30	8.85	24.00
Alkaline surfactant polymer	7.40	15.60	8.20	9.25	13.50
CO ₂ immiscible	0.25	78.00	0.72	2.95	6.70
CO ₂ miscible	0.30	46.00	0.70	1.20	1.80
Combustion	1.44	136.00	2.00	2.00	6.00
Hydrocarbon immiscible	0.80	52.00	2.00	2.20	4.90
Hydrocarbon miscible	0.10	160.00	0.32	0.46	0.83
Microbial	1.32	28.00	3.43	6.50	22.50
Nitrogen immiscible	0.15	20.00	0.20	0.60	4.35
Polymer	0.30	68.00	1.88	4.80	13.00
Steam	1.60	400.00	26.00	150.00	175.00
Surfactant polymer	0.32	288.00	3.25	7.00	18.00

Table 7. Statistical summarisation of oil temperature (F) from collected EOR projects

EOR method	Min.	Max.	q25	Mean	q75
Alkaline	75.00	205.00	120.00	132.50	165.00
Alkaline surfactant polymer	108.14	155.00	108.32	116.96	149.00
CO ₂ immiscible	78.00	289.00	124.50	148.00	184.50
CO ₂ miscible	80.00	250.00	104.00	106.00	140.00
Combustion	61.00	230.00	118.75	215.00	216.25
Hydrocarbon immiscible	146.00	220.00	150.25	158.00	160.00
Hydrocarbon miscible	94.00	290.00	165.00	189.00	206.00
Microbial	86.00	138.55	90.50	95.00	116.00
Nitrogen immiscible	82.00	288.00	131.00	135.27	171.00
Polymer	65.00	240.00	95.00	115.00	136.00
Steam	54.00	150.00	95.00	100.00	110.00
Surfactant polymer	68.00	200.00	74.00	104.00	133.70

Table 8. Statistical summarisation of API from collected EOR projects

EOR method	Min.	Max.	q25	Mean	q75
Alkaline	20.00	35.00	22.00	24.00	33.00
Alkaline surfactant polymer	22.00	33.69	27.00	33.69	33.69
CO ₂ immiscible	20.00	42.00	25.00	27.85	33.85
CO ₂ miscible	23.00	48.00	33.00	36.50	40.00
Combustion	21.50	39.00	28.00	33.00	33.00
Hydrocarbon immiscible	20.00	27.00	21.00	24.00	24.00
Hydrocarbon miscible	24.00	49.00	37.00	39.00	41.60
Microbial	23.00	44.30	31.80	33.00	38.50
Nitrogen immiscible	20.00	51.00	29.00	44.00	46.00
Polymer	20.00	48.00	26.08	33.00	38.00
Steam	16.00	47.00	24.50	25.00	26.25
Surfactant polymer	21.00	45.00	30.25	33.69	36.00

To provide an easy, straightforward, and comprehensive screening guideline, a boxplot matrix is created to visualise all the ranges for reservoir/fluid properties. A boxplot is shown in Figure 6, which reveals the minimum, 25th percentile (Q1), median, 75th percentile (Q3), and the maximum. The lower and upper limits are

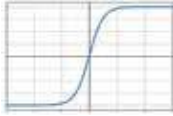
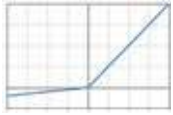
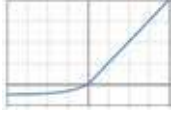
normally within the minimum and maximum values. In statistics, when the value is smaller than the lower limit or greater than the upper limit, it will be considered as outliers. However, for the construction of screening guidelines, the detected outliers are regarded as special cases after data cleansing that could not be ignored

because each case represents either an extreme reservoir/fluid situation or a new development for the implementation of an EOR technique. With the given data collected, 8 primary parameters, namely API, depth, area, porosity, permeability, oil saturation, temperature, and viscosity, are considered the background for the EOR guideline as shown in Figure 7. These boxplots illustrate the distribution of the above-mentioned parameters for the successful EOR projects that were used to obtain the required statistics involving the minimum, maximum, average, 1st quartile, 2nd quartile (median) and 3rd quartile for each variable. These parameters were determined from the successful EOR data set and then defined the intervals for the data distribution in horizontal axis. These statistical parameters for each EOR method are summarised in Tables 1 - 8, based on which we can make the scoring and rating for a given oil field. For example, considering surfactant as an EOR technique, the lower and upper limits of the variable saturation for successful projects (Figure 7d) are 30 and 96.9% and for a given range of Vietnam's oil fields are 40 and 80% (Table 9); $[30 - 96.9] \cap [40 - 80] = [40 - 80]$, which means the values within the range of (Figure 7) 40 and 80% of initial water saturation may be suitable for surfactant polymer injection method. Following the outcome of the boxplots and other similar plots such as scatter plots (Figure 3), the histogram technique can be used to represent the distribution of the data sets. As seen in Figure 3, the correlation coefficients are relatively small because most of the data collected here come from different fields and sites all over the world instead of one certain location.

4. Advanced EOR screening guideline by deep learning approach

Recent development of deep learning algorithms has been applied in many fields of the petroleum industry from exploration

Table 9. Common activation functions used in deep learning and ANN

Activation function	Plot	Equation
Sigmoid		$f(x) = \sigma(x) = \frac{1}{1+e^{-x}}$
Tanh		$f(x) = \tanh(x) = \frac{e^x - e^{-x}}{e^x + e^{-x}}$
ReLU		$f(x) = \begin{cases} 0, & x < 0 \\ x, & x \geq 0 \end{cases}$
Leaky ReLU		$f(x) = \begin{cases} \epsilon x, & x < 0 \\ x, & x \geq 0 \end{cases}$
ELU		$f(x) = \begin{cases} \alpha(e^x - 1), & x < 0 \\ x, & x \geq 0 \end{cases}$
Identity		$f(x) = x$

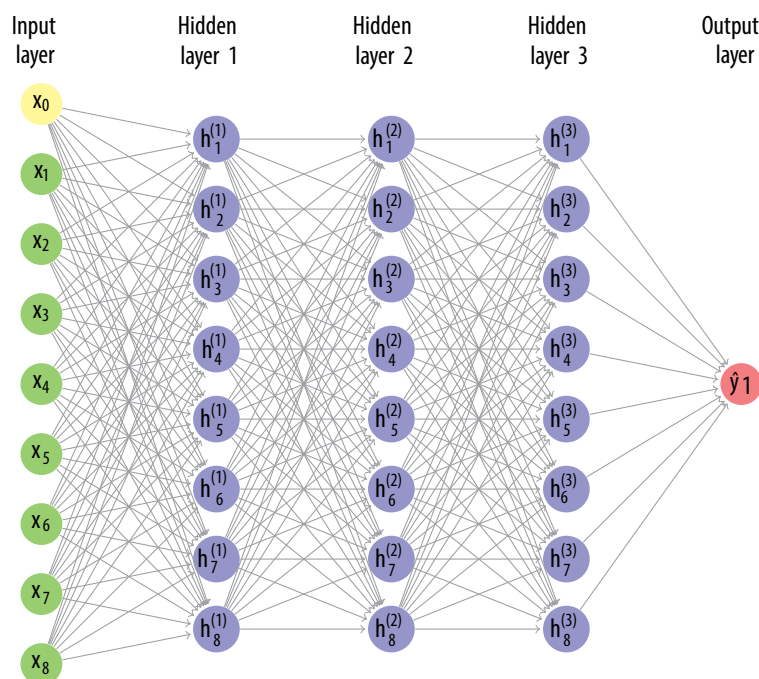


Figure 8. A deep learning network designed for this EOR screening problem, the input layer (x_1 to x_8) is made of 8 reservoir properties and the output layer will be an EOR method.

to production. The principle of deep learning is based on the artificial neuron network (ANN) approach in which the number of hidden layers is more than one while the ANN consists of only one hidden layer [20] as shown in Figure 8. In this problem for EOR selection, the deep learning network consists of an 8-input layer, 3 hidden layers with 8 neurons each and 1 output layer. However, the number of hidden layers as well as the number of neurons in each hidden layer are not optimised as it is beyond the scope of this research. The input layer consists of 8 reservoir properties (area, depth, porosity, permeability, and temperature) and fluid properties (viscosity and density (°API)), initial oil saturation denoted as x1 to x8 in Figure 8, while the output layer will be an EOR method. Each hidden layer is composed of basic processing elements called neurons. Each neuron is connected to the neurons of the adjacent layer with the connection weights between 0 and 1. The signals between the neurons are multiplied by the associated connection weights and added up together as Equation (1), and then used as the net input of the neuron as follows:

$$NET = \sum_{k=1}^n I_k W_k \quad (1)$$

where:

NET is the net input of the neuron;

I is the input variable;

W is the connection weight;

k is the running index;

n is the number of input variables.

Each neuron applies an activation function to its net input to determine its output signal, and the signal is transmitted to the next neuron.

The activation function is added to an artificial neural network in order to help the network learn complex

patterns in the data. Table 9 summarises the activation functions in terms of mathematical equations and their 1D plots. Among them, Sigmoid function is often used in ANN while ReLU is used in deep learning to avoid the vanishing gradient as reported by Giao and Kusan [21].

The connection weight function between the neurons is adjusted during the training processes. There are two ways of training, which are supervised and unsupervised training. For most typical neural networks, the connection weights are adjusted by the given input and corresponding output. This process is called supervised training. One of the widely used supervised networks is the feed-forward Back Propagation (BP) network which adjusts the connection weights during the back-propagation process. In this study, the BP network with the training algorithm of scaled conjugate gradient (SCG) - a new variation of the conjugate gradient method - is used.

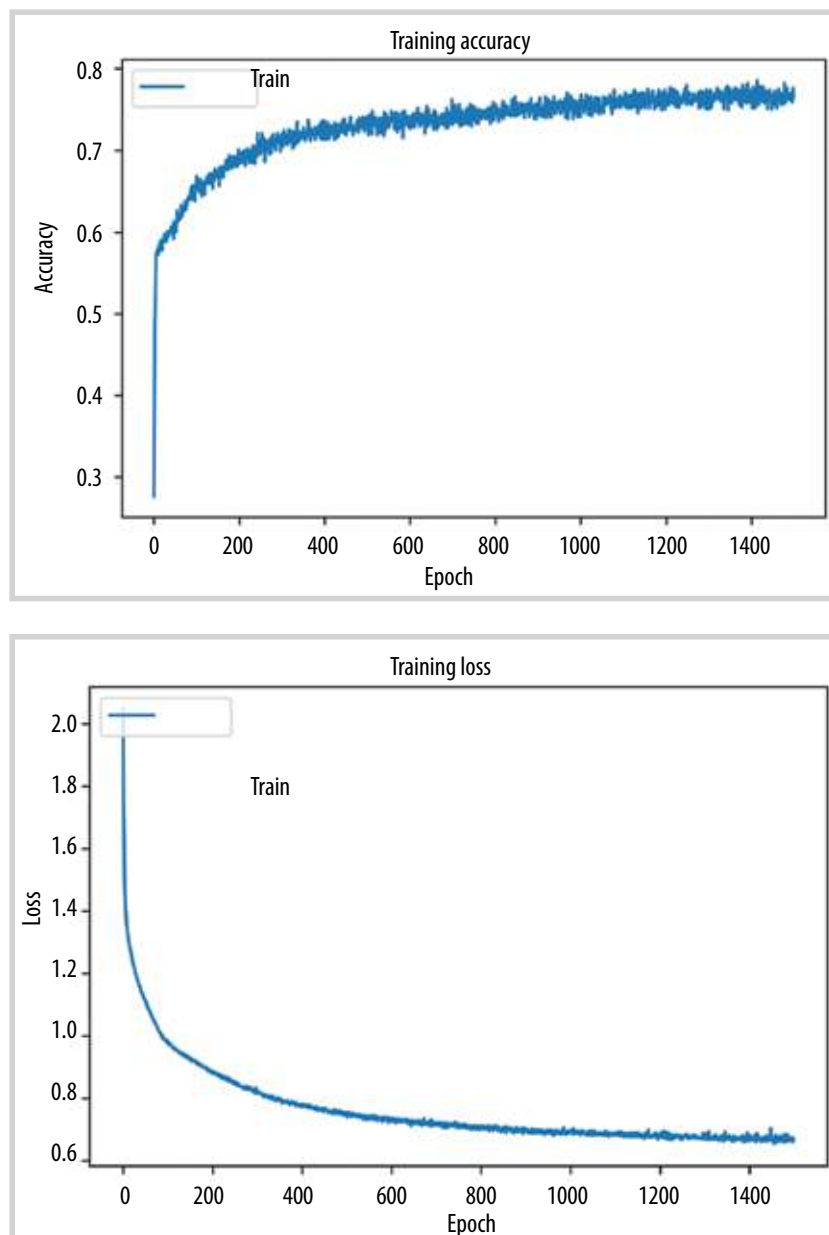


Figure 9. Training of result summaries.

Table 10. Vietnam oil field properties as input for EOR screening model

Field name	Depth (ft)	Temp (°C)	Area (arc)	Porosity (%)	Perm (mD)	API Gravity	Visc. (cP)	Oil saturation (%)	Reco-mmendation
Field 1	10168	230	1200	16.5	50	33	0.9	80	Polymer
Field 2	10004	212	1500	15	30	32	1.1	60	Polymer
Field 3	9840	203	1800	18	160	29	4	50	Polymer
Field 4	9184	90	800	19	253	38.9	0.7	50	Polymer
Field 5	8856	194	700	23.2	185	37.9	0.7	50	SP
Field 6	5904	183.2	900	19	300	37	0.8	50	SP
Field 7	6888	190	1000	26	1292	35.4	0.8	60	Hydro carbon Miscible
Field 8	10168	203	1020	18.8	293	37.9	0.8	60	Polymer
Field 9	10496	240	1300	12.04	31	38.7	0.7	40	Polymer
Field 10	10824	257	1200	10.25	20	38.7	0.7	40	Polymer
Field 11	10496	230	900	15	10	36	0.8	50	Polymer
Field 12	10496	203	900	22	247	37.7	0.8	50	Polymer
Field 13	10496	230	800	15	24.8	36	0.85	50	Polymer

SCG allows the avoidance of the line search per training iteration of Levenberg-Marquardt approach to scale the step size.

With the collected EOR projects, the output of each project is the successful EOR method applied to a certain oil field. So each EOR method has to be categorised as a unit vector instead of naming them as a single number. For example, with 12 EOR methods mentioned above the categorised vector will be a 12-row element unit vector in which vector (1 0 0 0 ... 0) will be for method 1; vector (0 1 0 0 ...0) for method 2 and (0 0 0 ... 1) will be for method 12, respectively. Consequently, the output layer will be a matrix of 12x1069. Similarly, the input layer will be a matrix of 8x1069 data corresponding to 8 parameters. For training purposes, the data will be split into 2 sets: 80% of data for training and the rest 20% for validation.

These learning processes are implemented under the sequential model of Tensorflow package [22]. The sequential model is simple, allowing us to build a model layer by layer. In the network model, the layer type is "dense" which is the standard layer and can work for most of training cases. Compiling the model takes two parameters: optimiser and loss.

The optimiser controls the learning rate. In this study, Adam optimiser will be used since it is generally a good tool in many cases. The Adam optimiser adjusts the learning rate throughout training. The learning rate determines how fast the optimal weights for the model are calculated. A smaller learning rate may lead to more accurate weights (up to a certain point), but it will take longer to compute the weights.

For the loss function, the mean square error is calculated by taking the average squared difference between the predicted and the actual values as defined in the following equation:

$$MSE = \frac{1}{N} \sum_{i=1}^N (f_i - y_i)^2 \tag{2}$$

where N is the number of data points, f_i and y_i are values returned by the training model and actual values of data point I, respectively. It is a popular loss function for regression problems. The closer to 0 it is, the better the model performed.

Figure 9 shows the result of training, including accuracy and training loss, respectively. The square correlation coefficient (r-square) between the predicted output from the training model and the one from 20% validating data is 0.89, which suggests that the training model is acceptable for further predicting. Once the training model was achieved, this model will be loaded with the input parameters (porosity, permeability, initial water saturation, viscosity, API (density), depth range, temperature, and area) from offshore oil fields of Vietnam (Table 10) to predict suitable EOR methods for these oil fields. The results are shown at the last column of Table 10. Here we can see that most of the recommended methods are polymer or surfactant polymer. Only one recommended method relates to gas miscible.

5. Conclusions

The following major conclusions were drawn from this study:

This study could successfully collect and provide the most up-to-date EOR-project data sets as the first step in analysing EOR data and establishing screening criteria.

With the new dataset collected from EOR projects all over the world, an updated graphical method was proposed to find the range of parameters for conventional EOR screening. The statistical analyses conducted on these data sets gave an overall outlook of EOR methods. Additionally, a boxplot served as a very helpful tool for exploring and displaying the screening-criteria data set. This tool was used to update the conventional EOR screening method, giving more reasonable and applicable EOR method to each oil field. For example, regarding the polymer and surfactant injection method, the ranges of API, viscosity (cP), permeability (mD), porosity (%), temperature (F), depth (ft) and initial oil saturation (%) are 21 - 45, 0.32 - 288, 1 - 1218, 10 - 34, 10 - 34, 68 - 200, 650 - 9460 and 30 - 96, respectively.

By applying the statistical analyses mentioned above for the input of the oil fields offshore Vietnam, it was found that the most recommended EOR method is chemical injection (polymer or polymer surfactant injection).

A deep learning network architecture was designed and tested in this study, consisting of an 8-input layer corresponding to eight reservoir properties, three 8-neuron hidden layers and an 1-output layer (the selected EOR method). Based on the initial DL prediction, the most recommended EOR method for mature oil fields in Vietnam is also polymer and polymer surfactant injection, with an exception of hydrocarbon miscible method being recommended for oil field No. 7.

Acknowledgement

This research is supported by the national EOR project "Study on the EOR technique selection from laboratory to the field pilot test for mature oil fields in the Cuu Long basin", Ref. No. ĐTDLCN.26/19. We would like to express our thanks to anonymous reviewer, Dr. Pham Huy Giao for valuable suggestions to improve the quality of the paper.

References

[1] Mark P. Walsh and Larry W Lake, *A generalized approach to primary hydrocarbon recovery*. Elsevier, 2003.

[2] Na Zhang, Mingzhen Wei, Jiayi Fan, Munqith Aldhaferia, Yandong Zhang and Baojun Bai, "Development of a hybrid scoring system for EOR screening by combining conventional screening guidelines and random forest

algorithm", *Fuel*, Vol. 256, pp. 1 - 10, 2019. DOI: 10.1016/j.fuel.2019.115915.

[3] J.P. Brashear and V.A. Kuuskraa, "The potential and economics of enhanced oil recovery", *Journal of Petroleum Technology*, Vol. 30, No. 9, pp. 1231 - 1239, 1978. DOI: 10.2118/6350-PA.

[4] J.J. Taber, F.D. Martin and R.S. Seright, "EOR screening criteria revisited - Part 1: Introduction to screening criteria and enhanced recovery field projects", *SPE Reservoir Engineering*, Vol. 12, No. 3, pp. 189 - 198, 1997. DOI: 10.2118/35385-PA.

[5] J.J. Taber, F.D. Martin and R.S. Seright, "EOR screening criteria revisited - Part 2: Applications and impact of oil prices", *SPE Reservoir Engineering*, Vol. 12, No. 3, pp. 10 - 24, 1997. DOI: 10.2118/39234-PA.

[6] Ahmad Al Adasani and Baojun Bai, "Analysis of EOR projects and updated screening criteria", *Journal of Petroleum Science and Engineering*, Vol. 79, No. 1 - 2, pp. 10 - 24, 2011. DOI: 10.1016/j.petrol.2011.07.005.

[7] Vladimir Alvarado, Aaron Ranson, Karen Hernandez, Eduardo Manrique, Justo Matheus, Tamara Liscano and Natasha Prospero, "Selection of EOR/IOR opportunities based on machine learning", *European Petroleum Conference*, 2002. DOI: 10.2118/78332-MS.

[8] Martina Siena, Alberto Guadagnini, Ernesto Della Rossa, Andrea Lamberti, Franco Masserano and Marco Rotondi, "A novel enhanced-oil-recovery screening approach based on Bayesian clustering and principal components analyses", *SPE Reservoir Evaluation Engineering*, Vol. 19, No. 3, pp. 382 - 390, 2016. DOI: 10.2118/174315-PA.

[9] D.R. Guerillot, "EOR screening with an expert system", *Petroleum Computer Conference*, San Jose, California, 1988. DOI: 10.2118/17791-MS.

[10] Ting-Horng Chung, Herbert B. Carroll and Rhonda Lidsey, "Application of fuzzy expert systems for EOR project risk analysis", *SPE Annual Technical Conference and Exhibition*, 1995. DOI: 10.2118/30741-MS.

[11] Mohamed Nageh, Mahmoud Abu El Ela, El Sayed El Tayeb and Helmy Sayyoub, "Application of using fuzzy logic as an artificial intelligence technique in screening criteria of the EOR technologies", *SPE North Africa Technical Conference and Exhibition*, 2015. DOI: 10.2118/175883-MS.

[12] Jong-Yong Lee and Jong-Se Lim, "Artificial neural network approach to selection of enhanced oil

recovery method", *Journal of the Korean Society of Mineral and Energy Resource Engineers*, Vol. 45, No. 6, pp. 719 - 726, 2008.

[13] Geraldo Ramos and Lateef Akanji, "Technical screening of enhanced oil recovery methods - A case study Block C in offshore Angolan oilfields", *First EAGE/ASGA Petroleum Exploration Workshop*, 2017. DOI: 10.3997/2214-4609.201702357.

[14] Geraldo A.R. Ramos, Bruno Elias and Kyari Yates, "Screening reservoir candidates for enhanced oil recovery in Angolan offshore projects", *Angolan Mineral, Oil and Gas Journal*, Vol. 1, No. 1, pp. 6 - 10, 2020. DOI: 10.47444/amogj.v1i1.3.

[15] G. Moritis, "CO₂ injection gains momentum", *Oil & Gas Journal*, Vol. 106, No. 15, pp. 46 - 57, 2006.

[16] G. Moritis, "California steam EOR produces less; other EOR continues", *Oil & Gas Journal*, Vol. 100, pp. 43 - 77, 2002.

[17] G. Moritis, "EOR continues to unlock oil

resources", *Oil & Gas Journal*, Vol. 104, No. 15, pp. 45 - 65, 2004.

[18] G. Moritis, "EOR oil production up slightly", *Oil & Gas Journal*, Vol. 96, No. 16, pp. 49 - 77, 1998.

[19] G. Moritis, "EOR weathers low oil prices", *Oil & Gas Journal*, Vol. 98, No. 12, pp. 39 - 61, 2000.

[20] Ian Goodfellow, Yoshua Bengio and Aaron Courville, *Deep learning*. MIT Press, 2016.

[21] Pham Huy Giao and Kushan Sandunil, "Application of deep learning in predicting fracture porosity", *Petrovietnam Journal*, Vol. 10, pp. 14 - 22, 2017.

[22] Tensorflow, "Tensorflow", 2020. [Online]. Available: https://www.tensorflow.org/api_docs/python/tf/keras/Sequential.

[23] Geraldo A.R. Ramos and Lateef Akanji, "Data analysis and Neuro-Fuzzy technique for EOR screening: Application for Angolan oil fields", *Energies*, Vol. 10, No. 7, pp. 10 - 33, 2017. DOI: 10.3390/en10070837.

INTERPRETATION OF INTERWELL CONNECTIVITY TESTS IN A WATERFLOOD SYSTEM

Dinh Viet Anh¹, Djebbar Tiab²

¹Petrovietnam Exploration Production Corporation

²University of Oklahoma

Email: anhdv@pvep.com.vn; dtiab@ou.edu

<https://doi.org/10.47800/PVJ.2021.06-02>

Summary

This study is an extension of a novel technique to determine interwell connectivity in a reservoir based on fluctuations of bottom hole pressure of both injectors and producers in a waterflood system. The technique uses a constrained multivariate linear regression analysis to obtain information about permeability trends, channels, and barriers. Some of the advantages of this new technique are simplified one-step calculation of interwell connectivity coefficients, small number of data points and flexible testing plan. However, the previous study did not provide either in-depth understanding or any relationship between the interwell connectivity coefficients and other reservoir parameters.

This paper presents a mathematical model for bottom hole pressure responses of injectors and producers in a waterflood system. The model is based on available solutions for fully penetrating vertical wells in a closed rectangular reservoir. It is then used to calculate interwell relative permeability, average reservoir pressure change and total reservoir pore volume using data from the interwell connectivity test described in the previous study. Reservoir compartmentalisation can be inferred from the results. Cases where producers as signal wells, injectors as response wells and shut-in wells as response wells are also presented. Summary of results for these cases are provided. Reservoir behaviours and effects of skin factors are also discussed in this study.

Some of the conclusions drawn from this study are: (1) The mathematical model works well with interwell connectivity coefficients to quantify reservoir parameters; (2) The procedure provides in-depth understanding of the multi-well system with water injection in the presence of heterogeneity; (3) Injectors and producers have the same effect in terms of calculating interwell connectivity and thus, their roles can be interchanged. This study provides flexibility and understanding to the method of inferring interwell connectivity from bottom-hole pressure fluctuations. Interwell connectivity tests allow us to quantify accurately various reservoir properties in order to optimise reservoir performance.

Different synthetic reservoir models were analysed including homogeneous, anisotropic reservoirs, reservoirs with high permeability channel, partially sealing fault and sealing fault. The results are presented in details in the paper. A step-by-step procedure, charts, tables, and derivations are included in the paper.

Key words: Interwell connectivity, multi-well testing, waterflood system, well test analysis, reservoir characterisation.

1. Introduction

The previous study carried out by Dinh and Tiab has introduced a new technique to infer interwell connectivity from bottom-hole pressure fluctuations in a waterflood system. The

technique was proven to yield good results based on numerical simulation models of various cases of heterogeneity [1].

In this study, an analytical model for multi-well system with water injection was derived for the technique. The model is based on an available solution for a fully penetrating vertical well in a closed rectangular multi-well system and uses the principle of superposition in space. Based on



Date of receipt: 5/4/2021. Date of review and editing: 5 - 13/4/2021.

Date of approval: 11/6/2021.

This article was presented at SPE Annual Technical Conference and Exhibition and licensed by SPE (License ID: 1109380) to the republish full paper in Petrovietnam Journal.

analytical analysis, a new technique to analyse data of interwell connectivity test was developed. This technique utilises the least squares regression method to calculate the average pressure change. Thus, reservoir pore volume, average reservoir pressure and total average porosity can be estimated from available input data. The results were verified using a commercial black oil numerical simulator.

The practical value of interwell coefficients was investigated. In order to derive the relationship between interwell connectivity coefficients and other reservoir parameters, a pseudo-steady state solution of the previously mentioned model was used. The wells were fully penetrating vertical wells flowing at constant rates. The investigation proves that the interwell coefficients between signal (active) and response (observation) wells are not only associated with the properties between the two wells but also the properties at the signal wells. To calculate Relative interwell permeabilities, we assumed the properties at the signal wells are constant. Thus, by varying permeability between well pairs to match the Relative interwell connectivity coefficient calculated from analytical model and simulation results, the interwell permeabilities can be found. Different cases of heterogeneous synthetic fields were considered including anisotropic reservoir, reservoir with high permeability channel, partially sealing fault and sealing fault. In the sealing fault case, the results indicated 2 groups of average reservoir pressure change corresponding to 2 reservoir compartments. Thus, reservoir compartmentalisation can be detected.

The technique presented in the previous paper requires several constraints including constant production rates and constant total injection rates. These constraints make it difficult to apply the technique in a real field situation where production rates are hardly kept constant. In this study, the systems with constant injection rates and changing production rates were investigated. The obtained interwell connectivity coefficients were almost the same as the results from the case with constant production rates and changing injection rates. The technique is also applicable for fields with only producers; where some producers are used as signal wells and others as response wells provided that all assumptions are valid. This suggests the technique is applicable to depletion fields as well. Also, response wells can act as shut-in wells.

This new study provides a tool to analyse reservoir heterogeneity and to have a better understanding of multi-well systems with the presence of both injectors and producers.

2. Literature review

In 2002, Albertoni and Lake developed a technique calculating the fraction of flow caused by each of the injectors in a producer [2]. This method uses a constrained Multivariate Linear Regression (MLR) model. The model introduced by Albertoni and Lake, however, considers only the effect of injectors on producers, not producers on producers. Albertoni and Lake also introduced the concepts and uses of diffusivity filters to account for the time lag and attenuation occurring between the stimulus (injection) and the response (production) [2]. Yousef et al. introduced the capacitance model in which a nonlinear signal processing model was used [3]. Compared to Albertoni and Lake's model which was a steady-state (purely resistive), the capacitance model included both capacitance (compressibility) and resistivity (transmissibility) effects. The model used flow rate data and could include shut-in periods and bottom hole pressures (if available). However, the technique is somewhat complicated and requires subjective judgement.

Recently, Dinh and Tiab [1] used a similar approach as Albertoni and Lake [2]; however, bottom-hole pressure data were used instead of flow rate data. Some constraints were applied to the flow rates such as constant production rate at every producer and constant total injection rate. Some advantages of using bottom-hole pressure data are: (a) Diffusivity filters are not needed, (b) Only minimal number of data points are required and (c) The programme for collecting data is flexible.

This study is to extend the work by Dinh and Tiab [1] on interwell connectivity calculation from bottom-hole pressure in a multi-well system. The purpose of this paper is to incorporate a pseudo-steady state analytical solution for closed system to the problem. Thus, other reservoir parameters such as relative interwell permeability, and reservoir pore volume can be quantified. This paper also provides in-depth understanding of the method and its applications.

3. Analytical approach

Numerous studies concerning multi-well systems have been carried out. Bourgeois and Couillens [4] provided a technique to predict production from well test analytical solution of multi-well system. Umnuayponwivat et al. investigated the pressure behaviour of individual well in a multi-well closed system [5]. Both vertical well and horizontal well pressure behaviours were considered.

Valko et al. developed a solution for productivity index for multi-well system flowing at constant bottom-hole pressure and under pseudo-steady state condition [6]. Marhaendrajana et al. introduced the solution for well flowing at constant rate in a multi-well system [7, 8]. The solution was used to analyse pressure build-up test and to calculate the average reservoir pressure using decline curve analysis. Lin et al. [9] proposed an analytical solution for pressure behaviours in a multi-well system with both injectors and producers based on the work by Marhaendrajana et al. [7].

3.1. Analytical model application

Considering a multi-well system with producers or injectors and initial pressure p_i , the solution for pressure distribution due to a fully penetrating vertical well in a close rectangular reservoir is as follows [8, 10]:

$$p_D(x_D, y_D, t_{DA}) = \sum_{i=1}^{n_{well}} q_{D,i} a_i(x_D, y_D, x_{wD,i}, y_{wD,i}, x_{eD}, y_{eD}, [t_{DA} - t_{sDA}]) \quad (1)$$

where the dimensionless variables are defined in field units as follows:

$$x_D = \frac{x}{\sqrt{A}} \quad (2)$$

$$y_D = \frac{y}{\sqrt{A}} \quad (3)$$

$$p_D = \frac{kh}{141.2q_{ref}B\mu} (p_{ini} - p(x, y, t)) \quad (4)$$

$$t_{DA} = 0.0002637 \frac{kt}{\varphi c_i \mu A} \quad (5)$$

a_i is the influence function equivalent to the dimensionless pressure for the case of a single well in bounded reservoir produced at a constant rate. Assuming $t_{sDA} = 0$, the influence function is given as:

$$a_i(x_D, y_D, x_{wD,i}, y_{wD,i}, x_{eD}, y_{eD}, t_{DA}) = \frac{1}{2} \sum_{m=-\infty}^{\infty} \sum_{n=-\infty}^{\infty} E_1 \left[\frac{(x_D + x_{wD,i} + 2nx_{eD})^2 + (y_D + y_{wD,i} + 2my_{eD})^2}{4t_{DA}} \right] + E_1 \left[\frac{(x_D - x_{wD,i} + 2nx_{eD})^2 + (y_D + y_{wD,i} + 2my_{eD})^2}{4t_{DA}} \right] + E_1 \left[\frac{(x_D + x_{wD,i} + 2nx_{eD})^2 + (y_D - y_{wD,i} + 2my_{eD})^2}{4t_{DA}} \right] + E_1 \left[\frac{(x_D - x_{wD,i} + 2nx_{eD})^2 + (y_D - y_{wD,i} + 2my_{eD})^2}{4t_{DA}} \right] \quad (6)$$

Equation 1 is valid for pseudo-steady state flow and can be rewritten as below:

$$p_{ini} - p(x, y) = \frac{141.2B\mu}{kh} \sum_{i=1}^{n_{well}} a_n[x_D, y_D, x_{wDn}, y_{wDn}, x_{eD}, y_{eD}, t_{AD}] q_n \quad (7)$$

Equation 7 is the pressure response at point (x_D, y_D) due to a well n at (x_{wDn}, y_{wDn}) in a homogeneous closed rectangular reservoir. The influence function (a_n) can be different for different wellbore conditions as well as flow regimes (horizontal well, partial penetrating vertical well, fractured vertical well, etc.). This study only considered the case of fully penetrating vertical well in a closed rectangular reservoir under pseudo-steady state condition.

Equation 7 is applicable to a field where all the wells are either producing or injecting. Lin and Yang [9] have extended the model to a field with both injectors and producers based on the model suggested by Equation 7 as shown below:

$$p_{ini} - p(x, y) = \frac{141.2B\mu}{kh} \left\{ \sum_{j=1}^{n_{pr}} a_j[x_D, y_D, x_{wDj}, y_{wDj}, x_{eD}, y_{eD}, t_{AD}] q_j - \sum_{i=1}^{n_{inj}} a_i[x_D, y_D, x_{wDi}, y_{wDi}, x_{eD}, y_{eD}, t_{AD}] q_i \right\} \quad (8)$$

where i and j denote injectors and producers, respectively. Equation 8 is for a homogeneous reservoir with initial reservoir pressure (p_{ini}) equal everywhere. Applying Equation 8 to each time interval of an interwell connectivity test, since the total injection and production are kept constant, the average reservoir pressure change is assumed to be constant for every time interval. The first term in the bracket on the right-hand side of Equation 8 is constant due to constant rates at every producer throughout the test. Applying to each time interval in the interwell connectivity test, assuming the initial pressure at the beginning of each interval increases at the same rate as the average reservoir pressure (Δp_{ave}), Equation 8 can be rewritten as:

$$p_{ave} - p(x, y) = \frac{141.2B\mu}{kh} \left\{ - \sum_{i=1}^{n_{inj}} a_i[x_D, y_D, x_{wDi}, y_{wDi}, x_{eD}, y_{eD}, t_{AD}] q_i \right\} + \Delta p_{pr} \quad (9)$$

where

$$\Delta p_{pr} = \frac{141.2B\mu}{kh} \sum_{j=1}^{n_{pr}} a_j[x_D, y_D, x_{wDj}, y_{wDj}, x_{eD}, y_{eD}, t_{AD}] q_j + \Delta p_{ave} \quad (10)$$

$$p_{ave} = p_{ini} - \Delta p_{ave}$$

Both Δp_{pr} and Δp_{ave} are assumed to be constant. Applying Equation 9 for a point at the circumference of the well bore of producer j' and taking into account the skin factor, we obtain:

$$p_{ave} - p_{wf,j'}(x_{wDj'}, y_{wDj'}) = \frac{141.2B\mu}{kh} \left\{ - \sum_{i=1}^{n_{inj}} a_{ij'} [x_{wDj'}, y_{wDj'} + r_{wDj'}, x_{wDi'}, y_{wDi'}, y_{eD}] q_i + s_j q_{j'} \right\} + \Delta p_{pr} \quad (11)$$

where the third term in the bracket accounts for the skin at well j' . For injector i' , we have:

$$p_{ave} - p_{wf,i'}(x_{wDi'}, y_{wDi'}) = \frac{141.2B\mu}{kh} \left\{ - \sum_{i=1}^{n_{inj}} a_{ii'} [x_{wDi'}, y_{wDi'} + r_{wDj'}, x_{wDi'}, y_{wDi'}, y_{eD}] q_i + s_i q_{i'} \right\} + \Delta p_{pr} \quad (12)$$

To simplify the problem, we assume all skin factors are equal to zeros. Equations 11 & 12 can be rewritten for each time interval as:

$$p_{ave} - p_{wf,j'} = - \frac{141.2B\mu}{kh} \left(\sum_{i=1}^I q_{ij'} a_{ij'} \right) + \Delta p_{pr} \text{ for } j' = 1..J \quad (13)$$

$$p_{ave} - p_{wf,i'} = - \frac{141.2B\mu}{kh} \left(\sum_{i=1}^I q_{ii'} a_{ii'} \right) + \Delta p_{pr} \text{ for } i' = 1..I \quad (14)$$

where $q_{ij'} = q_{i'} = q_i$ are the flow rates at injectors (signal wells).

3.2. Interpretation of interwell connectivity coefficients using bottom-hole pressure data

Now, let us consider the interwell connectivity test. In order to obtain better results, the reservoir should reach pseudo-steady state before the test begins. Different testing schemes were also considered including (a) injectors as response wells, (b) producers as both response and signal wells and (c) shut-in wells as response wells. The response wells need to be directly affected by the signal wells. The case where total injection equals to total production is not considered for the test due to the reason stated in the previous publication [1].

In the previous study, Dinh and Tiab [1] defined the interwell connectivity coefficients using the bottom-hole pressure data that satisfy the equation:

$$\hat{p}_j(\Delta t) = \beta_{0j} + \sum_{i=1}^I \beta_{ij} p_i(\Delta t) \text{ for } j = 1..J \quad (15)$$

where $\hat{p}_j(\Delta t)$ is the bottom-hole flowing pressure at producer j , β_{0j} is a constant and β_{ij} is the weighting coefficient accounting for the effect of bottom-hole

pressure at injector i (p_i) on producer j . Δt is the length of the time interval as the injection rates were changed after each time interval. Including the average reservoir pressure, p_{ave} to Equation 15, we have:

$$p_{ave} - p_{wf,j'}(\Delta t) = \beta_{0j'} + p_{ave} - \sum_{i=1}^I \beta_{ij'} p_{wf,i} \quad (16)$$

One of the properties of Equation 15 is:

$$\sum_{i=1}^I \beta_{ij'} = 1 \quad (17)$$

Thus Equation 16 becomes:

$$p_{ave} - p_{wf,j'} = \beta_{0j'} + \sum_{i=1}^I \beta_{ij'} (p_{ave} - p_{wf,i}) \quad (18)$$

Marhaendrajana et al. introduced the concept of interference effect as a regional pressure decline to analyse pressure build-up data at a production well [8]. Lin and Yang extended the work to a field with both injectors and producers [9]. Their solutions basically state that the pressure response of a well (injector or producer) in a multiwell system is affected by the flow rate at the well plus an interference effect due to other wells in the field flowing under the pseudo-steady state. The solution for a producer (j') can be written as:

$$p_{ini} - p_{wf,j'}(x_{wDj'}, y_{wDj'}, t) = \frac{141.2B\mu}{kh} [q_{j'}(a_{j'j'} - 2\pi t_{DA}) + 2\pi \Delta q_{tot} t_{DA}] \quad (19)$$

For injector i' , we have

$$p_{ini} - p_{wf,i'}(x_{wDi'}, y_{wDi'}, t) = \frac{141.2B\mu}{kh} [q_{i'}(a_{i'i'} + 2\pi t_{DA}) + 2\pi \Delta q_{tot} t_{DA}] \quad (20)$$

where $\Delta q_{tot} = \sum_{j=1}^{n_{pr}} q_j - \sum_{i=1}^{n_{inj}} q_i$. Equations 19 and 20 state that the pressure change at a producer or injector is a combination of two terms as shown on the right-hand sides of the two equations. The first term is proportional to the flow rate of the well itself and the second term accounts for the regional effect of other wells. In our case, the second term in the brackets is constant for each time interval. Using the material balance, we have:

$$\frac{\Delta p_{ave}}{\Delta t} = \frac{0.23394B}{c_t V_p} \Delta q_{tot} \quad (21)$$

where the constant 0.23394 is the conversion factor for field units and V_p is the reservoir pore volume in reservoir barrels. Applying the definition of t_{DA} (Equation 5) and Equation 21 to the second term in the right-hand side bracket, Equation 20 becomes:

$$p_{ini} - p_{wf,i}(x_{wDi}, y_{wDi}, t) = \frac{141.2B\mu}{kh} [q_i(a_{i'} + 2\pi t_{DA})] + \Delta p_{ave}(t) \quad (22)$$

Moving Δp_{ave} to the left-hand side, Equation 22 can be rewritten for each time interval of the interwell connectivity test as:

$$p_{ave}(t) - p_{wf,i}(x_{wDi}, y_{wDi}, t) = \frac{141.2B\mu}{kh} [q_i(a_{i'} + 2\pi t_{DA})] \quad (23)$$

$$or \ q_i = \frac{p_{ave}(t) - p_{wf,i}(x_{wDi}, y_{wDi}, t)}{\frac{141.2B\mu}{kh} [(a_{i'} + 2\pi t_{DA})]} \quad (24)$$

Substitute q_i defined in Equation 24 into Equation 13, we have:

$$p_{ave} - p_{wf,j'} = \sum_{i=1}^I [p_{ave} - p_{wf,i}(x_{wDi}, y_{wDi})] \frac{a_{ij'}}{(a_{ii} + 2\pi t_{DA})} + \Delta p_{pr} \quad (25)$$

Equation 25 can only be applied to the pseudo-steady state flow and equivalent to Equation 18 if the following condition satisfied:

$$\sum_{i=1}^I \beta_{ij'} = \sum_{i=1}^I \frac{a_{ij'}}{(a_{ii} + 2\pi t_{DA})} = 1 \quad (26)$$

Notice that Equation 25 does not depend on production history and holds true for any time interval assuming the pseudo-steady state flow. The sum $\sum_{i=1}^I \frac{a_{ij'}}{(a_{ii} + 2\pi t_{DA})}$ can be set to 1 by adjusting the time duration (Δt). The equivalent time duration (Δt_{eq}) obtained indicates the time of the pseudo-steady state required so that Equation 26 is satisfied at the response well. Thus, Equation 25 can be written as:

$$p_{ave} - p_{wf,j'} = \sum_{i=1}^I [p_{ave} - p_{wf,i}(x_{wDi}, y_{wDi})] \frac{a_{ij'}}{(a_{ii} + 2\pi t_{DA})} + \Delta p_{pr}(\Delta t_{eq}) \quad (27)$$

where $\sum_{i=1}^I \frac{a_{ij'}}{(a_{ii} + 2\pi t_{DA})} = 1$ and $\Delta p_{pr}(\Delta t_{eq})$ is the pressure change defined by Equation 10 corresponding to Δt_{eq} . $\Delta p_{pr}(\Delta t_{eq})$ depends on the pseudo-steady state initial pressure, the total field flow rate and the influence of producers, but not on the actual time interval. Thus, with the same total field flow rate (Δq_{tot}), assuming the pseudo-steady state has been reached, $\Delta p_{pr}(\Delta t_{eq})$ is constant with any test time interval (Δt). Equation 27 is true for any p_{ave} . Since Equations 27 and 18 are now equivalent, we should have:

$$\beta_{ij'} = \frac{a_{ij'}}{(a_{ii} + 2\pi t_{DA})} \text{ with } i = 1 \dots I \text{ and } j' = 1 \dots J \quad (28)$$

$$\beta_{0j'} = \Delta p_{pr}(\Delta t_{eq}) \quad (29)$$

Equation 28 indicates that the interwell connectivity coefficient β_{ij} reflects the effect of both the flow rates at the signal wells and the influence of other wells on the signal wells. Since $\sum_{i=1}^I \frac{a_{ij'}}{(a_{ii} + 2\pi t_{DA})} = 1$, p_{ave} on both sides is cancelled out and Equation 27 can also be written as:

$$p_{wf,j'} = \sum_{i=1}^I p_{wf,i}(x_{wDi}, y_{wDi}) \frac{a_{ij'}}{(a_{ii} + 2\pi t_{DA})} + \Delta p_{pr}(\Delta t_{eq}) \quad (30)$$

Even though $\sum_{i=1}^I \beta_{ij'}$ and $\sum_{i=1}^I \frac{a_{ij'}}{(a_{ii} + 2\pi t_{DA})}$ are both equal to 1, the meanings are different for each case. $\sum_{i=1}^I \beta_{ij'} = 1$ indicates the pressure fluctuation at the response wells due to signal wells only while $\sum_{i=1}^I \frac{a_{ij'}}{(a_{ii} + 2\pi t_{DA})} = 1$ indicates a state of pressure distribution due to pseudo-steady state flow after the period Δt_{eq} .

Since the interwell connectivity coefficients were calculated without the knowledge of pressure history during each time interval, it is reasonable to apply the pseudo-steady state equation (Equation 25) with the flow duration of Δt_{eq} to each pressure data. Thus, the original test system is now set to an equivalent pseudo-steady state system with the time interval of Δt_{eq} . The model works with the assumption that the bottom-hole pressures at the response wells reach pseudo-steady state before the rates at the signal wells are changed.

3.3. Model verification

In order to verify the analytical model, 2 homogeneous synthetic fields were used. One field has 5 injectors and 4 producers (the 5x4 synthetic field) and the other has 25 injectors and 16 producers (the 25x16 synthetic field). The used reservoir simulator was ECLIPSE 100 Black Oil Simulator. Figures 1 and 2 show the grid systems for the 2 models and the well locations with I and J indicating injector and producer respectively. The grid configuration for the 5x4 synthetic field was 73x73x5 and for the 25x16 synthetic field was 59x59x5. The dimensions for the 5x4 synthetic field were 3100 ft x 3100 ft x 60 ft and for the 25x16 synthetic field were 5900 ft x 5900 ft x 60 ft. The initial static reservoir pressure was 650 psia. Other reservoir properties for the homogeneous case are shown in Table 1. One-phase flow of water was assumed. The 5x4 synthetic field was run for 50 months representing 50 data points (time

Table 1. Input data for homogeneous simulation models

Horizontal permeability	$k_h = 100 \text{ mD}$	Water compressibility	$c_w = 1\text{E-}6 \text{ psi}^{-1}$
Vertical permeability	$k_v = 10 \text{ mD}$	Oil compressibility	$c_o = 5\text{E-}6 \text{ psi}^{-1}$
Porosity	$\varphi = 0.3$	Rock compressibility	$c_r = 1\text{E-}6 \text{ psi}^{-1}$
Viscosity	$\mu = 2 \text{ cp}$	Total compressibility	$c_t = 2.8\text{E-}6 \text{ psi}^{-1}$
Initial reservoir pressure	$p_i = 650 \text{ psi}$	Formation volume factor	$B = 1.03 \text{ bbl/STB}$
Water saturation	$S_w = 0.8$	Wellbore radius	$r_w = 0.355 \text{ ft}$

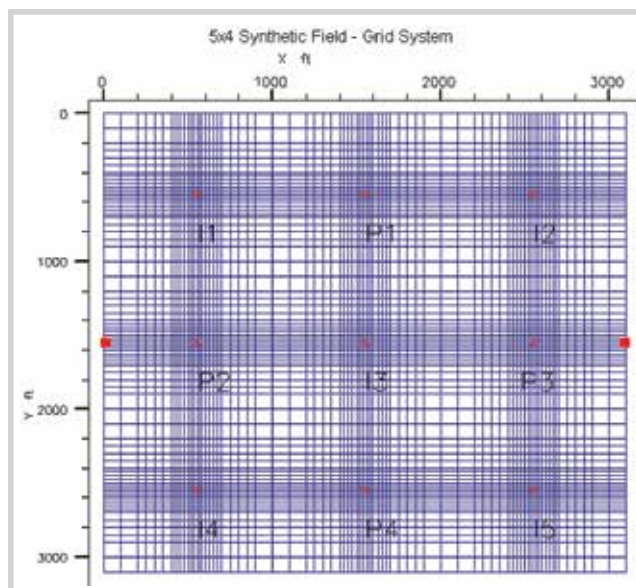


Figure 1. Grid system for the 5x4 synthetic field (73x73x5).

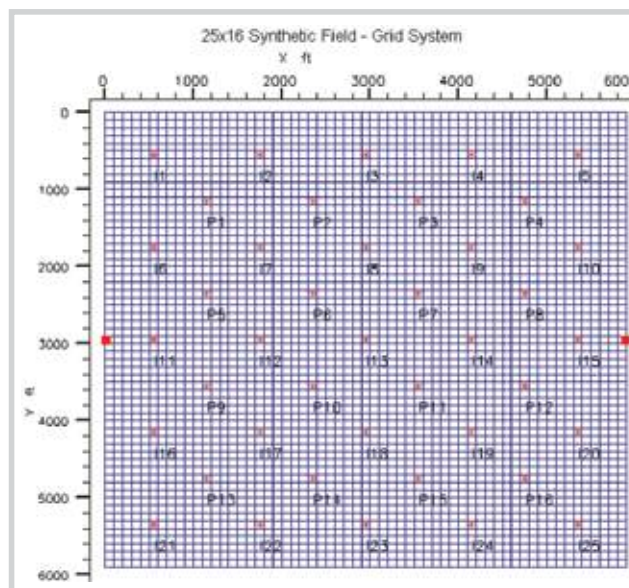


Figure 2. Grid system for the 25x16 synthetic field (59x59x5).

Table 2. Interwell connectivity coefficient results from MLR for the 5x4 synthetic field

	P1	P2	P3	P4	Sum
β_{0j} (psia)	-740.6	-740.3	-741.3	-741.0	-2963
I1	0.25	0.26	0.13	0.14	0.78
I2	0.25	0.14	0.26	0.14	0.78
I3	0.22	0.21	0.22	0.22	0.87
I4	0.14	0.25	0.14	0.25	0.78
I5	0.14	0.14	0.25	0.25	0.78
Sum	1.00	1.00	1.00	1.00	

Table 3. Interwell connectivity coefficient results from analytical solution with $\Delta t_{eq} = 12.63$ days for the 5x4 synthetic field

	P1	P2	P3	P4	Sum
I1	0.24	0.24	0.15	0.15	0.77
I2	0.24	0.15	0.24	0.15	0.77
I3	0.23	0.23	0.23	0.23	0.91
I4	0.15	0.24	0.15	0.24	0.77
I5	0.15	0.15	0.24	0.24	0.77
Sum	1.00	1.00	1.00	1.00	

interval, $\Delta t = 30$ days), while the 25x16 synthetic field was run for 130 months. However, only data after the 2nd month were used to better satisfy the condition of over all pseudo-steady states.

5x4 Synthetic field

Both Equations 27 and 30 were used to verify the analytical model. The bottom-hole pressure calculated from Equations 15 and 30 were compared. The coefficients

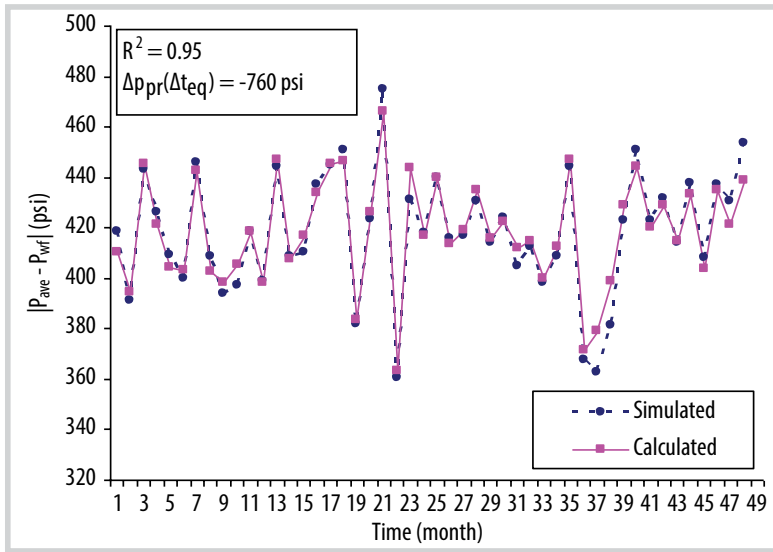


Figure 3. Absolute values of $(p_{ave} - p_{wrf})$ from Equation 28 and from simulation results for well P-1, the 5×4 homogeneous field.

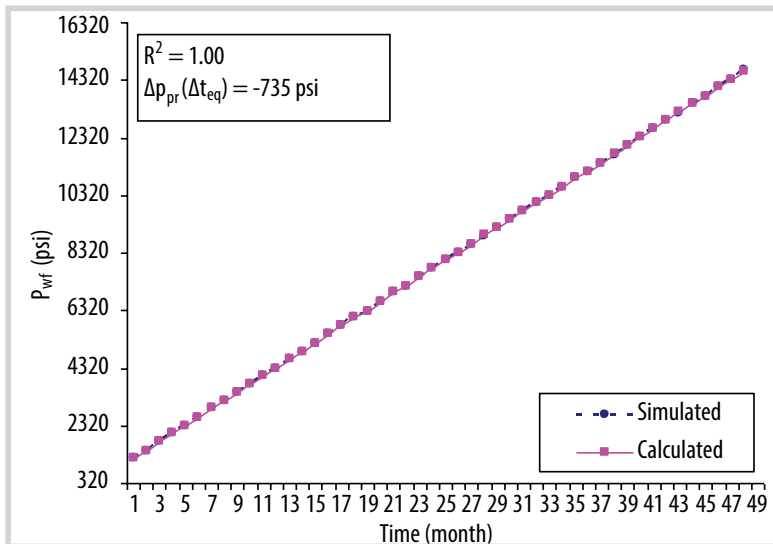


Figure 4. p_{wrf} results from Equation 30 and from simulation for well P-1, the 5×4 homogeneous field.

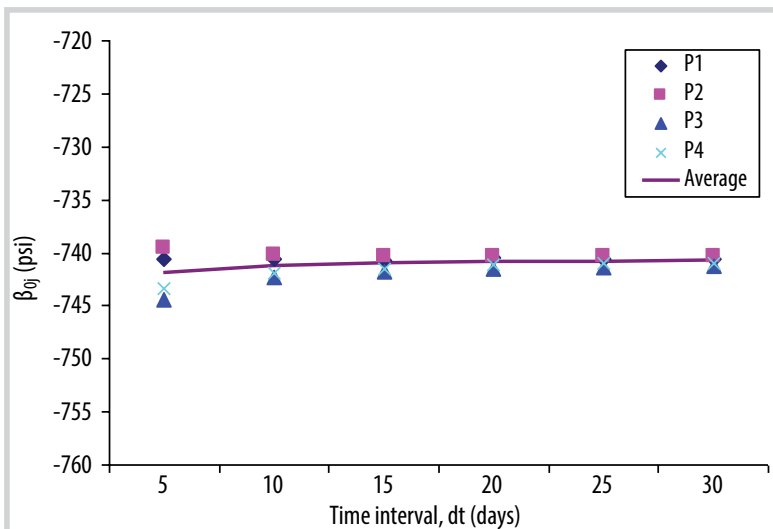


Figure 5. Plot of the term $\beta_{0j} = \Delta p_{pr}(\Delta t_{eq})$ versus different time interval (Δt) , the 5×4 homogeneous field.

calculated from the influence function were also compared to those obtained from simulation data. Investigation on the effect of different t_{eq} on the interwell connectivity coefficients was also carried out.

Tables 2 and 3 show the interwell connectivity coefficients obtained from simulation data using MLR technique [1] and calculated from analytical solution with equivalent time $\Delta t_{eq} = 12.63$ days. The coefficients for each well pair from both tables are close with the difference less than 10%.

Figures 3 and 4 show the results obtained from Equations 27 and 30 with the simulation results, respectively. The average pressures for analytical solution (Equation 27) were calculated using material balance equation (Equation 21). The constant term $\Delta p_{pr}(\Delta t_{eq})$ was calculated using trial-and-error method by matching 2 representative equivalent points on both graphs. The coefficient of determination (R^2) does not depend on this constant term. Good match is observed on Figure 3 with $R^2 = 0.95$. The error could be because the average reservoir pressure is not exactly constant due to the change in total compressibility. However, excellent match is observed in Figure 4. The constant terms $\Delta p_{pr}(\Delta t_{eq})$ for both cases are close to β_{0j} calculated from simulation data using MLR technique (Table 2).

Similar results were obtained for other producers. Thus, the analytical approach works well for the 5×4 homogeneous reservoir. Figure 5 shows a plot of the constant β_{0j} calculated from simulation results versus different length of the test time interval (Δt) . β_{0j} for different Δt are almost the same with less than 1% difference. Hence, the results agree with the analytical model that the term $\Delta p_{pr}(\Delta t_{eq}) = \beta_{0j}$ does not depend on the test time interval.

25×16 Synthetic field

Similar procedure was used to verify the application of an analytical model to

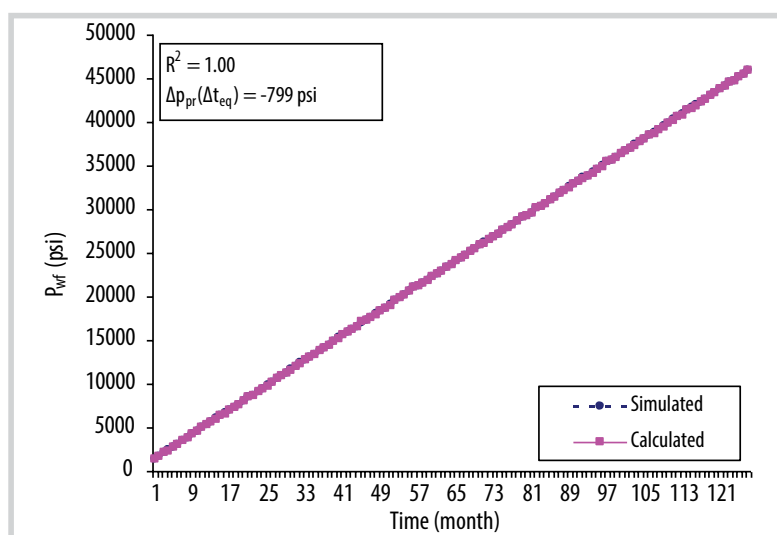


Figure 6. p_{wf} results from Equation 30 and from simulation for well P-1, the 25×16 homogeneous synthetic field ($\Delta t_{eq} = 5.87$ days).

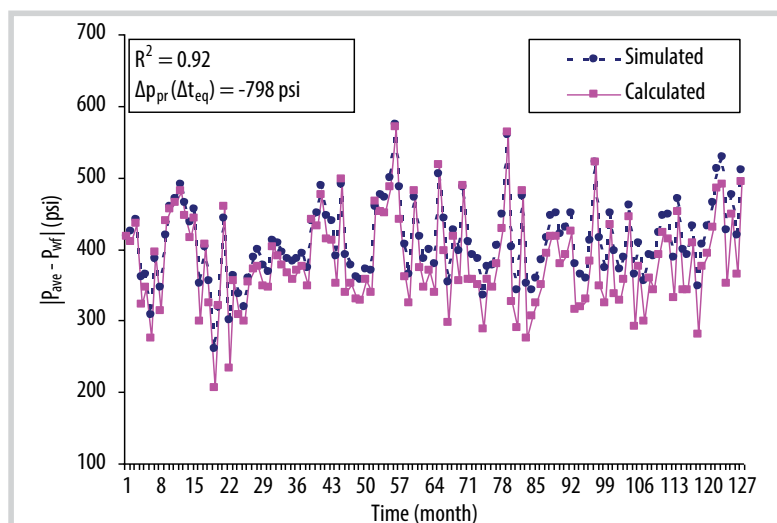


Figure 7. Absolute values of $(p_{ave} - p_{wf})$ calculated and simulated with p_{ave} taken from simulation results for well P-1, the 25×16 homogeneous synthetic field ($\Delta t_{eq} = 5.87$ days).

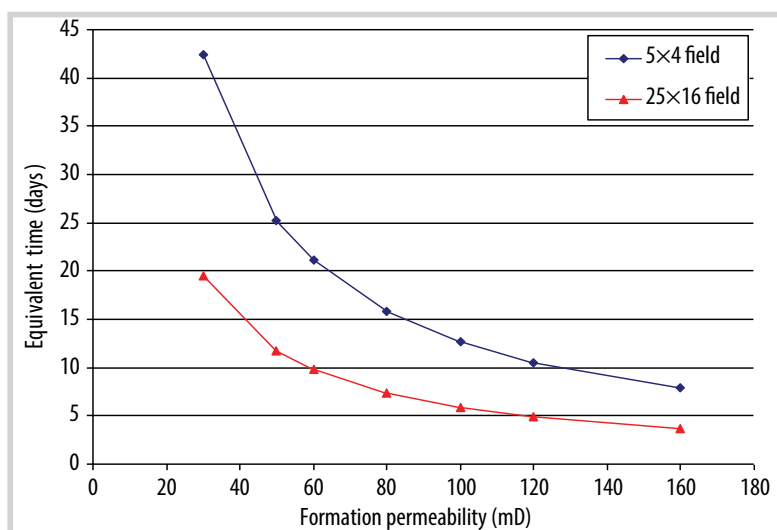


Figure 8. Equivalent time (Δt_{eq}) as a function of permeability, the homogeneous 5×4 and 25×16 synthetic fields.

the 25×16 synthetic field. The equivalent time was found to be 5.87 days ($\Delta t_{eq} = 5.87$ days). Again, Figure 6 shows the results obtained from Equation 30 for Well P1. Again, a perfect match was obtained for bottom-hole pressures calculated using Equation 30 and from simulation results. However, the pressure difference plots display a good match only at early time. The poor match at late time resulted in a low value of R^2 (0.42). At a later time, as more water was pumped in, the change of water saturation became more significant. Since water and oil compressibility were different, the change in water saturation would lead to a change in total compressibility. Thus, the constant average reservoir pressure change assumption was violated. P_{ave} used in Equation 27, which was calculated from material balance, was no longer accurate with changing total compressibility. When the actual average field pressure from simulation results was used for Equation 27, we obtained a much better match as shown in Figure 7 ($R^2 = 0.92$). Since excellent match was again obtained for bottom-hole pressure results even at late time (Figure 6), it was confirmed that once the well reaches pseudo-steady state, the bottom-hole pressure is independent from production history [6].

Different values of permeability were applied to the same reservoirs (the 5×4 and 25×16 synthetic fields) to investigate the behaviour of the equivalent time (Δt_{eq}). Plots of permeability of both the 5×4 and 25×16 synthetic fields vs. the equivalent time are shown on Figure 8. It is clear that as the permeability increases, Δt_{eq} decreases. The fact that Δt_{eq} of the 25×16 field was higher than that of the 5×4 field indicated that with the designed flow rates, the 25×16 field reached the pseudo-steady state quicker than the 5×4 field.

4. Calculation techniques for interwell connectivity tests

4.1. Least squares linear regression (LSLR) and multivariate linear regression (MLR) techniques

Albertoni and Lake [2] introduced the Multivariate Linear Regression (MLR) technique to solve a system of linear equations for interwell connectivity coefficients using flow rate data. Dinh and Tiab [1] used the same technique to calculate interwell connectivity coefficients from bottom-hole pressure data. Least squares linear regression is another technique to solve a system of linear equations by least square fitting [11, 12]. According to Yousef et al., MLR technique is equivalent to least squares linear Regression (LSLR) [13]. Thus, using either MLR or LSLR is an option based on convenience. In this study, both MLR and LSLR were used. More details about LSLR technique are provided below.

4.2. Calculation approaches

Consider a system of J producers and I injectors where injectors are signal wells and producers are response wells. All wells are fully penetrating vertical wells. The reservoir is assumed to be homogeneous with constant rock properties. The fluid saturations are assumed to be constant. Single phase flow of a slightly compressible fluid of constant viscosity is also assumed. In an interwell connectivity test as described by Dinh and Tiab [1], the injection rates were changed after a constant time interval (Δt) while the production rates were kept constant and equal throughout the test. The total injection and production rates were also kept constant. The reservoir was assumed to have reached the pseudo-steady state at the end of each time interval.

Equations 18 and 19 were used as models for the interwell connectivity test. Thus, the equations were applied to each time interval during the test. Since the total field-wise flow rate and the time interval are constant, the average reservoir pressure change is constant for every time interval. Let the superscript I be the order of the data points used for the test, we obtain a system of equations for L data points for producer j' as follows:

$$\begin{cases} \frac{141.2B\mu}{kh} \left(\sum_{i=1}^I q_{ij'}^{(1)} a_{ij'} \right) + \Delta p_{pr} = p_{ave}^{(1)} - p_{wf,j'}^{(1)}, \\ \frac{141.2B\mu}{kh} \left(\sum_{i=1}^I q_{ij'}^{(2)} a_{ij'} \right) + \Delta p_{pr} = p_{ave}^{(2)} - p_{wf,j'}^{(2)}, \\ \vdots \\ \frac{141.2B\mu}{kh} \left(\sum_{i=1}^I q_{ij'}^{(L)} a_{ij'} \right) + \Delta p_{pr} = p_{ave}^{(L)} - p_{wf,j'}^{(L)}, \end{cases} \quad (31)$$

Average pressure change calculation

Now, assuming constant B, μ , c_t and Δp_{ave} , we can subtract the previous equation in the system of Equation 31 from the next equation taking into account that Δp_{pr} stays constant. Thus, we have:

$$\begin{cases} \sum_{i=1}^I (q_{ij'}^{(2)} - q_{ij'}^{(1)}) M_{ij'} - \Delta p_{ave} = -(p_{wf,j'}^{(2)} - p_{wf,j'}^{(1)}) \\ \sum_{i=1}^I (q_{ij'}^{(3)} - q_{ij'}^{(2)}) M_{ij'} - \Delta p_{ave} = -(p_{wf,j'}^{(3)} - p_{wf,j'}^{(2)}) \\ \vdots \\ \sum_{i=1}^I (q_{ij'}^{(L)} - q_{ij'}^{(L-1)}) M_{ij'} - \Delta p_{ave} = -(p_{wf,j'}^{(L)} - p_{wf,j'}^{(L-1)}) \end{cases} \quad (32)$$

where $M_{ij'}$ are coefficients account for the state of the well regardless of production history. Since the total injection rate was kept constant, when one equation was subtracted from the other, the sum of the rate differences was equal to zero. The sum of the resulting coefficients ($M_{ij'}$) was also equal to zeros indicating that if the flow rates are kept constant and equal, the change of bottom-hole pressure is equal to the change of the average pressure. However, since $M_{ij'}$ were calculated without the information of production rates, they do not reflect the actual state and are not used in the analysis.

Equation 32 can be solved using either LSLR or MLR technique. In this study, LSLR was used to calculate Δp_{ave} . Δp_{ave} is positive when the average pressure increases and negative when it decreases. Assuming constant total compressibility and porosity, the reservoir pore volume (V_p) can be estimated using Equation 21. Knowing the initial static pressure, the average pressure after each time interval can be estimated by adding the total pressure change (Δp_{ave}). With the known total reservoir volume (V_b), the total porosity can also be calculated:

$$\phi_{tot} = \frac{V_p}{V_b} \quad (33)$$

Least squares linear regression (LSLR)

Considering the following model representing each data point:

$$Y = A_0 + C_1 A_1 + C_2 A_2 + \dots + C_l A_l + \epsilon \quad (34)$$

where the response is Y. The regression model parameters are A_0 and A_l , the explanatory variables are C_l and ϵ is random error [11, 12]. With (L-1) data sets, (L+1) estimated model parameters, we have the following equation:

$$\begin{bmatrix} Y_1 \\ Y_2 \\ \vdots \\ Y_{L-1} \end{bmatrix} = \begin{bmatrix} 1 & C_1^{(1)} & C_2^{(1)} & \vdots & \vdots & C_l^{(1)} \\ 1 & C_1^{(2)} & C_2^{(2)} & \vdots & \vdots & C_l^{(2)} \\ \vdots & \vdots & \vdots & \vdots & \vdots & \vdots \\ 1 & C_1^{(L-1)} & C_2^{(L-1)} & \vdots & \vdots & C_l^{(L-1)} \end{bmatrix} \times \begin{bmatrix} A_0 \\ A_1 \\ \vdots \\ A_l \end{bmatrix} \quad (35)$$

The short form of Equation 35 is:

$$Y = C \times A \quad (36)$$

By minimising the sum of the squared differences between the observed responses and the predicted responses for each set of $C_i^{(l)}$, the least squares estimation of the parameter vector A is (11, 12):

$$A = [C^T C]^{-1} C^T Y \quad (37)$$

where C^T is the transpose of C . For example, to solve Equation 32 for well j' , we consider $A_0 = -\Delta p_{ave}$, $A_i = M_{ij'}$, $C_i^{(l)} = (q_{ij'}^{(l+1)} - q_{ij'}^{(l)})$, and $Y_l = -(p_{wf, j'}^{(l+1)} - p_{wf, j'}^{(l)})$.

Relative interwell permeability calculation from interwell connectivity coefficients using bottom hole pressures

A direct relationship between interwell connectivity coefficients and the influence functions (a_{ij}) is presented in Equation 28, in which a_{ij} represents the connectivity between the 2 wells i and j' and the term $(a_{ii} + 2\pi t_{DA})$ is associated with the injector i . Thus, the permeability value in a_{ij} reflects the permeability between wells i and j' relative to the permeability given to the injector i in the term $(a_{ii} + 2\pi t_{DA})$. If permeability values given for every injector are equal, then the permeabilities in a_{ij} are relative to one another among injector - producer pairs and the permeability at the injectors. The equivalent time Δt_{eq} was calculated using trial-and-error technique with an assigned homogeneous permeability system to the injectors so that $\sum_{i=1}^l \frac{a_{ij'}}{(a_{ii} + 2\pi t_{DA})} = 1$. Thus, by varying permeability between each well pair so that $\frac{a_{ij'}}{(a_{ii} + 2\pi t_{DA})} = \beta_{ij'}$, the relative permeability among wells can be estimated.

The reference reservoir is homogeneous with permeability equal to the one given to the signal wells (injectors). We call the permeability assumed for the signal wells reference permeability (k_{ref}) and the permeability accounting for the flow property between signal and response relative wells interwell permeability (k_{ir}). The matching process can be carried out using trial-and-error method by varying relative interwell permeabilities until the total difference between interwell connectivity

coefficients from analytical model and simulation results for each response well equal zero. Different from the interwell connectivity coefficients, the relative interwell permeabilities do not depend on the distance between wells and the position of the wells.

4.3. Calculation procedures

Step 1: Obtain both flow rate and pressure data from the interwell connectivity test. The number of data points should be more than $l+1$ to get good results [1]. The time interval should be long enough for every well to reach the pseudo-steady state. However, if the reservoir is already in the pseudo-steady state, the time required for each well to reach the pseudo-steady state after each rate change will be much shorter than the time required for the reservoir to reach the pseudo-steady state from a static initial pressure [5]. The interwell connectivity coefficients can then be calculated using MLR method as described by Dinh and Tiab [1].

Step 2: Calculate the average reservoir pressure change corresponding to each producer, Δp_{ave} using Equation 32. Δp_{ave} for every producer should be close if all producers are connected to the same reservoir pore volume. The bulk volume (V_b) of the reservoir can also be calculated knowing the reservoir geometry. The pore volume and the total average porosity can then be calculated using Equations 21 and 33.

Step 3: Define a homogeneous pseudo-steady state reference reservoir by assuming a reference permeability (k_{ref}). The k_{ref} should be representative of the entire reservoir. Further details about the characteristics of k_{ref} will be discussed later. The equivalent time interval (Δt_{eq}) corresponding to the reference reservoir can be calculated using trial-and-error method as described before.

Step 4: Using k_{ref} and Δt_{eq} from Step 3, match the interwell connectivity coefficients from analytical equation (Equation 28) with those calculated from the bottom hole pressure data. The denominator in Equation 28, $(a_{ii} + 2\pi t_{DA})$, is associated with the injector i and is calculated using k_{ref} . The nominator is calculated using the relative interwell permeability (k_{ir}). Thus, k_{ir} is varied to obtain the match while k_{ref} is kept constant. The match is obtained when the percent error between interwell connectivity coefficients calculated from the analytical equation and simulation is 0%. The results include a value of k_{ir} for each injector - producer pair. These k_{ir} are relative interwell permeability corresponding to the assumed reference permeability.

Table 4. Relative interwell permeability results for the 5×4 homogeneous synthetic field ($k_{ref} = 100$ mD, $\Delta t_{eq} = 12.63$ days)

	P1	P2	P3	P4	Ave.
I1	105	109	93	98	101
I2	104	95	108	98	101
I3	95	94	97	95	95
I4	99	106	97	104	101
I5	97	97	105	106	101
Ave.	100	100	100	100	100

Table 5. Relative interwell permeability results from the pseudo-steady state equation for the 5×4 anisotropic synthetic field ($k_{ref} = 316$ mD, $\Delta t_{eq} = 4.0$ days)

	P1	P2	P3	P4	Ave.
I1	494	203	324	188	302
I2	490	326	204	191	303
I3	220	505	506	220	363
I4	197	201	323	486	302
I5	182	327	205	498	303
Ave.	317	313	312	317	317

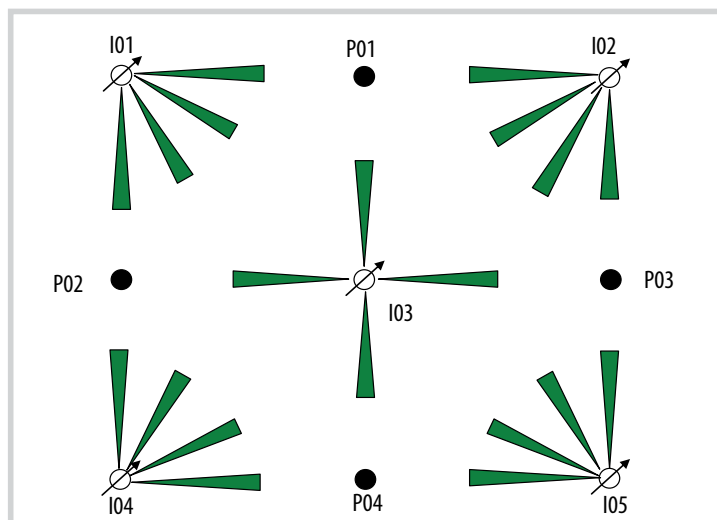


Figure 9. Representation of relative interwell permeability for the case of the 5×4 homogeneous reservoir.

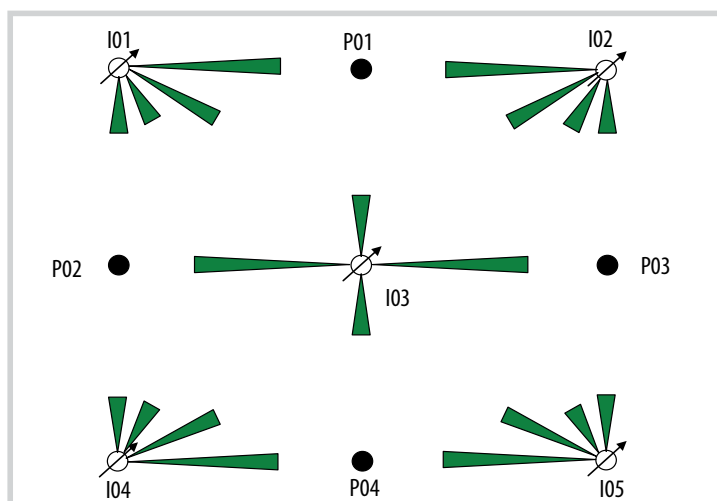


Figure 10. Representation of relative interwell permeability for the case of the 5×4 anisotropic reservoir.

Step 5: The obtained results are used to analyse the reservoir properties including high permeability channel, permeability barrier and reservoir compartmentalisation. More details are discussed in the next section.

5. Simulation results

The calculation approaches presented in the last section were applied to data from 2 synthetic fields, one with 5 injectors and 4 producers (the 5×4 synthetic field) and the other with 25 injectors and 16 producers (the 25×16 synthetic field). These synthetic fields are already described in the previous sections. Both homogeneous reservoirs and reservoirs with heterogeneity were considered.

5x4 Synthetic field

Consider a waterflood system of 5 injectors and 4 producers as shown in Figure 1, where production and injection rates were kept constant during constant time intervals. Injection rates were changed after each time interval but production rates and total injection rate stayed constant ($q_{tot} = \text{constant}$) as described by Dinh and Tiab [1]. The system was assumed to be in the pseudo-steady state so Equations 18 and 19 apply.

Homogeneous reservoir

The interwell connectivity coefficients calculated from simulation data and analytical

Table 6. Relative interwell permeability results from pseudo-steady state equation for the 5×4 synthetic field/reservoir with high permeability channel ($k_{ref} = 300$ mD, $\Delta t_{eq} = 4.21$ days)

	P1	P2	P3	P4	Ave.
I1	873	924	749	888	859
I2	156	161	219	182	179
I3	136	158	166	192	163
I4	173	97	199	125	148
I5	181	187	189	144	175
Ave.	304	305	304	306	

model were presented in the previous section. LSLR technique was used to calculate the average pressure change as described before. ΔP_{ave} is in perfect match with the results obtained from material balance and the resulting porosity was 0.301. By keeping the permeabilities associated with injectors constant at 100 mD, the interwell coefficient in Table 3 can be matched with those in Table 2 by adjusting the permeability between injector/producer pairs or the influence function a_{ij} . The resulting relative interwell permeabilities are shown in Table 4. Figure 9 shows the representation of the permeabilities in Table 4 in the form of inverse arrows. The lengths of the arrows are proportional to the permeability between injectors and producers. The relative interwell permeabilities are very close to each other and to the input formation permeability.

Anisotropic reservoir

In this case, the permeability in x direction (1,000 mD) is 10-fold the permeability in y direction (100 mD). The results for relative interwell permeability are shown in Table 5. The permeability at the injectors was set to the geometric average of the maximum and minimum permeability which equals 316 mD. The equivalent time (Δt_{eq}) was found to be 4.00 days.

Figure 10 shows the representation of the relative interwell relative permeabilities. The results agree with the actual permeability of the field with high permeability in x direction and low permeability in y direction. The results indicate that the relative permeability is not directional permeability between well pairs but rather be the average permeability of the effective area between the 2 wells. The interwell

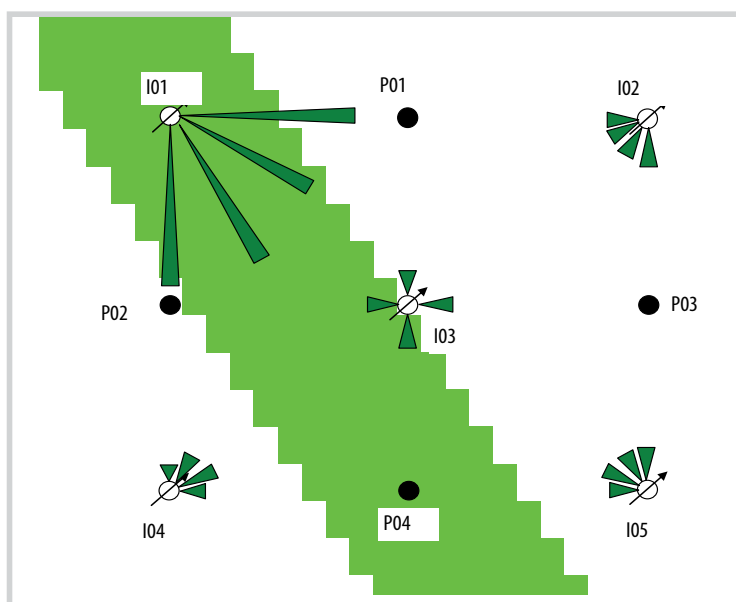


Figure 11. Representation of relative interwell permeability for the case of the 5×4 synthetic field with high permeability channel.

connectivity for some well pairs such as I1P2 and I2P3 is larger than the others such as I2P2 and I1P3. However, the permeabilities between I2P2 and I1P3 are larger than those of I1P2 and I2P3 even though the distance between the former pairs is less than the latter. Thus, the relative interwell permeabilities are independent of the distance between wells or the position of the wells. Results for the change of average reservoir pressure for this case are almost the same as the previous case, thus, the average pressure change does not depend on permeability.

Reservoir with high permeability channel

In this case, a high permeability channel was present as shown on Figure 11. The shaded area is the high permeability channels with permeability of 1000 mD which is 10-fold the permeability in other area of the reservoir (100 mD). For this case, permeability at the injectors was set to 100 mD. Again, the relative interwell permeability between the well pairs was calculated by matching the values of interwell connectivity coefficients calculated from the analytical model with the values obtained from MLR technique using simulation results. Some resulting permeabilities were lower

Table 7. Relative interwell permeability results from the pseudo-steady state equation for the 5×4 synthetic field/reservoir with partially sealing fault ($k_{ref} = 100$ mD, $\Delta t_{eq} = 12.63$ days)

	P1	P2	P3	P4	Ave.
I1	20	129	62	98	77
I2	249	65	174	95	146
I3	52	99	60	94	76
I4	79	111	87	106	96
I5	116	95	120	108	110
Ave.	103	100	101	100	

than the reservoir permeability, which was unreasonable. It was because well I1 was actually located in the high permeability zone and thus, assuming the permeability of well I1 (k_{ref}) was the same as the formation permeability would lead to unrealistic results. Thus, in order to address this problem, an approximate average reservoir permeability of 300 mD was assumed for well I1. The same permeability was applied to other injectors to guarantee comparable relative permeability. A new set of relative interwell permeabilities were found as shown in Table 6.

Representation of the relative interwell permeabilities is shown in Figure 11. A clear trend of the high permeability channel can be observed by looking at the relative interwell permeabilities on Figure 11. The flow in the channel seems to affect the relative interwell permeability between wells on each side of the channel. For example, k_{ir} for the pair I03-P02 is lower than k_{ir} for the pair I03-P03 even though the permeability between I03-P02 is higher. Thus, flow interference may affect the relative interwell permeability.

Reservoir with partially sealing fault

In this case, a reservoir with partially sealing fault similar to the case discussed by Dinh and Tiab [1] was investigated. The partially sealing fault is indicated by the shaded strip as shown on Figure 12. The fault was set to zero porosity and permeability. Permeability at injectors was equal to formation permeability of 100 mD.

The relative interwell permeability results are shown in Table 7. Figure 12

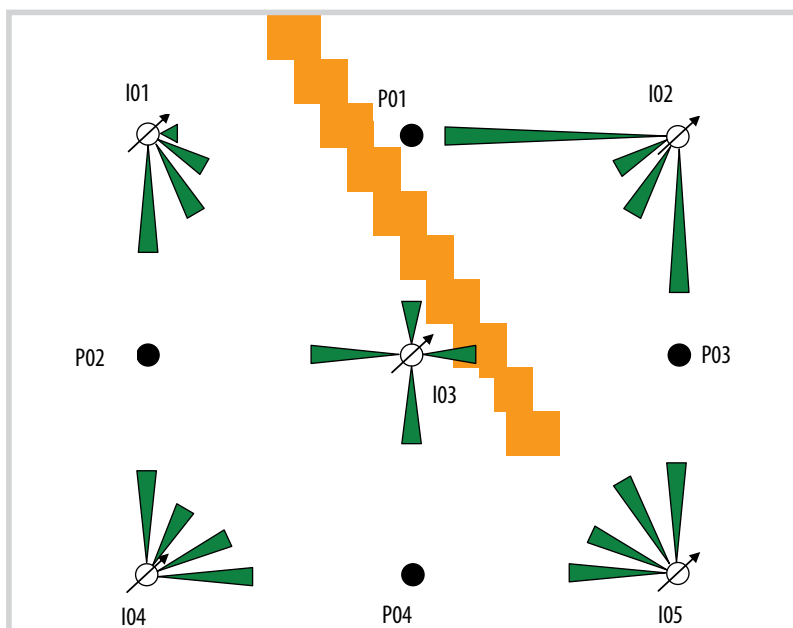


Figure 12. Representation of relative interwell permeability for the case of the 5×4 synthetic field with partially sealing fault.

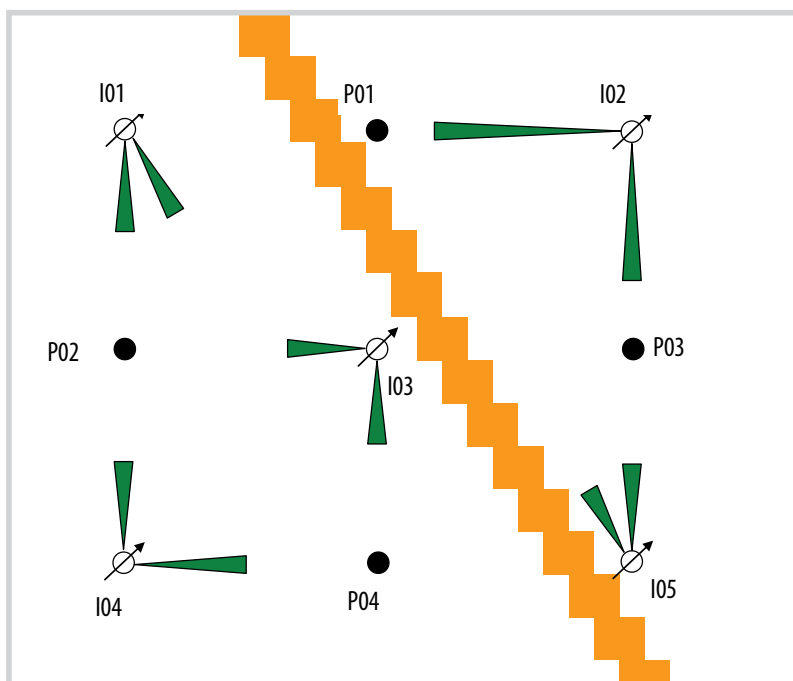


Figure 13. Representation of relative interwell permeability for the case of the 5×4 synthetic field with sealing fault.

Table 8. Change of average reservoir pressure results for the 5×4 synthetic field/reservoir with sealing fault ($k_{ref} = 100$ mD, $\Delta t_{eq} = 12.63$ days)

	P1	P2	P3	P4	Ave
Δp_{ave} (psia)	181.0	390.3	180.8	390.2	285.6
I1	-0.13	0.14	-0.18	-0.01	-0.18
I2	0.42	-0.24	0.30	-0.20	0.28
I3	-0.21	0.16	-0.23	0.19	-0.08
I4	-0.09	0.07	-0.12	0.12	-0.02
I5	0.00	-0.13	0.23	-0.11	0.00
Sum	0.00	0.00	0.00	0.00	

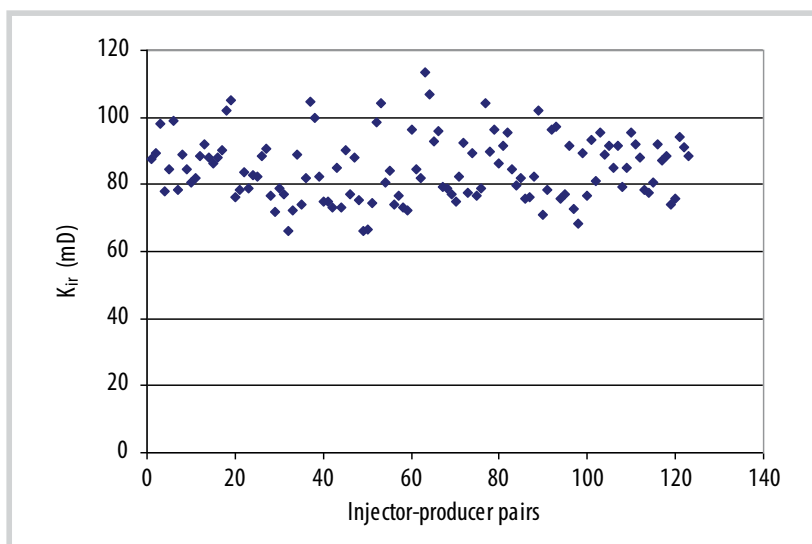


Figure 14. Plot of relative interwell permeability (k_{ij}) after cut-off ($\beta_{ij-cut-off} = 0.04$) for the 25×16 homogeneous synthetic field ($k_{ref} = 100$ mD, $\Delta t_{eq} = 5.87$ days).

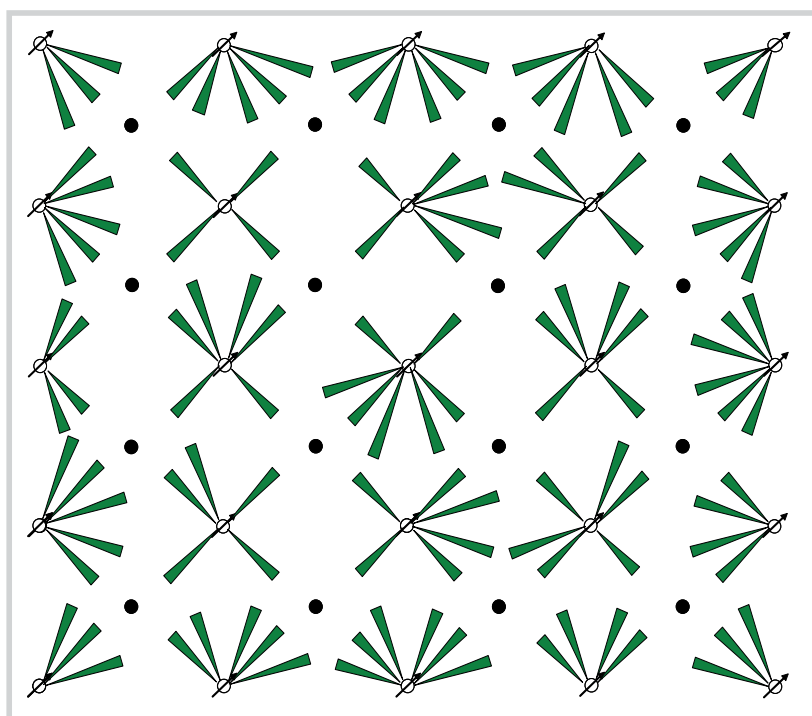


Figure 15. Representation of relative interwell permeability after cut-off ($\beta_{ij-cut-off} = 0.04$) for the case of the 25×16 homogeneous synthetic field ($k_{ref} = 100$ mD, $\Delta t_{eq} = 5.87$ days).

shows the representation of the relative interwell permeabilities in the form of reverse arrows. It is clear that the permeabilities of well pairs with wells on different side of the fault are small. Unlike the homogeneous case, the constant β_{oj} calculated for each producer were different indicating each producer was under different influence by other producers.

The average pressure change for this case is higher than that of the previous case indicating a decrease in pore volume. This is because the fault was set to zero porosity causing a decrease in overall pore volume. The calculated total porosity was 0.29, which is slightly lower than assigned formation porosity (0.30).

Reservoir with sealing fault

This case is similar to the partially sealing fault; however, the fault seals completely as shown in Figure 13. Thus, the reservoir is divided into two compartments. The results for interwell connectivity coefficients were similar to those presented in the previous publication [1]. Some coefficients are significantly small compared to others for the same producers. To simplify the calculation, a cut-off value was set at 0.1. Thus, any coefficients less than 0.1 were set to zeros. Since the relative interwell permeabilities do not exist at zero interwell coefficients, they were also set to zero.

The representation of relative interwell permeability results is presented

in Figure 13. The resulted average pressure change along with coefficient M_{ij} are shown in Table 8. It is obvious that there are 2 sets of average pressure changes (181 psi and 390 psi) corresponding to 2 groups of producers (P1, P3) and (P2, P4) suggesting 2 different reservoir pore volumes. From the relative interwell permeability results, we can identify the wells connected to the same pore volumes by analysing both relative interwell permeabilities and average pressure changes. The results indicate 2 groups of wells. One group of wells connected to the same pore volume includes well P1, P3, I2 and I5. The other group includes P2, P4, I1, I2 and I4. This agrees with the actual reservoir model setup. Thus, the new technique can be used to detect reservoir compartmentalisation and identify the wells that are in the same compartment.

The 25x16 synthetic field

Only the homogeneous case was considered for this field. As mentioned before, 128 data points were obtained to calculate interwell connectivity coefficients using MLR technique. Similar results to the results presented by Dinh and Tiab [1] were obtained. The interwell connectivity coefficients are very low for the well pairs that are too far apart. Since the percentage errors as mentioned in Step 4 were magnified for low interwell coefficients, a cut-off value of 0.04 was applied. Thus, the percentage errors of any coefficients lower than the cut-off value were set to zero, and the corresponding relative interwell permeability was considered as undetermined. Only relative interwell permeability corresponding to the connectivity coefficients higher than or equal to the cut-off values were calculated. The results are shown in Figures 14 and 15.

The relative interwell permeability results are close to one another. However, the average value for k_{ir} is slightly lower than the input permeability of 100 mD as shown in Figure 14. This could be due to cross flow effects among wells. As shown in Figure 15, only k_{ir} between well pairs that did not have any other well between them could be determined. The relative interwell permeabilities of the well pairs with farther distance were slightly higher than those with closer distance. This agreed with a conclusion drawn by Umnuyponwivat et al. [5] that “the interference effects are not always dominated by the nearby wells. Under certain conditions, farther wells may play more important roles on the well performance.”

6. Different flowing conditions at the response and signal wells

The previous study [1] considered injectors as signal wells (changing rates) and producers as response wells (constant rates). However, in a real field situation, it is not always possible to keep the production rates constant. Thus, different test designs should be considered. The characteristics of the analytical model discussed in the previous section indicate that either injector or producer can be used as response wells or signal wells. Hence, the technique should not be restricted to the case where injectors serve as signal wells and producers as response wells. In this section, we obtained simulation results from several scenarios to verify this theory. Resulting interwell connectivity and discussion on any necessary modification to the analytical solutions are also presented.

Tables 9 and 10 summarise the results for all the cases discussed in this section. The second column

Table 9. Interwell connectivity result summary for different test schemes for the 5x4 homogeneous synthetic field ($k_{ref} = 100$ mD, $\Delta t_{eq} = 12.63$ days)

Cases	Ave. % Error for β_{ij}	A	Δq_{tot} (STB/day)	Ave. Δp_{ave} (psi)	% Error for Δp_{ave}	Porosity
Base case	0.00%	0.0035	-800	286.0	0.01%	0.301
Constant injection	2.28%	0.0045	-800	285.6	0.12%	0.301
All producers	2.27%	0.0044	2,400	-930.3	8.30%	0.277
Shut-in producers	0.04%	0.0035	-2,000	711.5	0.63%	0.302
Shut-in injectors	2.35%	0.0431	2,000	-683.2	4.58%	0.315

Table 10. Interwell connectivity result summary for different test schemes for the 25x16 homogeneous synthetic field ($k_{ref} = 100$ mD, $\Delta t_{eq} = 5.87$ days)

Cases	Ave. % Error for β_{ij}	A	Δq_{tot} (STB/day)	Ave. Δp_{ave} (psi)	% Error for Δp_{ave}	Porosity
Base case	0.00%	0.0059	-3600	353.0	0.58%	0.303
Constant injection	0.70%	0.0059	-3600	352.5	0.70%	0.303
Shut-in producers	1.37%	0.0072	-10000	964.6	2.45%	0.308
Shut-in injectors	420.85%	0.1307	10000	-970.6	1.74%	0.306

shows the average percent error of interwell connectivity coefficients compared to the base case (constant production rate and changing injection rate in homogeneous reservoir). The 3rd column presents the asymmetric coefficients (A). The 4th column is the total field flow rates. The 5th and 6th columns show the Δp_{ave} results and their percent error compared to the material balance solution, respectively. The last column is the calculated porosities with input porosity of 0.3 for all the cases.

6.1. Constant injection rates and changing production rates

For this case (constant injection), the injectors of the 5x4 homogeneous synthetic field described before were converted to producers and the producers were converted to injectors. Thus, the 5x4 synthetic field now has 5 producers and 4 injectors. Flow rates of the new producers are the same as of the original injectors except they are now producing flow rates. The new injectors were maintained at constant rates (850 STB/day) so that the difference between total injection and total production was the same as the base case. The results are shown in Table 9.

Determination coefficients of $R^2=1$ and the low asymmetric coefficient $A = 0.004482$ indicate good results. The coefficients and average pressure change are almost the same as for the case of constant production rates and changing injection rates (Table 9).

Similar results were obtained for the 25x16 synthetic field with asymmetric coefficient $A = 0.0059$. Almost the same Δp_{ave} was also obtained. Table 10 summarises the results.

A few changes are required for the analytical model in this case. The negative sign in front of the first terms on the right-hand side of both Equations 13 and 14 become positive and the Δp_{pr} becomes:

$$\Delta p_{pr} = - \frac{141.2B\mu}{kh} \sum_{j=1}^{n_{inj}} a_j [X_{Dj}, Y_{Dj}, X_{wDj}, Y_{wDj}, X_{eDj}, Y_{eDj}, t_{AD}] q_j + \Delta p_{ave} \quad (38)$$

j and i are now standing for injectors and producers, respectively. Equation 19 should be used instead of Equation 20 to derive the flow rates for active wells (producers).

6.2. All production wells with constant rates at response wells

In this case (all producers), for the 5x4 homogeneous field, the injectors in the base case were converted to producers and acted as signal wells. Thus, all wells in the system were producers. The response wells were set to constant production rate of 100 barrels/day. The results are shown in Table 9. Poorer result was obtained for Δp_{ave} with the percentage error compared to the material balance result

of 8.3% (Table 9). This was because as all wells were producing, the water saturation decreased leading to changing total compressibility or deviation from original assumption. Thus, Δp_{ave} was actually different for each time interval.

Similar approach was applied to the 25x16 homogeneous synthetic field. However, with the original flow rates, when all wells are producing, it was impossible to maintain the production rates as scheduled due to quick depletion of the reservoir. Thus, no results were obtained for the 25x16 synthetic field in this case. Therefore, the challenge to carry out the interwell connectivity test when all wells are producing is to maintain the scheduled production rates and make adjustments to the change in total compressibility.

6.3. Shut-in wells as response wells

In this case, all response wells in the previous cases were shut-in (shut-in producers and shut-in injectors). The results obtained were also similar for both changing injection rates and changing production rates. Both cases of shut-in producers for the constant production rate and changing injection rate case and shut-in injectors for constant injection rates and changing production rates case for the 5x4 homogeneous synthetic field were investigated. Results for the shut-in injector case ($A = 0.0431$) were not as good as the results for the shut-in producers ($A = 0.0035$) as shown in Table 9. The reason could be a more significant change in total compressibility in the case of shut-in injectors.

The same approach was applied to the 25x16 homogeneous synthetic field. The case of all producers with shut-in wells as response wells could be simulated for this field. Good results were obtained for the case of shut-in producer and changing injection rates (Table 10). However, poor results with an average percent error of $\beta_{ij} = 420.85\%$ were obtained for shut-in injectors and active producers even after a cut-off value of 0.04 was applied to the interwell connectivity coefficients as shown in Table 10. Again, these errors were due to the significant change in total compressibility as water was drawn from the reservoir and the decreasing reservoir pressure leading to weak signals from active producers.

As seen in Tables 9 and 10, with a negative total field flow rate (total injection is higher than total production), the calculated Δp_{ave} are positive indicating an increase in reservoir pressure and vice versa. The results for the base case and the constant injection case are very close indicating the roles of injectors and producers can be switched without significantly affecting the interwell connectivity results.

7. Conclusions and recommendations

The previous study by Dinh & Tiab [1] has been extended in this study. A pseudo-steady state flow solution for a well in a multi-well system was used to model the interwell connectivity test. The model was verified using 2 synthetic reservoir models, one with 5 injectors and 4 producers and the other with 25 injectors and 16 producers. Results from the model fit well with the simulation results. Average reservoir pressure change can be calculated, and the total reservoir porosity can be estimated. By defining a reference permeability, the interwell connectivity can be presented in terms of the relative interwell permeability. Some of the conclusions and recommendations drawn from this study are:

- The analytical model presented in this study works well with the interwell connectivity test with the assumption that the pseudo-steady state has been reached at the end of each time interval.
- Tests that are longer than required (more data points) may create errors because of deviation from the constant total compressibility assumption due to the change of total reservoir saturation. Thus, an adequate number of data points should give better results.
- The relative interwell permeability does not depend on the position and the distance between wells. Thus, it provides an additional parameter to evaluate interwell connectivity.
- The average reservoir pressure change with the interwell connectivity information can be used to identify reservoir compartmentalisation as well as the wells connected to each compartment.
- Results from this study have shown that the signal wells could be either producers or injectors, and so are the response wells. The response well could also be either flowing or shut-in. Thus, this study provided more flexibility in design of interwell connectivity tests to fit a field situation.

- Further investigation on the characteristics of relative interwell permeability and the effect of interwell flow on the interwell permeability should be conducted.
- Interwell connectivity tests with varied test time intervals and multi-phase flow should be investigated.
- Extension of the study to include wells with different well bore conditions such as horizontal wells and hydraulic fractured wells is recommended.
- Extension of the study to infinite reservoirs and closed reservoirs with different shapes is also recommended.

Nomenclature

- \hat{p}_j = modelled pressure change (psia)
- ϕ = porosity, fraction
- ϕ_{tot} = total field porosity, fraction
- a = influence function
- A = asymmetric coefficient or area (ft²)
- B = formation volume factor (rbbl/STB)
- c_o = oil compressibility (psi⁻¹)
- c_r = rock compressibility (psi⁻¹)
- c_t = total compressibility (psi⁻¹)
- c_w = water compressibility (psi⁻¹)
- E_1 = exponential integral function one
- h = formation thickness (ft)
- I = total number of signal or active wells (injectors) or injector indicator in well names
- J = total number of response wells (producers), producer indicator or productivity index, (STB per day/psi)
- k = permeability (mD)
- k_{ir} = interwell relative permeability (mD)
- k_{ref} = reference permeability (mD)
- $LSLR$ = least square linear regression
- M = coefficients in average pressure change calculation
- m, n = numbers of calculation terms
- MLR = multivariate linear regression
- n_{inj} = total number of injectors
- n_{pr} = total number of producers

n_{well} = total number of wells
 p = pressure (psia)
 p_{ave} = average pressure (psia)
 p_{ini} = initial pressure (psia)
 p_j = pressure at the observation well (psia)
 p_{wf} = bottom-hole flowing pressure (psia)
 q = flow rate (STB/day)
 q_{ref} = reference flow rate (STB/day)
 R^2 = coefficient of determination
 r_w = wellbore radius (ft)
 s = skin factor, dimensionless
 t = time (hours)
 t_s = starting time (hours)
 V_b = reservoir bulk volume (ft³)
 V_p = pore volume (ft³)
 x = coordinate or dimension in x-direction (ft)
 x_e = dimension of study area in the x-direction (ft)
 x_w = individual well x-coordinate (ft)
 y = coordinate or dimension in y direction (ft)
 y_e = dimension of study area in the y direction (ft)
 y_w = individual well y-coordinate (ft)
 β_{0j} = additive constant term in MLR
 β_{ij} = weighting coefficient in MLR
 Δp = pressure change/difference (psi)
 Δp_{ave} = average pressure change (psi)
 Δp_{pr} = pressure change corresponding to influence of response wells and change in average pressure (psi)
 Δq_{tot} = field total flow rate (STB/day)
 Δt = time interval (hours)
 Δt_{eq} = equivalent pseudo-steady state time interval
 μ = fluid viscosity (cp)

Subscripts

ave = average
 D = dimensionless quantity
 DA = dimensionless corresponding to area

e = boundary value
 eq = equivalent
 i' = investigated signal/active well (injector)
 i = signal or active well (injector) index
 ini = initial value
 j = response/observation well (producer) index
 j' = investigated response/observation well (producer)
 tot = total
 w = well
 wf = flowing conditions

Superscripts

l = order of data point
 L = total number of data points
 T = transposed

References

- [1] Djebbar Tiab and Dinh Viet Anh, "Inferring interwell connectivity from well bottom hole pressure fluctuations in waterfloods", *SPE Reservoir Evaluation & Engineering*, Vol. 11, No. 5, pp. 874 - 881, 2008. DOI: 10.2118/106881-PA.
- [2] Alejandro Albertoni and Larry W.Lake, "Inferring interwell connectivity only from well-rate fluctuations in waterfloods", *SPE Reservoir Evaluation and Engineering Journal*, Vol. 6, No. 1, pp. 6 - 16, 2003. DOI: 10.2118/83381-PA.
- [3] A.A.Yousef, P.Gentil, J.L.Jensen, and Larry W.Lake, "A capacitance model to infer interwell connectivity from production and injection rate fluctuations", *SPE Annual Technical Conference and Exhibition, Dallas, Texas, 9 - 12 October 2005*.
- [4] M. Bourgeois and P. Couillens, "Use of well test analytical solutions for production prediction", *European Petroleum Conference, London, United Kingdom, 25 - 27 October 1994*. DOI: 10.2118/28899-MS.
- [5] Suwan Umnuyayponwivat, Erdal Ozkan, and R.Raghavan, "Pressure transient behavior and inflow performance of multiple wells in closed systems", *SPE Annual Technical Conference and Exhibition, Dallas, Texas, 1 - 4 October 2000*. DOI: 10.2118/62988-MS.
- [6] P.P.Valko, L.E.Doublet, and T.A. Blasingame, "Development and application of the multiwell

productivity index (MPI)”, *SPE Journal*, Vol. 5, No. 1, pp. 21 - 31, 2000. DOI: 10.2118/51793-PA

[7] Taufan Marhaendrajana, “*Modeling and analysis of flow behavior in single and multiwell bounded reservoirs*”, PhD dissertation, Texas A&M University, Texas, May 2000.

[8] T.Marhaendrajana, N.J.Kaczorowski, and T.A.Blasingame, “Analysis and interpretation of well test performance at Arun field, Indonesia”, *SPE Annual Technical Conference and Exhibition, Houston, Texas, 3 - 7 October 1999*. DOI: 10.2118/56487-MS.

[9] Jia En Lin and Hui-Zhu Yang, “Analysis of well-test data from a well in a multiwell reservoir with water injection”, *SPE Annual Technical Conference and Exhibition, Anaheim, CA, 11 - 14 November 2007*. DOI: 10.2118/110349-MS.

[10] Dinh Viet Anh and Djebbar Tiab, “Inferring interwell connectivity in a reservoir from bottomhole

pressure fluctuations of hydraulically fractured vertical wells, horizontal wells, and mixed wellbore conditions”, *Petrovietnam Journal*, Vol. 10, pp. 20 - 40, 2020. DOI: 10.47800/PVJ.2020.10-03.

[11] Jerry Lee Jensen, L.W.Lake, Patrick William Michael Corbett and D.J.Goggin, *Statistics for petroleum engineers and geoscientists*. New Jersey: Prentice Hall, 1997.

[12] Ali Abdallah Al-Yousef, “*Investigating statistical techniques to infer interwell connectivity from production and injection rate fluctuations*”, PhD dissertation, University of Texas at Austin, Austin, Texas, May 2006.

[13] Steven C.Chapra and Raymond P.Canale, *Numerical methods for engineers, 2nd edition*. McGraw-Hill, 1988.

TRANSPORT OF OIL/WATER PARTITIONING COMPONENTS DURING WATER INJECTION

Huynh Thi Thu Huong, Nguyen Huu Quang, Le Van Son, Tran Trong Hieu

Centre for Applications of Nuclear Technique in Industry, Vietnam Atomic Energy Institute

Email: huonghtt@canti.vn

<https://doi.org/10.47800/PVJ.2021.06-03>

Summary

The oil/water partitioning components such as alkylphenols and aliphatic acids naturally exist in crude oil compositions at different initial concentrations of hundreds or even thousands of ppm depending on the location of the reservoir compared to the site of original rocks. During contact with sweeping injection brine, those compounds diffuse from oil phase to water phase due to oil/water partitioning behaviours. As a result, their concentration in oil contacting with water will be attenuating during water injection. Their concentration profile in water injection history contains the information related to diffusion in oil and water phase, interstitial velocity of water and oil saturation.

This paper presents the research results of theoretical model and numerical model of the washed-out process of alkylphenols in the late stage of water injection. The research results have proposed approximate analytical expression for concentration of alkylphenols at the late stage of water flooding. In this regard, at the sufficient large injection volume the alkylphenol concentration attenuates exponentially and the attenuation rate depends on parameters such as partitioning coefficient, oil saturation and interstitial velocity of water and oil and diffusion coefficients. The simulation concentration results obtained from UTCHEM simulator for the 5-spot model showed a good match with analytical calculation results.

The research results can be used as the basis for developing methods to assess water flooding systems as well as oil saturation. The results can also be used for study of transport of non-aqueous phase liquid (NAPL) in environmental contamination.

Keywords: Residual oil saturation, waterflooding, tracer, partitioning organic compounds, enhanced oil recovery.

1. Introduction

Alkylphenols are aromatic compounds consisting of phenol nuclei and alkyl groups generated by alkylation and isomerisation reactions in the source rock during petroleum formation. For years, the existence and origin of the organic phenolic compounds such as alkylphenols and aliphatic acids in petroleum have been studied as indicators to classify petroleum according to the origin of hydrocarbons as well as to indicate petroleum migration pathways [1 - 4]. The concentration distribution of alkylphenols and their oil/water partition characteristics were used by Taylor, Larter, and Dale to study petroleum migration in the North Sea fields [4]. Lucach, Bowler, and Larter studied the Dhahaban hydrocarbon system in Oman based on the distribution variation of alkylphenols [5].

In the process where oil comes into contact with the injection water, because of oil/water partition properties the alkylphenols diffuse from oil phase to water phase, causing attenuation of their concentration in the two phases over time. The attenuation rate of alkylphenol concentration depends on several factors such as partition coefficient, diffusion coefficient, interstitial velocity of phases, and the amount of remaining oil in pore volume. Sinha, Asakawa, and Pope proposed a method using alkylphenols as natural tracers to determine residual oil saturation in the swept area based on their residence time in water phase during water injection [6].

In Vietnam, the Tracer Laboratory of the Centre for Applications of Nuclear Techniques in Industry (Vietnam Atomic Energy Institute) has studied the transport of alkylphenols during waterflooding in oil recovery since 2014. The authors have proposed an analytical model describing the attenuation of alkylphenol concentration in produced water over water injection time and conducted



Date of receipt: 17/8/2020. Date of review and editing: 17/8 - 10/12/2020.

Date of approval: 11/6/2021.

experiments to validate the analytical model [7 - 9]. The study results also considered the possibility of using alkylphenols as the natural partitioning tracers to evaluate oil saturation and determine the water contribution proportion of injection wells to production wells.

2. Theory

Alkylphenols (APs) are trace compositions in crude oil formed along with hydrocarbons during geochemical processes, which have the initial concentration in the oil phase in the range from several ppm to thousands of ppm depending on the field. During water injection, alkylphenols diffuse from oil phase to water phase at the water-oil contact boundary in pore spaces.

The advection-dispersion equation in oil-water phase contact of alkylphenols with the assumption that their concentration between phases instantaneously reaches equilibrium is expressed as Equation (1) [10]:

$$\phi \frac{\partial}{\partial t} (S_w C_w + K_d S_o C_w) + \nabla \cdot (S_w \phi \vec{v}_w^* C_w + K_d S_o \phi \vec{v}_o^* C_w) - \nabla \cdot [(S_w \phi \vec{D}_w^* + K_d S_o \phi \vec{D}_o^*) \nabla C_w] = 0 \tag{1}$$

in which, ϕ is porosity of media, C_w is APs concentration in water phase [M/L³]; S_w and S_o are the saturation of water phase and oil phase, respectively ($S_w + S_o = 1$); K_d is APs partition coefficient; \vec{v}_w^* and \vec{v}_o^* are interstitial velocity of water phase and oil phase, respectively [L/T]; \vec{D}_w^* and \vec{D}_o^* are dispersion tensors of APs in water phase and oil phase, respectively [L²/T], t is time [T].

Suppose that the porous media is infinite homogeneous, the saturation of the phases is constant, and the interstitial velocity of phases is constant in the pore, the initial and boundary conditions are as follows:

$$\text{Initial condition: } C_w(x, 0) = \begin{cases} C_o & x \in [0, +\infty) \\ 0 & x \in (-\infty, 0) \end{cases} \tag{2}$$

$$\text{Boundary condition: } C_w(-\infty, t) = 0 \tag{3}$$

$$\left. \frac{\partial C_w(x, t)}{\partial x} \right|_{x \rightarrow +\infty} = 0 \tag{4}$$

The one-dimensional analytical solution describing the concentration of APs in water phase $C_w(x, t)$ is described as:

$$C_w(x, t) = \frac{1}{2} \times C_o \times \left[1 + \text{Erf} \left(\frac{x - \frac{C^*}{A} \times t}{2 \times \sqrt{\frac{B \times t}{A}}} \right) \right] \tag{5}$$

in which, A, B and C* are parameters depending on APs partition coefficient, oil saturation, dispersion coefficient in phases, and pore velocity of water and oil:

$$\begin{aligned} A &= 1 + (K_d - 1)S_o \\ B &= (1 - S_o)D_{Lw}^* + K_d S_o D_{Lo}^* \\ C^* &= (1 - S_o)v_{wx}^* + K_d S_o v_{ox}^* \end{aligned}$$

At $x = L$ when $t \rightarrow \infty$, the approximate form of $\text{Ln}C_w$ is shown in Equation (6):

$$\text{Ln}[C_w(L, t \rightarrow \infty)] = -\frac{C^{*2}}{4 \times A \times B} \times t - \frac{1}{2} \times \text{Ln}(t) + \text{Ln} \left[\frac{A \times \sqrt{\frac{B}{A}} \times C_o \times \left(-1 + e^{\frac{C^* \times L}{2 \times B}} \right)}{2 \times C^* \times \sqrt{\pi}} \right] \tag{6}$$

Equation (6) shows that the value of $\text{Ln}(t)$ is very small compared to t , so it can be considered that $\text{Ln}C_w$ is approximately linear dependent on the time of water injection. Figure 1 illustrates $\text{Ln}C_w$ according to Equation (5) and the approximate solution according to Equation (6), representing the attenuation of APs concentration with different partition coefficients in water phase over injection time. When injection time t is sufficiently long or the injected volume is large enough, $\text{Ln}C_w$ is almost linear over injection time, in which the slope of $C^*2/$

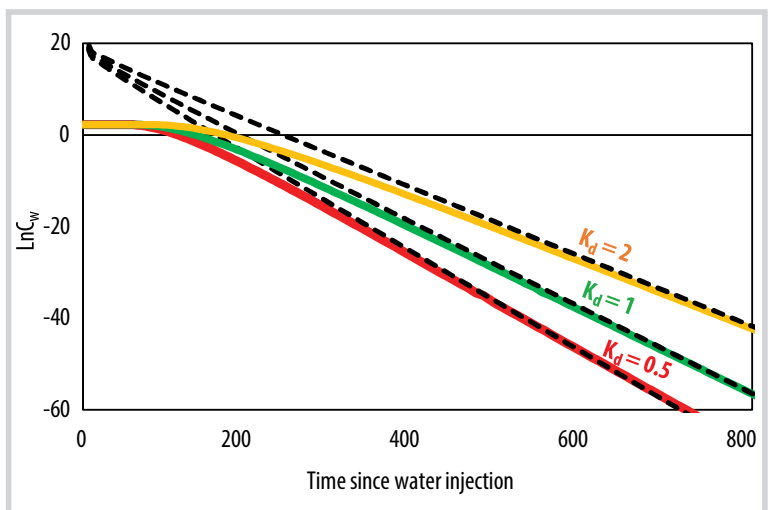


Figure 1. Illustrating $\text{Ln}C_w$ according to Equation (5) - solid lines and approximate solutions according to Equation (6) - dashed lines, for APs having $K_d = 0.5$, $K_d = 1$ and $K_d = 2$. When t is large, the value of $\text{Ln}C_w$ decreases linearly over time. The smaller the K_d , the faster the time to reach the linear asymptotic.

(4AB) represents the decline rate of APs concentration during water sweeping. With the same injection conditions and oil saturation, the smaller the K_d is, the greater the dispersibility into water phase becomes and the faster the concentration decreases, and vice versa.

The slope is described as

$$a = \frac{C^{*2}}{4 \times A \times B} = \frac{[(1 - S_o) \times v_{wx}^* + K_d S_o v_{ox}^*]^2}{4 \times [1 + (K_d - 1) \times S_o] \times [(1 - S_o) \times D_{Lw}^* + K_d \times S_o \times D_{Lo}^*]} \quad (7)$$

Let $a = a_i + a_m$, in which:

$$a_i = \frac{(1 - S_o)^2 \times v_{wx}^{*2}}{4 D_{Lo}^* S_o^2 \times K_d^2 + 4 (D_{Lo}^* + D_{Lw}^*) (1 - S_o) S_o K_d + 4 D_{Lw}^* (1 - S_o)^2} \quad (8)$$

$$a_m = \frac{2(1 - S_o) S_o v_{wx}^* v_{ox}^* K_d + S_o^2 v_{ox}^{*2} K_d^2}{4 D_{Lo}^* S_o^2 \times K_d^2 + 4 (D_{Lo}^* + D_{Lw}^*) (1 - S_o) S_o K_d + 4 D_{Lw}^* (1 - S_o)^2} \quad (9)$$

We have

$$\frac{a_m}{a_i} = \left(\frac{S_o}{1 - S_o} \right)^2 \times \left(\frac{v_{ox}^*}{v_{wx}^*} \right)^2 K_d^2 + 2 \times \frac{S_o}{1 - S_o} \times \frac{v_{ox}^*}{v_{wx}^*} \times K_d \quad (10)$$

and

$$\frac{v_{xo}^*}{v_{xw}^*} = \frac{1 - S_o}{S_o} \times \frac{f_o}{f_w} \quad (11)$$

in which, f_o and f_w are the oil cut and the water cut, respectively. Replace Equation (11) to Equation (10):

$$\frac{a_m}{a_i} = \left(\frac{f_o}{f_w} K_d \right)^2 + 2 \frac{f_o}{f_w} K_d \quad (12)$$

From the above equations, recall the decline rate of $\text{Ln}C_w$ ($L, t \rightarrow \infty$) be the leaching rate at the late stage of water flooding:

$$a = \frac{\left(1 + \frac{f_o}{f_w} K_d \right)^2 (1 - S_o)^2 v_{wx}^{*2}}{4 D_{Lo}^* S_o^2 K_d^2 + 4 (D_{Lo}^* + D_{Lw}^*) (1 - S_o) S_o K_d + 4 D_{Lw}^* (1 - S_o)^2} \quad (13)$$

At the late stage of water flooding, oil is almost immobile as also known as residual oil, $f_o = 0$ and $S_o = S_{or}$, the attenuation of APs concentration in the production water is in accordance with the exponential law of the injection time or respectively the injection volume. Obviously, the decline rate depends on the partition coefficient of APs (K_d), the oil saturation (S_o), the dispersion coefficients of APs in phases (D_{Lo}^* , D_{Lw}^*) and the pore velocity of water v_{wx}^* .

3. Simulation results

The advection-dispersion transport of APs from the oil phase into water phase during the water injection has been simulated on 1/4 5-spot models using UTCHEM (The University of Texas's Chemical Simulator software), developed by the University of Texas [11].

UTCHEM was used to run 3D homogeneous single-layered reservoir models with 1/4 5-spot pattern, including 2 specific cases:

- Immobile oil model having initial oil saturation and residual oil saturation of 0.35;
- Mobile oil model having initial oil saturation of 0.65 and residual oil saturation of 0.35.

The models have the size of 165 m × 165 m × 12 m divided into 55 × 55 × 4. The flow rate of injection water is 65.34 m³/d.

The general parameters of the models are:

- Porosity $\phi = 0.2$, water viscosity $\mu_w = 0.7$ cp, oil viscosity $\mu_o = 4$ cp;
- Longitudinal and transverse dispersivity are $\alpha_{DL} = 0.03$ m, $\alpha_{DT} = 0.003$ m;

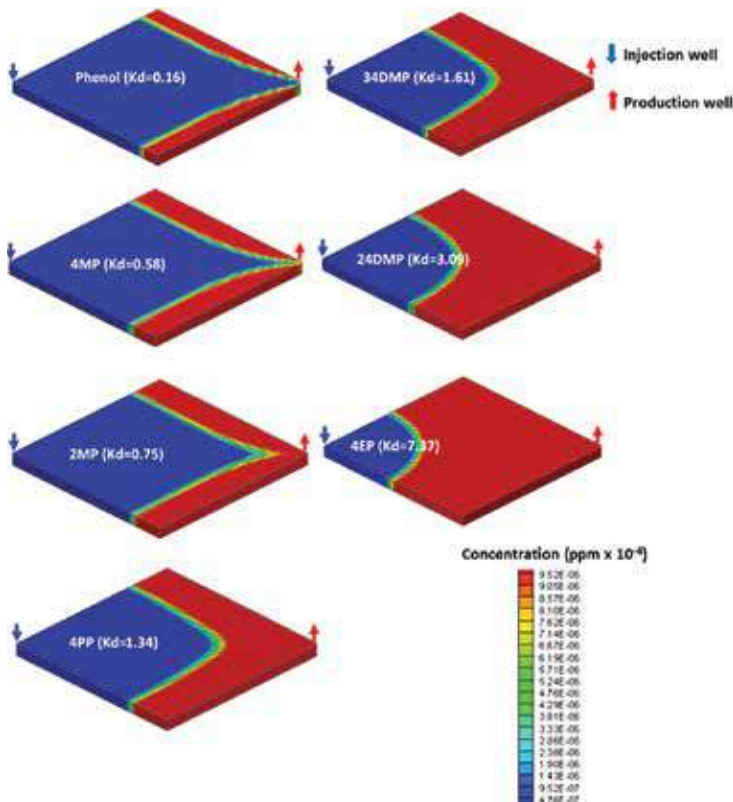


Figure 2. Illustration of APs concentration distribution in space at water injection of 0.6 PV in mobile oil model ($S_{oi} = 0.65$, $S_{or} = 0.35$).

Table 1. The partition coefficient K_d of APs and initial concentration of APs used in the models

Alkylphenols	Partitioning coefficient $K_d = C_o/C_w$	Initial concentration in oil phase (mg/L)	Initial concentration in water phase (mg/L)
Phenol	0.16	1.6	10
4-Methylphenol (4MP)	0.58	5.8	10
2-Methylphenol (2MP)	0.75	7.5	10
4-Propylphenol (4PP)	1.34	13.4	10
3,4-Dimethylphenol (34DMP)	1.61	16.1	10
2,4-Dimethylphenol (24DMP)	3.09	30.9	10
4-Ethylphenol (4EP)	7.37	73.7	10

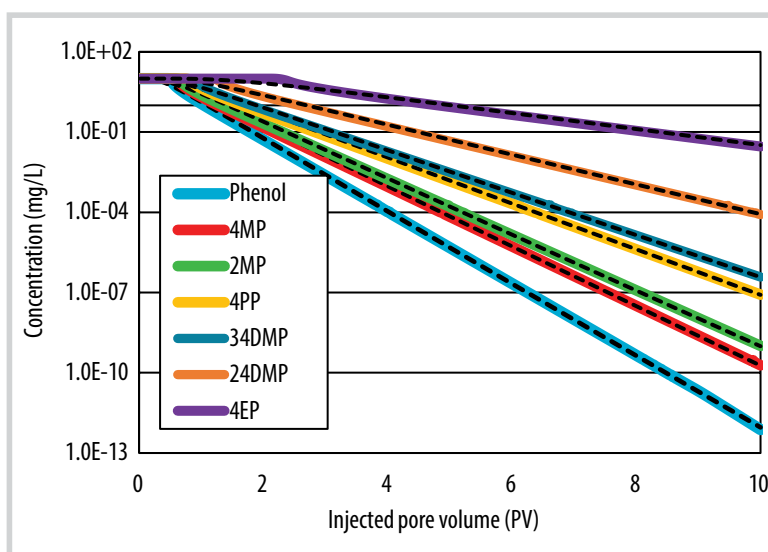
- Relative permeability curve is described by Corey model: critical water saturation $S_{cwr} = 0.3$, residual oil saturation $S_{or} = 0.35$, water endpoint: 0.15, oil endpoint 0.85, water exponent: 1.5, oil exponent: 2, endpoint mobility ratio: 1.

The APs initial concentration in oil phase and water phase and partition coefficient between phases determined in the experimental data of the Tracer Laboratory of CANTI are listed in Table 1. All compounds are supposed to have the same density, alkane number and chemical properties but different in partition coefficient.

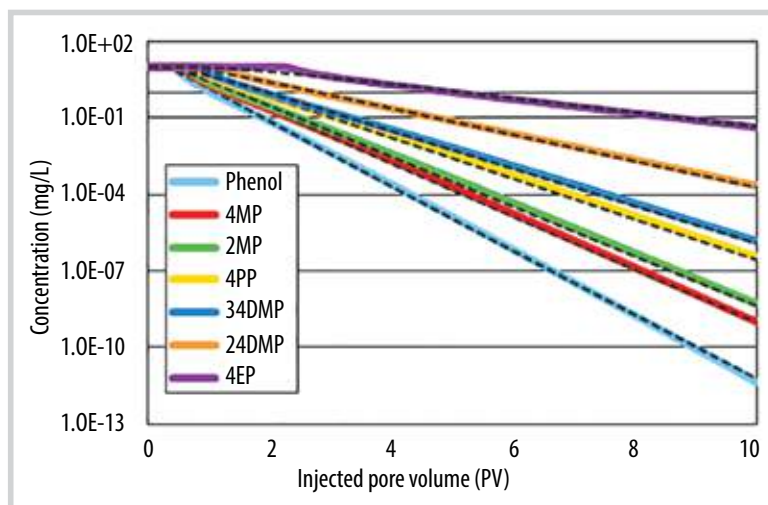
The water injection takes place up to 10 PV of the model to investigate the APs concentration decrease at the end of the injection stage. It is assumed that the concentration of APs between phases instantaneously reaches equilibrium while oil and water are in contact. Figure 2 illustrates the spatial concentration distribution of APs at water injection of 0.6 PV for the mobile oil model.

Figure 3 shows the concentration of APs in produced water in both models, in which the smaller the K_d is, the faster the leaching rate becomes, and vice versa.

The concentration obtained from calculation of the analytical solution in accordance with Equation (5) matches well with the simulation data in both models of mobile and immobile oil at the late stage of water injection (> 2 PV). The root mean square error (RMSE) between the simulation data and the calculation



(a)



(b)

Figure 3. Concentration curves of APs in produced water of the 1/4 5-spot having immobile oil ($S_{oi} = S_{or} = 0.35$, a) and the 1/4 5-spot having mobile oil ($S_{oi} = 0.65 S_{or} = 0.35$, b). Solid lines present the simulation data from UTCHEM software, while dashed lines present the calculation results of Equation (5).

tion data during the injection stage is shown in Table 2. The results show that the value of RMSE from 0 - 2 PV is greater than that at the

Table 2. The root mean square error (RMSE) between the simulation data and the analytical solution during the injection stage

Water injection (PV)	Phenol ($K_d = 0.16$)	4MP ($K_d = 0.58$)	2MP ($K_d = 0.75$)	4PP ($K_d = 1.34$)	34DMP ($K_d = 1.61$)	24DMP ($K_d = 3.09$)	4EP ($K_d = 7.37$)
	Immobile oil model						
0 - 1	1.445	1.585	1.638	1.813	1.883	1.174	0.123
1 - 2	0.080	0.130	0.150	0.170	0.220	1.930	1.950
2 - 3	0.003	0.010	0.015	0.044	0.064	0.183	2.382
3 - 4	< 0.001	< 0.001	< 0.001	0.005	0.009	0.062	0.177
4 - 5	< 0.001	< 0.001	< 0.001	< 0.001	0.001	0.015	0.197
5 - 10	< 0.001	< 0.001	< 0.001	< 0.001	< 0.001	0.002	0.059
Mobile oil model							
0 - 1	1.115	1.377	1.469	1.744	1.849	1.285	0.215
1 - 2	0.118	0.161	0.169	0.147	0.169	1.939	2.103
2 - 3	0.001	0.004	0.006	0.018	0.029	0.109	2.469
3 - 4	< 0.001	0.002	0.003	0.007	0.007	0.025	0.118
4 - 5	< 0.001	< 0.001	< 0.001	0.002	0.003	0.004	0.144
5 - 10	< 0.001	< 0.001	< 0.001	< 0.001	< 0.001	0.002	0.046

end of the injection stage, in which the APs with higher K_d represents the higher RMSE value.

5. Conclusions

The analytical solution of the advection-dispersion equation describing the attenuation of concentration of APs compounds in produced water was approximated as an exponential function at the late stage of water flooding when the injection time or injected volume is large (>1 PV). The analytical solution was validated by applying the ¼ 5-spot model to calculate the concentration of 7 AP compounds to compare with the results of numerical simulation using UTCHEM simulator. The results show that, when the injection time is large enough to reach injection of 2 PV or more, the approximate analytical solution matches quite well with the simulation results. The RMSE value is less than 0.2 for the APs having K_d less than 3. The analytical solution also shows that the APs concentration in produced water decreases exponentially over injection time and the factors affect the concentration attenuation rate include partition coefficient, diffusion coefficients, interstitial velocity and oil saturation. The approximate solution obtained in this study provides a better understanding of the factors influencing the attenuation of the APs concentration than the semi-experimental formula proposed by Huseby et al [10].

The research results can be used as the basis for developing the methods of assessment of water flooding sys-

tem as well as oil saturation. The results can also be used for study of transport of non-aqueous phase liquid (NAPL) in environmental contamination.

Acknowledgements

This research work has been implemented through the Project entitled “Study on the application of oil saturation determination method using partitioning organic compounds in oilfields” under the grant of Vietnam’s Ministry of Science and Technology.

References

- [1] Marisa Ioppolo - Armanios, *The occurrence and origins of some alkylphenols in crude oils*. Curtin University of Technology, 1996.
- [2] Steve Later and Barry Bennet, “Now you see them, now you don’t, now you might see them again! A review of the systematics of alkylphenol occurrence in conventional and heavy oil petroleum systems”, *2011 CSPG/CSEG/CWLS Conference, Calgary, Alberta, Canada, 9 - 11 May, 2011*.
- [3] B.Bennett and S.R.Larter, “Partition behaviour of alkylphenols in crude oil/brine systems under subsurface conditions”, *Geochimica et Cosmochimica Acta*, Vol. 61, No. 20, pp. 4393 - 4402, 1997. DOI: 10.1016/S0016-7037(97)88537-7.
- [4] Paul Taylor, Steve Larter, Martin Jones, Jason Dale, and Idar Horstad, “The effect of oil-water-rock partitioning

on the occurrence of alkylphenols in petroleum systems", *Geochimica et Cosmochimica Acta*, Vol. 61, No. 9, pp. 1899 - 1910, 1997.

[5] Sandra O.Lucach, Bernard F.J.Bowler, Neil Frewin, and Steve R.Larter, "Variation in alkylphenol distributions in a homogeneous oil suite from the Dhahaban petroleum system of Oman", *Organic Geochemistry*, Vol. 33, No. 5, pp. 581 - 594, 2002.

[6] R.Sinha, K.Asakawa, G.A.Pope, and K.Sepehmoori, "Simulation of natural and partitioning interwell tracers to calculate saturation and swept volumes in oil reservoirs", *SPE/DOE Symposium on Improved Oil Recovery, Tulsa, Oklahoma, 17 - 21 April 2004*.

[7] Nguyễn Hồng Phan, Nguyễn Hữu Quang, Tô Bá Cường, Huỳnh Thị Thu Hương, và nnk, "Phát triển mô hình mô phỏng quá trình vận động của các chất chỉ thị tự nhiên (NPIT) để đánh giá trữ lượng dầu trong khai thác", Viện Năng lượng Nguyên tử Việt Nam.

[8] Huỳnh Thị Thu Hương, Lê Thanh Tài, Nguyễn Hữu Quang, and Lê Văn Sơn, "Determination of contribution proportion of injection wells in oil production by interwell tracer method using partitioning organic compounds

from crude oil", *Petrovietnam Journal*, Vol. 6, pp. 24 - 29, 2019.

[9] Tô Bá Cường, Nguyễn Hồng Phan, and Nguyễn Hữu Quang, Interwell tracer method using partitioning compounds naturally existing in crude oil for determination of residual oil saturation, *Petrovietnam Journal*, Vol. 10, pp. 38 - 43, 2016.

[10] Olaf Huseby, A.Haugan, J.Sagen, Jiri Muller, Barry Bennett, S.R.Larter, Eustathios S.Kikkinides, A.K.Stubos, Faraz Yousefian, Jean-Francois Thovert, and P.M.Adler, "Transport of organic components from immobile and bypassed oil in porous media", *Applied Chemical Engineering*, Vol. 49, No. 5, pp. 1085 - 1094, 2003. DOI: 10.1002/aic.690490504.

[11] Center for Petroleum and Geosystems Engineering, University of Texas, "Reservoir engineering research program. Volume II: Technical documentation for UTCHEM - 9.0 - A three-dimensional chemical flood simulator", 2000. [Online]. Available: http://www.xn--oy2b1712qo85afq62g.kr/download/gms/UTCHEM_Tech_Doc.pdf.

COMPARATIVE ANALYSIS OF FINANCIAL ASSURANCE INSTRUMENTS FOR OIL AND GAS DECOMMISSIONING AND MINE RESTORATION

Le Thi Huyen

Petrovietnam University

Email: huyenlt@pvu.edu.vn

<https://doi.org/10.47800/PVJ.2021.06-04>

Summary

This paper introduces how different bonding mechanisms for oil and gas decommissioning and mine restoration can ensure operators' accomplishment of restoration/decommissioning liability and affect their budget. Four mechanisms presented and compared herein include surety bonds, cash collateral bonds, decommissioning and abandonment provisions, and lease-specific abandonment accounts.

The author also provides some cautions and recommends amendments for each mechanism to be efficiently applied to oil and gas decommissioning in Vietnam so as to assure operators' decommissioning duties without discouraging their potential investments.

Key words: Financial assurance, bonding mechanisms, decommissioning, restoration.

1. Introduction

In an oil and gas or a mining project, decommissioning¹ or restoration² occurs at the closure phase³ when extraction or production operations terminate. Since no more revenues are created, financial assurance mechanisms aim to provide adequate funds for such work [2]. Lessons show that there are many cases where unplanned and premature closures occurred [4] and financial assurance is particularly helpful in such cases, whether in the mining industry or the oil and gas industry [5, 6]. Therefore, selecting a financial assurance mechanism or a bonding approach that can ensure full restoration or decommissioning is crucial to the regulator. Meanwhile, given that bonds can restrict the operator's operating capital which reduces when the deposit amount is high [7], choosing a bond instrument that does not discourage the operator's investment and simultaneously assures their compliance is not less critical to any regulator. Given such context, this paper aims to address three key questions: (i) how different types of bond instruments guarantee fulfillment of restoration/decommissioning liability, (ii)

how they affect the operator's budget, and (iii) which type of bond instruments is most effective in ensuring the operator's compliance without highly discouraging their investment?

Vietnam has a great potential of oil and gas resources. In 2017, Vietnam's crude oil reserves were 4.4 billion barrels, ranking third in Asia, after China and India and could be enhanced in the future since the country's waters were largely unexplored [8]. However, as in other regions, many offshore oil and gas fields in Vietnam are reaching the end of their productive lives [9, 10] and hence will be decommissioned soon. In addition, any offshore platforms will be eventually decommissioned. Therefore, timely amendment for improvement of Vietnam's legislation on oil and gas decommissioning to be applied to existing projects and new ones is critical. With recommendations for Vietnam's relevant legislation, this research contributes to ensuring sufficient financial guarantee funds for full oil



Date of receipt: 2/7/2020. Date of review and editing: 2 - 29/7/2020.

Date of approval: 11/6/2021.

¹ The research uses the term "decommissioning" to refer to the process that contains all activities related to removing and disposing offshore platforms [1].

² The research uses the term "restoration" to refer to the activities that repair mined land and are undertaken after mining operations (extraction) cease as part of the mining project.

³ The life cycle of a mine comprises eight phases: design, exploration, permitting, construction, operations, decommissioning/closure, post-closure and relinquishment [2]. Likewise, an oil and gas project life consists of six phases which are lease, exploration, development, production, closure and post-closure [3].

and gas decommissioning throughout the project life without discouraging operators' investments.

2. Methods

This research is the continuation of the study of Ferreira and Suslick [1, 5, 11-13] regarding different bonding regimes for offshore decommissioning. Ferreira and his colleagues focused on evaluating the effects of alternative bond options on the operator's net present value (or payoff) and the government earnings in hypothetical oil-producing projects in the Brazilian Continental Shelf [5]. Whereas this research focuses on the extent to which different bond approaches can assure full decommissioning or restoration work to be delivered without discouraging the operator's investment. This research also differs from Ferreira and Suslick's study in terms of methodological approach. Ferreira and Suslick applied a financial valuation model for bonding approaches based on discounted cash flow and sensitivity analyses for the hypothetical oil-producing projects [5]. Differently, this research compares different bonding mechanisms as specified in Vietnam's legislation, Ferreira and Suslick's scenarios, and the literature. The effects of some bonding mechanisms on operators and the government are contextualised in oil field X in Vietnam and three opencast coal mines in East Ayrshire, Scotland.

Four types of data were collected for the research, comprising documentation, two informal conversations and a telephone conversation. Data about oil field X was collected between March 2019 and July 2020. Whereas data about three opencast coal mines in East Ayrshire, Scotland, were collected from March 2016 to April 2018 as part of the data for the author's PhD study and all such data were documented.

3. Overview of bonding mechanisms

Liability risks can be decreased by bonding mechanisms in respect of: (i) creating impetus for complying with contract requirements; (ii) indemnifying the government and taxpayers sensibly from failure; and (iii) providing environmental protection against possible damages due to not implementing appropriate closure activities [13]. Bonding mechanisms can be in the form similar to insurance policies (surety bonds), the form of an upfront fund that covers full restoration/decommissioning costs at the project approval stage (cash collateral bonds), the form of fund paid in annual portions during the project life (decommissioning and

abandonment provisions), or the form of an account within a specified period (lease-specific abandonment accounts) [1, 5, 11, 14]. The followings are an overview of these financial assurance instruments.

3.1. Surety bonds

In the context of the mining industry and the oil and gas industry, surety bonds are agreements among three parties: the operator who is required to undertake site restoration/decommissioning as approved by the government, the government who must ensure the accomplishment of restoration/decommissioning work and a surety company who guarantees the availability of funds for restoration/decommissioning work irrespective of the operator's financial capacity [7, 15]. Surety bonds have been favoured by a number of mining companies because of the relatively small payments required [16].

Since the surety company's responsibility is limited to the insured amount, the bond value may not fully cover the decommissioning cost [15]. In addition, surety bonds are maintained by operators' annual premiums [1] which are not aimed to pay for losses to the same level as traditional insurance premiums because in fact, a great amount of the premiums for surety bonds are underwriting fees [15]. Furthermore, unlike insurance policies, of which premiums are calculated to cover anticipated payments, surety bonds are issued based on credit worthiness principles: If there is higher financial uncertainty given the operator's reputation, the surety issuer may charge a higher premium [7]. Then it is important that the government must precisely calculate the bond value and strictly monitor it during the project life to ensure its sufficiency for the entire restoration/decommissioning work. Another problem is that if the operator goes into liquidation, the surety company may not have to pay out the whole value of the bond, but they will never have responsibility for the exceeding value [15]. Therefore, effective negotiations with surety company are essential for the government's success in securing the whole bond value.

3.2. Cash collateral bonds

Cash collateral bonds can be in the form of letters of credit, certificates of deposit, cash or real property and are the least preferred option for mining companies since they require huge expenditures [16]. In this mechanism, an amount of cash equivalent to the whole restoration/decommissioning cost is deposited upfront with a

governmental agency or to an insured bank account [1, 14]. The interest earned from the account is either added to the bond value or returned to the operator [14]. The operator is not allowed to utilise the deposited cash to undertake the required work and can only receive it back when the work completes [1].

3.3. Decommissioning and abandonment provisions

Under the decommissioning and abandonment provision mechanism, the total decommissioning cost is paid by the operator in annual portions throughout the field's life cycle or producing life [1, 17, 18]. Different from cash collateral bonds, the fund collected in this mechanism can be used by the operator to implement the required work [1]. As the name suggests, this mechanism is used in the oil and gas industry and although its application to the mining industry has not been found in the literature, it can be understood similarly.

3.4. Lease-specific abandonment accounts

Different from the decommissioning and

abandonment provisions, the lease-specific abandonment account approach requires the operator to pay the decommissioning cost within four years since production or by the start of the year when the operator is expected to have produced 80% of the economically recoverable reserves, whichever is earlier; the first payment is equivalent to 50% of the total bond value [5, 12]. This approach only applies to the field's producing life [12]. Like cash collateral bonds, this mechanism requires operators to use out-of-pocket funds to cover decommissioning activities and the deposited cash is only returned to operators upon completion of the required activities [5]. Similar to the decommissioning and abandonment provisions, the literature review does not show whether this approach has been utilised in the mining industry; however, it can have similar application.

4. Results

4.1 Surety bonds

Surety bonds are more advantageous to operators than cash collateral bonds in the aspect that the operators

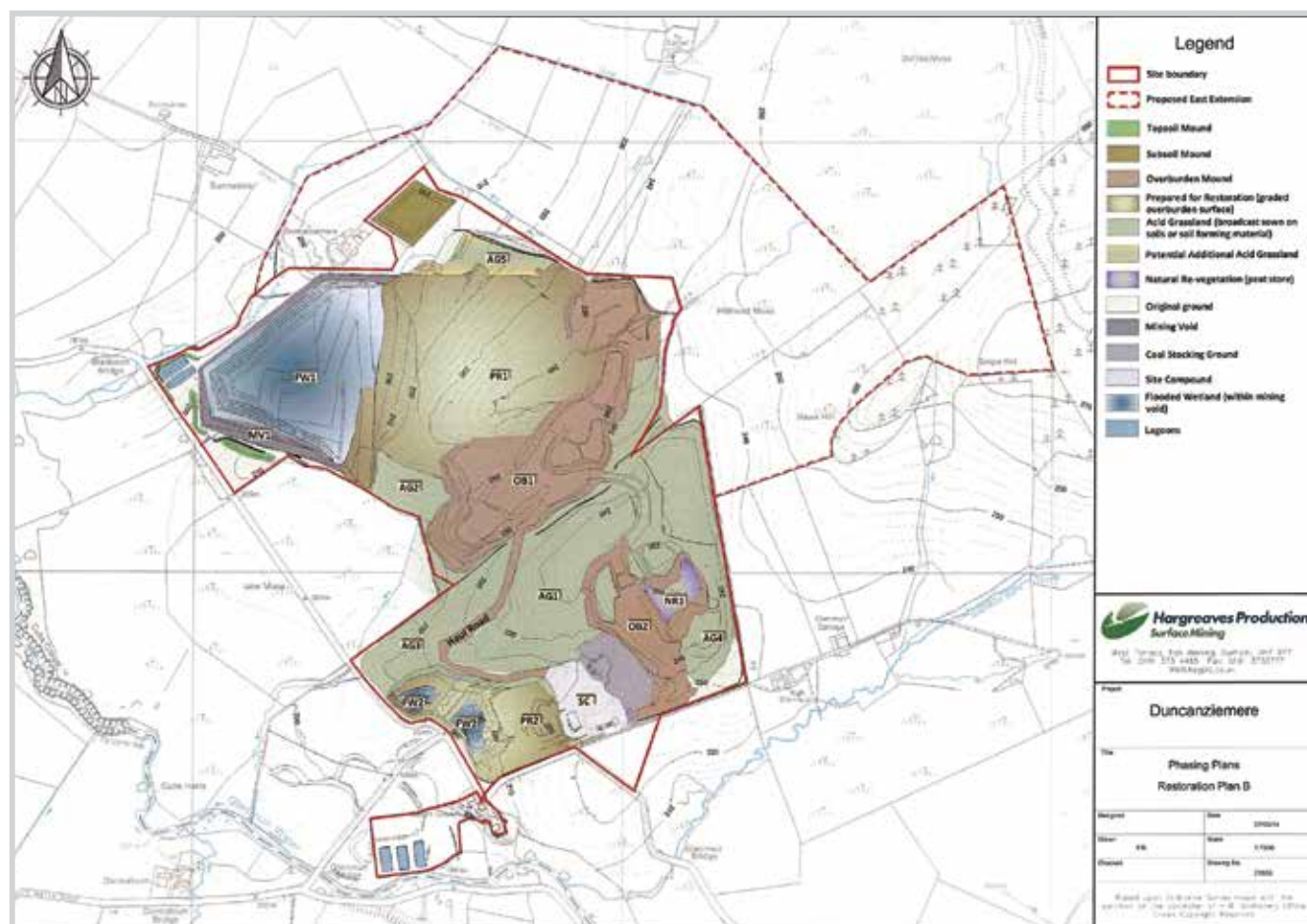


Figure 1. Restoration Plan B for Duncanziemere complex in 2014 [29].

do not have to pay for a large upfront fund [1]; if being calculated precisely and monitored strictly, they are more beneficial to regulators than the decommissioning and abandonment provisions because if the operators go bankrupt at some point in the project life, the regulators will be paid by the surety company for full restoration/ decommissioning work. Experience from Dunstonhill Surface Mine (Dunstonhill), Duncanziemere Surface Mine (Duncanziemere) and Netherton Surface Mine (Netherton) - three opencast coal mines in East Ayrshire, Scotland, showed that calculating and monitoring surety bonds are critical.

Dunstonhill, Duncanziemere and Netherton were operated by Scottish Coal (Dunstonhill) and Aardvark (Duncanziemere and Netherton) after being granted planning permissions on 29 March 2010, 30 March 2011 and 19 October 2010 respectively [19 - 21]. Nevertheless, Scottish Coal went into liquidation on 19 April 2013 and the same situation happened to Aardvark on 16 May 2013 [22]. In order to be granted planning permissions for the sites, the mining companies were required to lodge restoration and aftercare bonds at the planning stage to ensure fulfilment of the restoration and aftercare obligations as specified in the Section 75 Agreements [20 - 22]. Those restoration and aftercare bonds are surety bonds [23 - 26]. Dunstonhill was provided with a restoration bond valued at GBP 4.2 million and an aftercare bond worth GBP 0.377 million [22] whereas Duncanziemere and Netherton were granted restoration bonds of GBP 2.6 million and GBP 4.5 million respectively [21, 22]. However, at the time of the operators' liquidation, the estimated costs for restoring the sites according to the original restoration plans would be GBP 10.241 million, GBP 6.593 million, and GBP 11.811 million respectively [22]. Those wide gaps between the bond values and the restoration costs were caused by East Ayrshire Council's failures in calculating and monitoring the bonds at the planning stage and during the operations phase [27]. For example, the schedule of restoration and aftercare liabilities for Dunstonhill related the bond quantum to specific time periods [23]. However, no compliance monitoring was executed after the signing of the Section 75 Agreement, particularly by an independent mining engineer (who should be appointed by the Council) to guarantee the operational and restoration works on site were pursuant to the approved scheme and hence could make any necessary adjustment to the bond quantum for sufficient coverage of the outstanding restoration

work [27]. Especially, the Council's lack of monitoring led to the bond for Duncanziemere having expired without being replaced by Aardvark [28] and it became unsecured due to not having been called in by the Council before its expiry [29].

The cases of Dunstonhill and Netherton also showed negotiations with bond providers are crucial for securing bond values. After the liquidation of Scottish Coal and Aardvark, East Ayrshire Council had a lot of challenges in this regard. In relation to Netherton, the bond provider made the final offer of GBP 3.96 million, equivalent to 88% of the maximum value of the bond after some negotiations with the Council [30]. Regarding Dunstonhill, given the potential decreases of the restoration bond values, the Council managed to call in the bond prior to the expiry dates [31]. The first bond call was repudiated by the bond provider who, after the second call, only agreed to present a cumulative offer of GBP 6 million for Dunstonhill and Ponesk (another opencast coal site in East Ayrshire - the author) [32, 33]. This means the original bond value for Dunstonhill was reduced by GBP 1.2 million.

4.2 Decommissioning and abandonment provisions

The financial assurance instrument currently applied to the oil and gas industry in Vietnam can be categorised as decommissioning and abandonment provision. Particularly, oil operators in Vietnam shall, within one year since the production of the first oil and gas flow, establish a financial guarantee fund to which annual payments shall be made according to the previous formula:

$$Payment\ level = \frac{\begin{matrix} The\ production\ within\ the\ year \\ \times\ (Total\ decommissioning\ cost \\ -\ The\ paid\ balance) \end{matrix}}{Remaining\ recoverable\ reserves} \quad [34]$$

or the present formula:

$$E_n = \frac{A_n \times (B_n - C_{(n-1)} - I_{(n-1)})}{D_n}$$

in which:

- E_n : The level of payment in the year n; the calculation unit is USD.
- A_n : The production in the year n, defined by the actual production in the respective year; the calculation unit is barrel of oil equivalent.
- B_n : The total decommissioning cost updated in the year n, $B_n = (b_1 - b_2)$, in which:

+ b_1 : The total decommissioning cost estimated in the (most recently approved) decommissioning plan; the calculation unit is USD.

+ b_2 : The cost estimate defined in the (most recently approved) decommissioning plan corresponding to the equipment, property or structure decommissioned up to the year (n-1); the calculation unit is USD.

- $C_{(n-1)}$: The balance of the financial guarantee fund on December 31st of the year (n-1), defined by the total balance of all the bank accounts to which PVN sends the financial guarantee fund of the respective field, and certified in writing by the relevant commercial banks; the calculation unit is USD.

- $I_{(n-1)}$: The profit from the savings accounts received by organisations and individuals after PVN, on behalf of them, fulfils all the duties to the national budget (if any) for the year (n-1).

- D_n : The remaining recoverable reserves, $D_n = d_1 - d_2$, in which:

+ d_1 : The recoverable reserves defined in the economic development plan or the early production plan already approved by authorities up to the end of the year n; the calculation unit is barrel of oil equivalent.

+ d_2 : The total production accumulated from the relevant field(s) up to the year (n-1); the calculation unit is barrel of oil equivalent [35].

Following the above-mentioned formulas, operators only deposit in the financial guarantee fund part of the decommissioning cost during the project life. This could lead to financial burdens on taxpayers if the operators go into liquidation [1]. Therefore, the mechanism does not ensure the compliance [1] as the operators may choose to liquidate at some point of the project to avoid the remaining financial liability if the field production does not compensate for the decommissioning cost.

Slightly different from the Brazilian hypothetical cases where no interest would be earned from the fund [1], pursuant to Vietnam's legislation, interest will be earned and added to the fund after all financial duties to the Government of Vietnam have been fulfilled [34, 35]. This helps reduce the financial burden on the operator as their actual total payment is less than the total decommissioning cost. Particularly, PVN will deposit the fund in a separate interest-bearing account in a stable credit institution in Vietnam [34, 35]. PVN will

transfer part of the fund to the operator for undertaking decommissioning activities if being called during the project life [35]. If the decommissioning work is not implemented wholly or partially by the operator, PVN can use the fund for fulfilling the work [34, 35].

4.3 Cash collateral bonds

Compared to surety bonds and decommissioning and abandonment provisions, cash collateral bonds are likely the most reliable approach to ensure full restoration/decommissioning work to be undertaken. This is because operators have to deposit an amount of money equal to full restoration/decommissioning cost in an escrow account in advance and the government completely controls such account until the bond is released after the completion of the required operations [1]. This was probably the reason why East Ayrshire Council chose this bonding approach for Duncanziemere after the liquidation of the previous operator. Particularly, the Council approved another mining company to extract the remaining coal and restore the site to a revised restoration plan but required such mining company to deposit in advance a sufficient amount of money into an escrow account which would be used if they did not fulfil the task [29].

However, the problem of cash collateral bonds is that the operators have to pay in advance (prior to extraction/production) for an upfront fund which covers the whole restoration/decommissioning work and cannot be used by the operators for implementing restoration/decommissioning activities. This means the operators must pay double for restoration/decommissioning activities during the project life, which requires large capital and is not attractive to investors. Investments from large companies like mining ones are important for the local and regional areas. For example, the development at Dunstonhill would create totally 276 jobs including indirect jobs through offering or retaining about 120 jobs for directly employed staff and continuing support for local businesses [36]. The development at Duncanziemere would provide 36 jobs and sustain indirect employment in supplying mechanical, engineering and fleet services to opencast sites [37]. Meanwhile, Netherton would provide or retain about 110 direct jobs [38] and support indirect employment for local subcontractors, trades and small businesses related to the site operations and coal haulage [40]. In fact, all the mines are located in rural areas where the unemployment rates were high [37, 38, 40 - 42] and most of the employees were expected to reside within

15 kilometres of the site or within East Ayrshire [36, 37, 39]. Therefore, such job provision was considered to contribute substantially to the local economies [37, 38, 43, 44]. Likewise, the oil and gas industry can play an important role in the economic development of a region or even a nation. Tremendous investment activities in oil and gas exploration and production have made Vung Tau - the oil and gas hub of Vietnam - become a prosperous city and contribute significantly to the nation's economy [45]. Between 2006 and 2015, PVN made an average annual contribution of 20 - 25% of the total national budget and 18 - 25% of the GDP [46]. Since 2015, despite facing many difficulties, PVN has still contributed about 9 - 11% of the total national budget and 10 - 13% of the GDP annually [46].

4.4 Lease-specific abandonment accounts

Another approach mentioned by Ferreira and Suslick [5] that has not been applied in the oil and gas industry in Vietnam and the mining industry in Scotland is lease-specific abandonment account. This approach seems to be beneficial to both regulators and operators.

For regulators, it is assured that, by the end of the maximum 4-year period since production, they have held the fund that can cover all required decommissioning activities. It is safer than the decommissioning and abandonment provision approach if the production lasts more than 4 years and much safer than surety bonds though a bit riskier than cash collateral bonds. Although there may be cases where the operator is insolvent before the fourth year, the regulator is assured to have held at least half of the total decommissioning cost from the initial payment, which, following Vietnam's legislation, must be fulfilled within one year since the first oil and gas production [34, 35] instead of an undefined date within 4-year time in the Brazilian hypothetical context [5]. Again, this approach is safer than the decommissioning and abandonment provision if the production lasts more than 2 years, much safer than surety bonds and safe by half of the cash collateral bond mechanism.

For operators, this mechanism is more advantageous than the cash collateral bond approach in the aspect that their initial payment does not have to cover the whole decommissioning cost. However, compared to

the decommissioning and abandonment provision and surety bond options, it is less advantageous. If the project lasts 10 years, their annual payments to the fund are spread over the project life in the former and thus the total payment within 4 years is much less than the total decommissioning cost; whereas their annual premiums for 4 years to maintain the bond in the latter are even much lower than the total decommissioning cost⁴.

5. Discussion

Given the problems associated with surety bonds, the author does not recommend this approach to oil and gas decommissioning in Vietnam. Surety bonds only serve as a form of financial guarantee and operators still have to pay for their restoration/decommissioning activities on their own [1]. If the operator is solvent to complete the task, the bond will be released and the premium payment will be terminated. On the contrary, the bond issuer will finance restoration/decommissioning activities [1]. This explains firms' choice of going into liquidation when seeing that they would not be able to produce adequate profits to fund the required work like the cases of Scottish Coal and Aardvark in East Ayrshire, Scotland in 2013. In addition, the bond issuer will not have to pay the whole bond value and the experiences in East Ayrshire show that negotiations with bond issuers to reclaim the maximum bond value is very challenging.

The cases of opencast coal mines in East Ayrshire also showed what mining companies would do to avoid restoration liabilities. After the liquidation of Aardvark, two companies namely OCCW (Duncanziemere) Limited and OCCW (Netherton) Limited, which were actually hived down from the interest of Aardvark, were set up to continue coaling operations at Duncanziemere and Netherton and undertake the remaining restoration liabilities [47]. It should be noted that these liabilities addressed the revised restoration schemes only, which are at lower levels than the original ones [21, 29]. The situation seems to be similar in the oil and gas industry because small spurious firms can be set up from big ones to circumvent decommissioning obligations if no stringent financial guarantee regime is in place [5].

As aforementioned, the decommissioning and abandonment provision approach has been

⁴This comparison only considers annual premiums of which the rates in the offshore surety industry are often between 1 and 3% but can be up to 5% of the covered loss [15]. There might be cases where operators also have to collateralise 100% of the bond to keep the bond in place [15].

applied to decommissioning of oil and gas projects in Vietnam. This approach is more advantageous to operators than cash collateral bonds and lease-specific abandonment accounts in the aspect that they can pay the decommissioning fund in annual portions over the project's or the field's lifetime. For regulators, while this approach can avoid the issues associated with securing bond money if the operators go into liquidation under the surety bond option, it does not ensure compliance of full financial liability until the end of the project as mentioned earlier. In the case of oil field X developed by Truong Son Joint Operating Company (Truong Son JOC) from 24 November 2008 and then by Petrovietnam Exploration Production Corporation (PVEP) since 24 November 2013 [48, 49], the financial liability was entirely fulfilled by the previous operator. Particularly, Truong Son JOC, before handing over the field in 2013, had revaluated the financial guarantee fund and added to the fund to ensure its adequacy for decommissioning operations, given the early cessation of the Production Sharing Contract⁵. Doing this way, Truong Son JOC complied with Article 20 of Decision 40/2007/QĐ-TTg which requires that within one year before the end of the petroleum contract or the expiry of the petroleum production period, operators must recalculate the financial guarantee fund and must add to the fund if it is not sufficient for decommissioning [34]. While in Vietnam so far there have never been cases of oil companies liquidating to avoid decommissioning liability and apart from laws, there would be contractual terms binding operators' liability, the potential deficiency of decommissioning funds during the project life under this bonding mechanism should be paid attention to by Vietnamese regulators. Additionally, since the fund deposited by the operator during the project life will be managed by PVN [34, 35], administrative issues will arise and need to be handled by the Group diligently.

Regarding cash collateral bonds, while the upfront fund shall be paid by the operator prior to coal extraction or oil and gas production as in the Scottish and Brazilian cases respectively, it can be paid within one year since the production of the first oil and gas flow following Vietnam's legislation for the timing of establishing the financial guarantee fund [34, 35]. This is quite sensible to regulators because under the current law, projects which are determined during the exploration phase to be

unnecessary or unused for future petroleum activities must be decommissioned within this phase and the operators do not have to pay for a financial guarantee fund in such cases [35]. In addition, requiring the operators to pay for the financial guarantee fund within one year since the first oil and gas production is more attractive to investors since it gives them more time to accumulate profits from the project. However, there is a risk of noncompliance if the operators liquidate just within this period.

Similar to the decommissioning and abandonment provisions, if the cash collateral bond approach is applied to oil and gas decommissioning in Vietnam, it can be amended such that the upfront funds can be used by the operators to implement decommissioning activities during the project life upon calling PVN. Moreover, interest earnings from the upfront fund should be returned to the operator annually like in the Brazilian cases [1] to support its capital needs. These help reduce financial burdens on the operator and thus also attract more investment. Again, since the upfront fund will be managed by PVN in Vietnamese cases [34, 35], administrative issues will arise and need to be resolved diligently by the Group. Furthermore, compliance monitoring must be undertaken stringently by the Government in collaboration with PVN to ensure the money withdrawn from the upfront fund equates to the decommissioning work carried out by the operator on site.

Whereas, like cash collateral bonds, if the lease-specific abandonment account approach is applied to oil and gas decommissioning in Vietnam, it can be amended so as the money in the account can be utilised by the operator to undertake the decommissioning work during the project process upon calling PVN. Also, interest earnings from the account can be returned to the operator yearly like in the Brazilian cases [5] to support its capital needs. These will also help attract more investment from the operators. Again, similar to the decommissioning and abandonment provision and cash collateral bond options, the account will be managed by PVN in Vietnamese cases [34, 35], therefore, the Group needs to be diligent in dealing with administrative issues arising. Also, the Government in collaboration with PVN must have strict compliance monitoring to make sure the money withdrawn from the account corresponding to the decommissioning work implemented by the operator on site.

⁵The production of the field X should have been ceased when Truong Son JOC terminated the Production Sharing Contract; however, PVEP, on behalf of PVN which was assigned by the Government of Vietnam, continued the operations of the field in order to maximise the oil extraction and thus does not have financial liability for the field decommissioning.



Figure 2. Large flooded hole with steep wall at Dunstonhill opencast coal mine in April 2013 after being abandoned.

So how about the existing oil and gas projects in Vietnam that have been operated for more than 10 or 20 years? Since the decommissioning and abandonment provision approach has been applied to them, the government in collaboration with PVN needs to check the balance of the financial guarantee fund for each project and monitors the site to assess the outstanding decommissioning liability. If the fund is inadequate for undertaking the outstanding work, the operator must add to the fund immediately or as soon as possible. This is especially important for projects executed via joint ventures or production sharing contracts between PVN and international firms since the latter may go into liquidation at any time. It is not only reasonable but also fair because the projects have lasted more than 10 or 20 years, bringing certain profits to the operators from oil sales.

6. Conclusions

The comparison of different bonding instruments with practices from the oil and gas industry in Vietnam and the opencast coal mining industry in Scotland shows the outbalance of each instrument to the government and the operators.

Cash collateral bonds are most advantageous to the government since they ensure the site is fully restored or decommissioned. Contrarily, this option is least advantageous to operators who have to make double payment for the restoration/decommissioning cost during the project life.

The second choice for the government should be the lease-specific abandonment account option because by the end of the fourth year, the government will have held the fund that can cover the total decommissioning cost.

For the operator, lease-specific abandonment accounts are more favourable than cash collateral bonds because the initial payment is equivalent to only half of the restoration/decommissioning cost.

The third desirable option for the government should be decommissioning and abandonment provisions. Getting annual moneys until the year when the operator goes in liquidation (if this is the case), it is more reliable for the government than the surety bond option in which they need to calculate the bond quantum precisely and monitor carefully throughout the project phases to ensure the bond money is adequate for the remaining restoration/decommissioning liability. The operator is more advantageous with this option than with the cash collateral bonds and lease-specific abandonment accounts since they can pay the decommissioning fund in annual portions over the whole project life or the field's producing life.

Among the four options, surety bonds are least reliable to the government due to issues associated with bond securing while the operator may not undertake the required restoration/decommissioning during the project life and go into liquidation near the end of the project to avoid using their out-of-pocket funds in addition to the annual premiums to maintain the bond to cover restoration/decommissioning activities. However, if the government is successful in bond securing, they are more advantageous than under the decommissioning and abandonment provision approach due to being paid by the surety company for the exact outstanding restoration/decommissioning liability in case the operator becomes insolvent at some point of the project life. On the contrary, the operator is most advantageous under this approach. Clearly, with this approach, the operator does not have to pay either an upfront fund equal to the total restoration/decommissioning cost like with the cash collateral bonds or payments equating to the total restoration/decommissioning cost within four years or an initial payment equivalent to half of the restoration/decommissioning cost like with the lease-specific abandonment accounts. If the project lasts more than 10 years and the operator chooses to liquidate just after the fourth year of production/extraction, the annual premiums to keep the bond in place within four years are much lower than the annual payments out of the total restoration/decommissioning cost and thus the operator is more beneficial than with

the decommissioning and abandonment provision approach.

If the afore-mentioned bond instruments are applied to oil and gas decommissioning in Vietnam, some amendments need to be considered. Cash collateral bonds and lease-specific abandonment accounts will become more advantageous to the operator if the upfront fund in the former and the money in the account in the latter can be used by the operator to carry out decommissioning activities during the project and any interest earnings can be returned to the operator annually to support its capital needs. In addition, the upfront fund for cash collateral bonds and the initial payment for lease-specific abandonment accounts can be deposited within one year since the production of the first oil and gas. Regarding the decommissioning and abandonment provision approach which has been applied to oil and gas decommissioning in Vietnam, the Government should be cautious of the potential deficiency of decommissioning funds if operators go into liquidation at some point within the project life. For all those types of bond instruments, the Government in collaboration with PVN needs to monitor operators' compliance stringently to ensure the money withdrawn from the financial guarantee fund is equivalent to the decommissioning work execution. Furthermore, as the manager of the financial guarantee fund, PVN needs to deal with any arising administrative issues diligently.

Acknowledgement

This work was funded by Petrovietnam University under grant code GV1903.

References

- [1] D.F. Ferreira and S.B. Suslick, "A new approach for accessing offshore decommissioning: A decision model for performance bonds", *SPE International Conference on Health, Safety, and the Environment in Oil and Gas Exploration and Production, Stavanger, Norway, 26 - 28 June, 2000*. DOI: 10.2118/61219-MS.
- [2] World Bank Multistakeholder Initiative, "Towards sustainable decommissioning and closure of oil fields and mines: A toolkit to assist government agencies". 2010.
- [3] Silvana Tordo, *Fiscal systems for hydrocarbons: Design issues*. World Bank, 2007.
- [4] Alison Leigh Browne, Daniela Stehlik, and Amma

Buckley, "Social licences to operate: for better not for worse; for richer not for poorer? The impacts of unplanned mining closure for "fence line" residential communities", *Local Environment*, Vol. 16, No. 7, pp: 707 - 725, 2011. DOI: 10.1080/13549839.2011.592183.

[5] D.F. Ferreira and S.B. Suslick, "Identifying potential impacts of bonding instruments on offshore oil projects", *Resources Policy*, Vol. 27, No. 1, pp. 43 - 52, 2001. DOI: 10.1016/S0301-4207(01)00007-1 .

[6] P.H. Whitbread-Abrutat, A.D. Kendle, and N.J. Coppin, "Lessons for the mining industry from non-mining landscape restoration experiences", *Mine Closure 2013*, Australian Centre for Geomechanics, pp. 625 - 640, 2013. DOI: 10.36487/ACG_rep/1352_52_Whitbread-Abrutat.

[7] David Gerard, "The law and economics of reclamation bonds", *Resources Policy*, Vol. 26, No. 4, pp. 189 - 197, 2000. DOI: 10.1016/S0301-4207(00)00033-7.

[8] U.S. Energy Information Administration, "Vietnam". [Online]. Available: <https://www.eia.gov/international/analysis/country/VNM>.

[9] D. Burdon, S. Barnard, S.J. Boyes, and M. Elliott, "Oil and gas infrastructure decommissioning in marine protected areas: System complexity, analysis and challenges", *Marine Pollution Bulletin*, Vol. 135, pp. 739 - 758, 2018. DOI: 10.1016/j.marpolbul.2018.07.077.

[10] Vietnam News, "PVN sets target of adding up to 30m tonnes to oil reserves", 15/3/2019. [Online]. Available: <https://vietnamnews.vn/economy/507134/pvn-sets-target-of-adding-up-to-30m-tonnes-to-oil-reserves.html>.

[11] D.F. Ferreira and S.B. Suslick, "Financial assurance bonds: An incentive mechanism for environmental compliance in the oil sector", *SPE International Conference on Health, Safety and Environment in Oil and Gas Exploration and Production, Kuala Lumpur, Malaysia, 20 - 22 March, 2002*. DOI: 10.2118/74025-MS.

[12] Doneivan F. Ferreira, Saul B. Suslick, and Paula C.S.S. Moura, "Analysis of environmental bonding system for oil and gas projects", *Natural Resources Research*, Vol. 12, No. 4, pp. 273 - 290, 2003. DOI: 10.1023/B:NARR.0000007806.90842.8f.

[13] Doneivan Ferreira, Saul Suslick, Joshua Farley, Robert Costanza, and Sergey Krivov, "A decision model for financial assurance instruments in the upstream petroleum sector", *Energy Policy*, Vol. 32, No. 10, pp. 1173 - 1184, 2004. DOI: 10.1016/S0301-4215(03)00080-6.

[14] Katherine Lynn Baker, *Costs of reclamation on Southern Appalachian Coal Mines: a cost-effectiveness analysis for reforestation versus hayland/pasture reclamation*. Virginia Polytechnic Institute and State University, 2008.

[15] Mark J. Kaiser, Brian F. Snyder, "Supplemental bonding in the Gulf of Mexico: the potential effects of increasing bond requirements", *International Journal of Oil, Gas and Coal Technology*, Vol. 2, No. 3, pp. 262 - 279, 2009.

[16] Ryan Yonk, Josh.T. Smith, and Arthur R. Wardle, "Exploring the policy implications of the surface mining control and reclamation act", *Resources*, Vol. 8, No. 1, pp. 1 - 18, 2019. DOI: 10.3390/resources8010025.

[17] Flávia Kaczelnik Altit and Mark Osa Igiehon, "Decommissioning of upstream oil and gas facilities", *Proceedings of the 53rd Annual Rocky Mountain Mineral Law Institute, The Rocky Mountain Mineral Law Foundation, 2007*. [Online]. Available: http://content.schweitzer-online.de/static/catalog_manager/live/media_files/representation/zd_std_orig__zd_schw_orig/000/046/457/9781905783236_content_pdf_1.pdf.

[18] F. Jahn, M. Cook, and M. Graham, "Chapter 18: Decommissioning", *Developments in Petroleum Science*, Vol. 55, pp. 419 - 425, 2008. DOI: 10.1016/S0376-7361(07)00018-0.

[19] East Ayrshire Council, "Planning permission for application Ref. 09/0511/PP dated 30 March 2011", *Planning Application Ref. 09/0511/PP, East Ayrshire Council, 2011*. [Online]. Available: <http://eplanning.east-ayrshire.gov.uk/online/applicationDetails.do?activeTab=documents&keyVal=KMPQAYGF01B00>.

[20] East Ayrshire Council, "Planning enforcement notice for Dunstonhill site opencast coal mine, near Patna", 2/4/2015.

[21] East Ayrshire Council, "Planning enforcement notice for Netherton opencast coal mine, Skares", 2/4/2015.

[22] East Ayrshire Council, "Opencast mining in East Ayrshire - Steps to recovery", 19/9/2013.

[23] East Ayrshire Council, "Minute of agreement among East Ayrshire Council, The Scottish Coal Company Limited, SRG Estates Limited, the Scottish Ministers, and Diana Mary Wheeler", *Planning Application Ref. 08/0783/FL, East Ayrshire Council, 2010*.

[24] East Ayrshire Council, "Minute of variation of minutes of agreement among East Ayrshire Council, Aardvark TMC Limited, The Partners of and Trustees for the Firm of Young Brothers, The Dumfries Estate Trustees and The Scottish Ministers", *Planning Application Ref. 09/0891/PP, East Ayrshire Council, 2010.*

[25] East Ayrshire Council, "Minute of variation among East Ayrshire Council, ATH Resources Plc, Aardvark TMC Limited, and Denise Tait Chambers", *Planning Application Ref. 09/0511/PP, East Ayrshire Council, 2011.*

[26] East Ayrshire Council, "Decommissioning, restoration, aftercare and mitigation financial guarantees", 21/5/2014.

[27] Jim Mackinnon, Chris Norman, James Fowlie, "Report of Independent Review of regulation of opencast coal operations in East Ayrshire", East Ayrshire Council, 2014.

[28] East Ayrshire Council, "East Ayrshire Council response regarding the restoration bonds of Dunstonhill, Duncanziemere and Netherton", *Email communication to the author, 23/7/2018.*

[29] East Ayrshire Council, "Application Ref. 13/0865/PP at Duncanziemere Surface Coal Mine, Lugar by OCCW (Duncanziemere) Limited", 4/4/2014.

[30] East Ayrshire Council, "Update Report - Netherton Opencast coal site restoration bond", 13/8/2014.

[31] East Ayrshire Council, "Dunstonhill Opencast site restoration bond", 19/2/2014.

[32] East Ayrshire Council, "Update report - Dunstonhill and Ponesk Opencast coal site restoration bonds", 4/6/2014.

[33] East Ayrshire Council, "Update report - Dunstonhill and Netherton Opencast coal sites - Revised restoration schemes", 1/4/2015.

[34] Thủ tướng Chính phủ, *Quyết định về việc thu dọn các công trình cố định, thiết bị và phương tiện phục vụ hoạt động dầu khí*, Quyết định 40/2007/QĐ-TTg, 21/3/2007.

[35] Thủ tướng Chính phủ, *Quyết định về việc thu dọn các công trình, thiết bị và phương tiện phục vụ hoạt động dầu khí*, Quyết định 49/2017/QĐ-TTg, 21/12/2017.

[36] Scottish Coal Company Limited, "Dunstonhill Surface Mine – Amended Planning Application Supporting Statement & Supplementary Environmental Information", *Planning Application Ref. 08/0783/FL, East Ayrshire Council, 2009.*

[37] East Ayrshire Council, "Application Ref. 09/0511/PP: Proposed extension to Laigh Glenmuir Surface Mine, land at Duncanziemere, near Lugar, Cumnock by Aardvark TMC Limited", *Head of Planning and Economic Development to the Southern Local Planning Committee dated 27 May 2010, Planning Application Ref. 09/0511/PP, East Ayrshire Council, 2010.*

[38] East Ayrshire Council, "Application Ref. 09/0891/PP: Phased extraction of coal by surface mining methods with progressive restoration and ancillary works on land at Netherton, off Newfield road, near Cumnock by Aardvark TMC Limited", *Head of Planning and Economic Development to the Southern Local Planning Committee dated 25 June 2010, East Ayrshire Council, 2010.*

[39] SLR Consulting Limited, "Planning Application for Proposed Surface Mining Operations at Netherton, New Cumnock, East Ayrshire: Environmental Statement, Planning Statement and Pre-Application Consultation Report", *Planning Application Ref. 09/0891/PP, East Ayrshire Council, 2009.*

[40] East Ayrshire Council, "Application Ref. 08/0783/FL: Extraction of coal by surface mining methods with restoration to forestry, parkland, public access and nature conservation interests, Dunstonhill, Lethanhill, Patna by the Scottish Coal Company Limited", *Head of Planning and Economic Development to the Special Southern Local Planning Committee dated 17 December 2009, Planning Application Ref. 08/0783/FL, East Ayrshire Council, 2009.*

[41] East Ayrshire Council and East Ayrshire Health and Social Care Partnership, *Southern locality profile - Local outcome improvement plan summary needs assessment 2017*. The Community Planning Partnership, 2017.

[42] The Scottish Government, "Local area labour markets in Scotland: Statistics from the annual population survey 2013", 7/5/2014. [Online]. Available: <http://www.gov.scot/Resource/0044/00449714.pdf>.

[43] East Ayrshire Council, "Application Ref. 05/0232/FL: Proposed extraction of coal by opencast method, restoration of site and associated engineering works at Laigh Glenmuir farm, near Cumnock by ATH Resources plc", *Head of Planning, Development and Building Standards to the Development Services Committee dated 11 January 2006, Planning Application Ref. 05/0232/FL, East Ayrshire Council, 2006.*

[44] RPS Planning & Development, "Dunstonhill Surface Mine Environmental Statement - Chapter 5: Need,

Benefits & Socio-economic Impacts of the Development”, *Planning Application Ref. 08/0783/FL, East Ayrshire Council, 2008.*

[45] Petrovietnam Technical Services Corporation, “Vung Tau - A long-standing Vietnam oil and gas hub”, *Company News*, 2014.

[46] Petrovietnam, “Tập đoàn Dầu khí Quốc gia Việt Nam: 44 năm đồng hành, phát triển cùng đất nước, 2019”, [Online]. Available: <http://www.pvn.vn/Pages/detail.aspx?NewsID=a20f8571-5483-491a-80df-3fbd808cd5c5>.

[47] Hargreaves Services PLC, “Acquisition of assets from Aardvark”, 16/5/2013. [Online]. Available: <https://>

www.investegate.co.uk/hargreavesservsplc--hsp-/rns/acquisition-of-assetsfromaardvark/201305160700118376E/.

[48] Viện Dầu khí Việt Nam (VPI), “Chương trình quản lý an toàn dự án vận hành mỏ X”, 2017.

[49] Tổng công ty Thăm dò Khai thác Dầu khí, “Biện pháp phòng ngừa và ứng phó sự cố hóa chất công trình mỏ X”, 2015.

[50] Lê Thị Huyền, “So sánh các cơ chế bảo đảm tài chính cho công tác thu dọn mỏ dầu khí ngoài khơi và phục hồi môi trường mỏ khoáng sản”, *Tạp chí Dầu khí*, Số 11, tr. 56 - 65, 2020.

AN OVERVIEW OF THE GASOHOL MARKET IN VIETNAM, THE NEXT DIRECTION?

Nghiem Thi Ngoan, Dao Minh Phuong, Pham Ba Nam

Vietnam Petroleum Institute

Email: ngoannt@vpi.pvn.vn

<https://doi.org/10.47800/PVJ.2021.06-05>

Summary

To ensure energy security, reduce greenhouse gas emissions and increase agricultural output, the Vietnamese government has issued several policies to promote gasohol, resulting in remarkable achievements in gasohol development in recent years. However, unexpected limitations have been seen by other countries after a period of using this fuel such as air pollution, threats to food security, deterioration of natural forest area and severely depleted freshwater resources. This paper presents an overview of the current state of Vietnam's gasohol market and a brief analysis of policy, supply - demand - price information, from which some hindrances are identified and a few more optimistic directions to develop this type of fuel in the future are proposed.

Key words: Gasohol, ethanol, feedstock.

1. Current status of gasohol development in Vietnam

1.1. Gasohol related policies

With the objectives of ensuring energy security, protecting the environment, reducing greenhouse gas emissions and stabilising agricultural product output, on 20 November 2007, the Prime Minister issued Decision No. 177/2007/QĐ-TTg approving the scheme for developing biofuels up to 2015 with a vision to 2025 (hereinafter referred to as "the Scheme"), aiming to increase bioethanol and vegetable oil production to 250 thousand tons by 2015 and 1.8 million tons by 2025. To implement the Scheme, on 22 November 2012, the Prime Minister signed Decision No. 53/2012/QĐ-TTg to promulgate a roadmap to apply the ratio of blending biofuels and traditional fuels (hereinafter referred to as "the Roadmap") with some main targets as follows:

For E5 gasoline:

- From 1 December 2014, gasoline to be produced, blended, and traded for consumption by road motor vehicles in the provinces and cities of Hanoi, Ho Chi Minh City, Hai Phong, Da Nang, Can Tho, Quang Ngai, and Ba Ria - Vung Tau would be E5.

- From 1 December 2015, gasoline to be produced, blended, and traded for consumption by road motor vehicles in the whole nation would be E5.

For E10 gasoline:

- From 1 December 2016, gasoline to be produced, blended, and traded for consumption by road motor vehicles in the provinces and cities of Hanoi, Ho Chi Minh City, Hai Phong, Da Nang, Can Tho, Quang Ngai, and Ba Ria - Vung Tau would be E10.

- From 1 December 2017, gasoline to be produced, blended and traded for consumption by road motor vehicles in the whole nation would be E10.

According to the Government Office's Announcement No. 255/TB-VPCP dated 06/6/2017, as of 1 January 2018, only production of E5 RON 92 and RON 95 mineral gasoline would be allowed. The Government also introduced special consumption tax (SCT) incentives in Official Dispatch No. 17125/BTC-CST dated 25 November 2014. Specifically, the SCT rate for mineral gasoline is 10%, for E5 is 8%, and for E10 is 7%. Thus, in case that E5 and mineral gasoline have the same taxable price, the net price of the former is 3% lower than that of the latter. These government's efforts to bring E5 gasoline closer to consumers are not strong enough to make any significant change [1].



Date of receipt: 24/6/2020. Date of review and editing: 24/6 - 22/9/2020.
Date of approval: 11/6/2021.

1.2. Potential feedstock for bioethanol production in Vietnam

In Vietnam, ethanol is produced mainly from cassava - the third most popular crop after rice and corn. This value chain includes stages from cassava planting, cassava slicing after harvest to blending products, distribution and use of bioethanol.

Cassava is planted mainly in lowland and plains with a slope of over 8%. According to data of the General Statistics Office (GSO), the cassava planting area of the country in 2018 reached more than 566.3 thousand hectares with a total output of 9.96 million tonnes of fresh tubers. Tay Ninh is the province having the highest cassava productivity, reaching over 1.86 million tons per year, followed by Gia Lai with more than 1.18 million tons per year.

Cassava is the main feedstock for ethanol production. It is also considered the most suitable source of raw materials for bioenergy development in Vietnam based on the advantages of cultivation, the capacity to ensure supply as well as the reasonable price for long-term development. Compared to other raw materials, rice is the most important food crop ensuring food security in the country, and cannot be used as raw materials for bio-alcohol production; maize productivity is inadequate to meet the needs of food and livestock in the country; sugar molasses can also produce bio-alcohol but its production

cost (VND 5,000 - 10,000/kg) is higher than that of cassava while the production efficiency is lower (1 ton of sugar molasses produce 0.18 tons of ethanol while 1 ton of cassava produced 0.33 tons of ethanol) [3].

1.3. Bioethanol production

By 2019, Vietnam has had 7 ethanol plants with a total capacity of 612 million litres/year. Four of the plants are designed to use 1.05 million tons of cassava to produce 420 million litres of bioethanol per year for gasohol blending.

Unstable feedstock is the first difficulty that manufacturers cannot solve on their own. Although cassava is an abundant raw material in biofuel production, the lack of planning and mechanisms to help farmers develop production areas makes the supply for plants unsteady. Raw material deficiency is a crucial factor that drives many factories to operate at a high cost since raw materials account for 60% of the production cost.

The business of E5 RON 92 gasoline is conducted throughout the distribution system, thus the existing infrastructure is considered an advantage for the spreading of biofuel products. However, E5 is highly volatile fuel, resulting in the fact that transportation and storage costs as well as fuel loss are higher than those of gasoline.

Petrolimex focuses on investing in a small number of blending stations that have large capacity for distribution

Table 1. Planting area and crop productivity for bioethanol production in Vietnam [2]

Content	Corn	Sugarcane	Cassava
Area (thousand ha)			
2010	1,125.7	261.1	498.0
2018	1,039.0	261.0	515.3
Growth 2010 - 2018 (%)	-0.96	0.13	0.55
Productivity (thousand tons)			
2010	4,625.7	16,161.7	8,595.6
2018	4,905.9	17,836.5	9,960.3
Growth 2000 - 2018 (%)	0.78	1.43	2.03

Table 2. Bioethanol plants in Vietnam [4]

No	Plant	Location	Capacity (million litre/year)	Operation year	Status
1	Bioethanol Dung Quat	Quang Ngai	100	2014	Stop production
2	Bioethanol Binh Phuoc	Binh Phuoc	100	2012	Stop production
3	Ethanol Tung Lam	Dong Nai	72	2011	Operation
4	Bioethanol Dai Tan	Quang Nam	125	2010	Sold to Tung Lam Operation
5	Ethanol Dac To	Kon Tum	65	2011	Stop production
6	Ethanol Dai Viet	Dak Nong	50	2008	Stop production
7	Bioethanol Phu Tho	Phu Tho	100	-	Not yet operated
	Total		612/197		Total/Operation

within a certain radius and that can easily be accessed by waterways or pipelines. Meanwhile, PVOIL establishes many small capacity blending stations across the country to ensure an adequate supply for the entire distribution system of 540 petrol stores of its own and more than 3,000 stores operated by general agents, agents, and franchisees.

PVOIL's strategy helps to respond quickly to the rising demand for E5 gasoline. It is also efficient in reducing costs, losses and time of transportation from the blending station to the distribution place, and improving the interactive support among stations if any problem occurs. This is an advantage when the bio-gasoline market becomes more popular and demand increases sharply in the short term. Petrolimex's strategy shows that the enterprise aims to be a central hub with the capability to distribute large

volume, reduce labour cost, and flexibly co-ordinate when the supply-demand market of E5 gasoline fluctuates.

1.4. Gasohol demand

According to statistics from petroleum trading companies, E5 gasoline consumption increased rapidly in 2018 after the release of Announcement No. 255/TB-VPCP. Specifically, E5 gasoline accounted for 50% of the national petrol filling stations, E5 consumption increased to 3,560 thousand m³, making up 40% of the total gasoline consumption, which previously did not exceed 9%.

There are many factors affecting the demand for bio-gasoline such as product quality, consumer habits, and access to bio-gas stations, etc. However, price is considered the key factor, which greatly affects the demand for E5 in Vietnam.

Table 3. Domestic supply 2019 [4]

No	Enterprises	Number of blending station	Capacity (million m ³)
1	Petrolimex	7	1.8
2	PVOil	12	1.67
3	Saigon Petro	2	0.66
4	Military Petrochemical Joint Stock Company - MIPEC	3	0.108
5	Nam Song Hau Petroleum Investment and Trading Co., Ltd	1	0.072
6	Dong Thap Petroleum Trading Limited Company	2	0.1728
7	Thanh Le Trading Import Export Company Limited	2	0.576
8	Nam Phuc Investment Joint Stock Company		1.9
9	Thien Minh Duc Joint Stock Company		
10	Trading - Investment - Investment Construction Bach KhoaViet		
11	Hai Linh Co., Ltd		
	Total		6.9

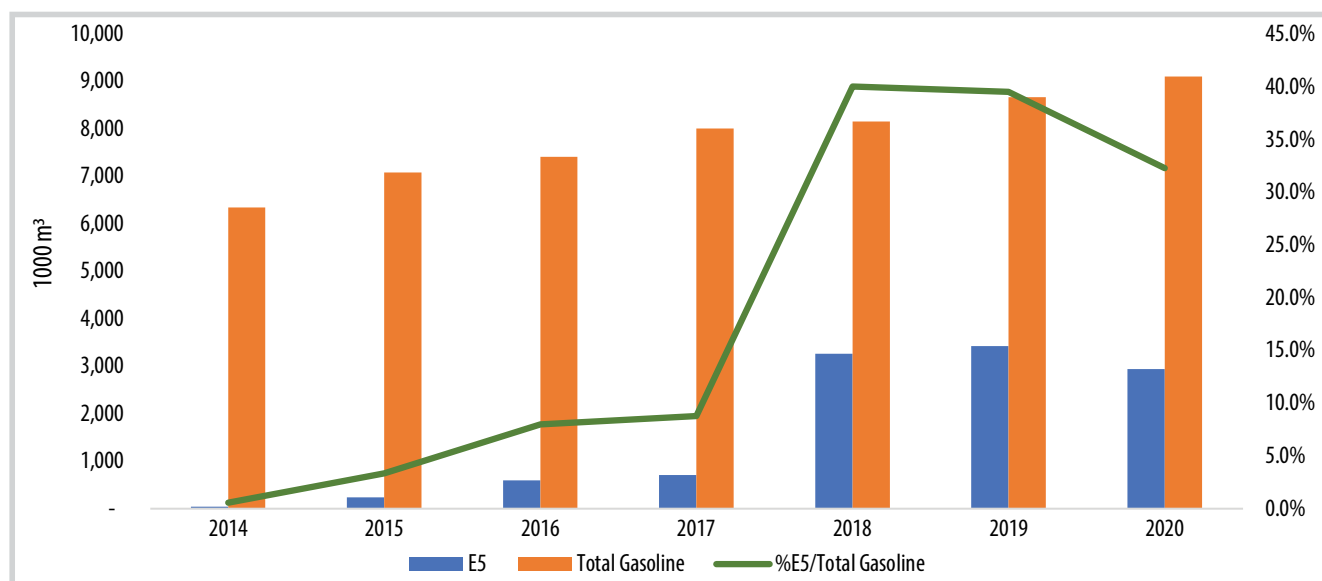


Figure 1. E5/total gasoline consumption in Vietnam during 2014 - 2020 [4].

Although E5 consumption increased sharply in 2018, it is trending down in the market. If in 2018, the consumed E5 was more than 3.2 million m³, equivalent to 40% of the total gasoline sold on the market, in 2020, this number decreased to 32%.

This shows that the government's price supporting policy for E5 gasoline has not yielded impressive results, because the deviation between E5 and RON 95 gasoline is quite small, and not attractive enough to consumers.

In terms of demand, according to Wood Mackenzie forecast, Vietnam's gasohol development rate in the 2020

- 2025 period will be 5% per year, equivalent to about 4 million m³; whilst the growth rate in the 2026 - 2030 period will be about 3%, corresponding to 4.7 million m³ by 2030.

1.5. Gasohol prices

Price of gasohol is described in Figures 2, 3.

The Government has incentives for E5 and mineral gasoline through the composition of excise tax, environmental protection tax, and stabilisation fund. However, the price difference between E5 and RON 95 gasoline is quite small, about VND 1,400 - 1,600/litre.

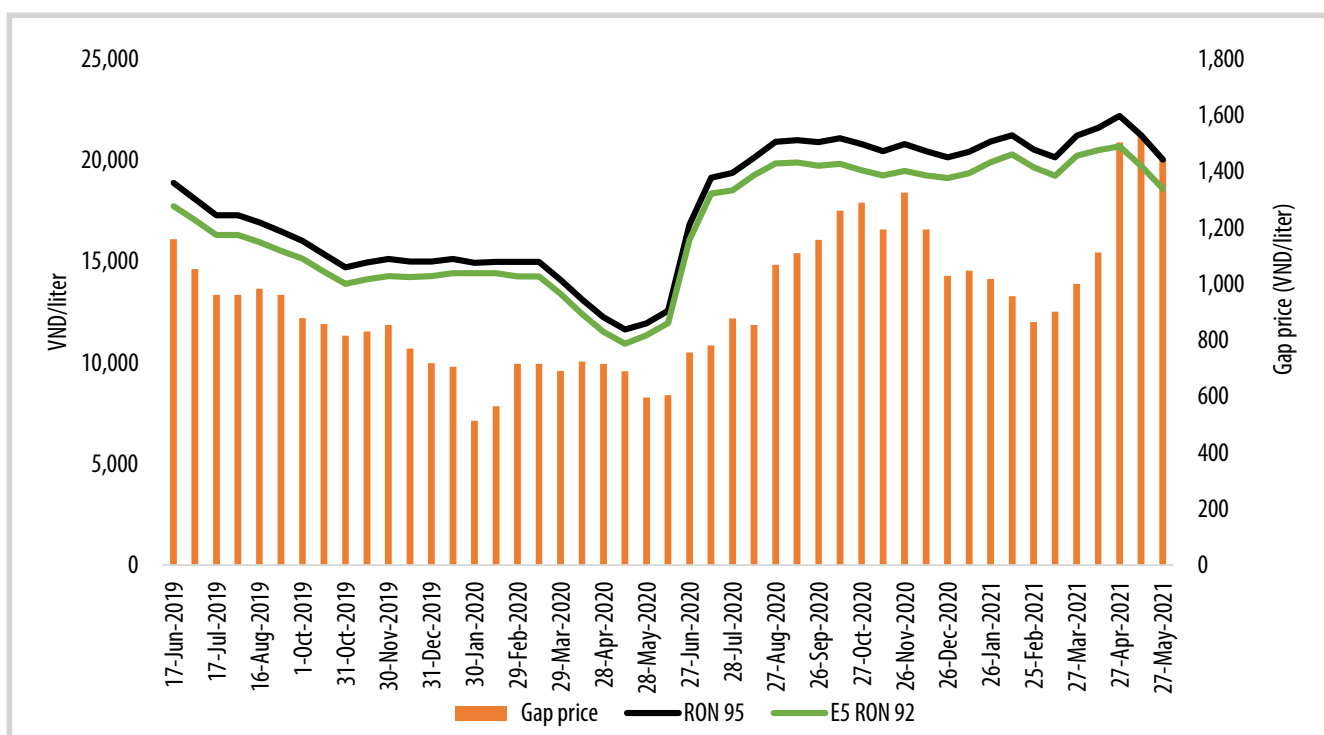
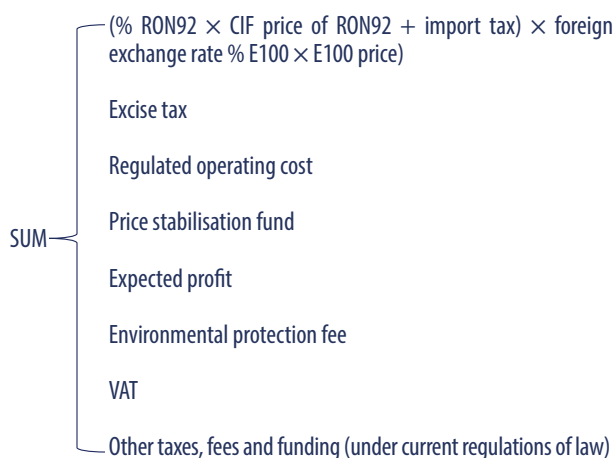


Figure 2. Retail prices of gasoline and gasohol in Vietnam [4].



Which:

No	Information	Calculation unit	95 gasoline	E5
1	Excise tax	%	10	8
2	Standard cost	VND/litre	1,250	1,250
3	Stabilisation fund	VND/litre	Depends on each petroleum business management documentary	
4	Standard profit	VND/litre	300	300
5	Environmental protection fee	VND/litre	4,000	3,800
6	VAT	%	10	10

Figure 3. Pricing structure of gasohol in Vietnam [5].

2. Policies for production and use of biofuel in some countries

Compared to other countries, Vietnam introduced gasohol to the market later. This fuel has been widely used in the US, Europe, and many developed countries since the 70s of the last century. In Southeast Asia, Thailand

has been one of the biggest gasohol producers and consumers for the last 10 years.

There are various measures being used to promote gasohol development around the world, but two important policies are price subsidies and obligatory blending, with Thailand and the USA as the two representatives respectively.

Table 4. Policies of production and use of biofuels in some countries [6 - 8]

Country	Biofuel mandates	Fuel excise tax reduction/exemption and other policy mechanisms
Australia	<ul style="list-style-type: none"> - No national renewable fuel target - New South Wales: 5% biodiesel and 6% ethanol (volume) - Queensland: 0.5% biodiesel and 4% ethanol (volume) 	<ul style="list-style-type: none"> - Producer grant scheme (fuel excise reduction)
Brazil	<ul style="list-style-type: none"> - 27% ethanol and 10% biodiesel (volume) - 100% hydrous ethanol is also marketed in all gas stations in Brazil. 	<ul style="list-style-type: none"> - There are tax incentives for biofuel producers, blenders and users including tax incentives for ethanol-flex fuel vehicles, tax incentives for ethanol fuel and federal tax exemptions and incentives for biodiesel production
Japan	<ul style="list-style-type: none"> - 500 million litres of ethanol mandate (volume) - Introducing 10 million litres (crude oil equivalent) of second generation biofuels (volume) 	<ul style="list-style-type: none"> - No diesel oil delivery tax for B100 - A special tax incentive for the consumption of ethanol - Import of bio-ETBE encouraged through a zero tariff
Sweden	<ul style="list-style-type: none"> - GHG emission reduction of 2.6% for gasoline and 19.3% for diesel 	<ul style="list-style-type: none"> - The tax exemption has varied from full to reduced tax exemption. From January 2018, all biofuels are fully exempted from tax
The United States (US)	<ul style="list-style-type: none"> - Volume targets for biofuels including conventional corn-based ethanol and advanced, cellulosic and diesel biofuels 	<ul style="list-style-type: none"> - California’s Low-Carbon Fuel Standard (LCFS) - Biodiesel producer’s credit
India	<ul style="list-style-type: none"> - No official national mandate for ethanol and biodiesel use in the transportation sector - The 20% and 5% blending targets are proposed (volume) 	<ul style="list-style-type: none"> - No excise tax exemption/reduction for ethanol and biodiesel - Deregulated diesel prices - Allow 100% foreign direct investment in biofuel technologies - Over USD 30 million investment in biofuel R&D and second-generation ethanol technology - Biofuel imports are banned but the import of feedstock for production of biodiesel is permitted to the extent necessary
Germany	<ul style="list-style-type: none"> - GHG reduction of 3.5%/4%/6% in the fuel mix for the entire fuel sector from 2015/2017/2020 onwards 	<ul style="list-style-type: none"> - There is no tax relief for FAME biodiesel, HVO/HEFA fuels, vegetable oils and ethanol: - FAME biodiesel, HVO/HEFA fuels and vegetable oils have the same fuel tax as diesel fuel (€ 0.4104/litre) - Ethanol has the same fuel tax as gasoline fuel (€ 0.6545/litre) - The fuel tax for CNG and biomethane is € 0.0139/kWh until 2023 - A carbon tax is indirectly applied via CO₂ tax for passenger cars
Thailand		<ul style="list-style-type: none"> - An excise tax exemption and the price subsidies are provided by the State Oil Fund (see Table 5, 6 for details) - Producers/Investors can take advantage of a 0% import tax for equipment produced outside Thailand and exemption of corporate income tax for up to 8 years, with an additional 50% reduction for 5 years - Thailand’s government provides over THB 1.5 trillion (USD 45.7 million) in financial support over the next 10 years to ensure success of bioeconomy - The government also supports the manufacturing of vehicles that are compatible with E20 and E85 gasohol. Improvements in the fuel efficiency of vehicles is promoted by setting the excise tax rate for Eco-cars (less than 1,300 cc engines with fuel consumption rate of no more than 5 litres per 100 kilometres) at 17% compared to 30% for E10 vehicles. An additional 3% reduction in the excise tax rate was provided for the manufacturing of Eco-cars that are able to use E85 gasohol. This helped increase annual sales of E20 and E85 passenger cars, which account for approximately 60% of total passenger cars

Table 5. Excise tax rates applied on gasoline and similar products in Thailand in 2019 [11]

Gasoline products	Tax rate (Baht per litre)
Unleaded gasoline	6.50
Gasoline other than unleaded gasoline	6.50
E10	5.85
E20	5.20
E85	0.975

Table 6. Oil fund levied on petroleum products in Thailand in 2019 (Baht/litre) [12]

Products	Retail price	Oil fund
Unleaded gasoline 95	35.33	7.77
Gasohol 95 E10	27.68	1.81
Gasohol 95 E20	24.67	-1.08
Gasohol 95 E85	20.04	-6.68
Gasohol 91 E10	27.41	1.82

In the world rankings, Thailand stood in the 6th position in terms of ethanol production and the 7th in terms of consumption in 2018 [9]. This country has introduced gasohol to the domestic market early, since 2002. Thailand’s government imposed many policies to promote the gasohol demand and supply, of which fiscal policies are most important. By reducing excise tax and offering subsidies through the State Oil Fund, gasohol was made 20 - 40% cheaper than the premium gasoline. These government price subsidies have led to increase of gasohol consumption up to 97% of total gasoline consumption in 2019 [8, 10]. Table 5 describes more detail.

Since 2007, E10 has been introduced nationwide in Thailand. The National Oil Fund was adjusted many times lower for gasohol, especially E85. Table 6 shows the differences of this factor among the types of gasoline in 2019.

Although using gasohol can reduce CO₂, bad air quality persists in Thailand’s major cities. The Air Quality Index (AQI) used by cities to determine levels of air pollution measured 175 in Bangkok in January 2019, while AQI levels under 25 are considered to be acceptable for humans to breathe regularly, according to the World Health Organisation. The reason given is that ethanol increases gasoline vapour pressure (RVP), eventually leading to increased volatile organic compound (VOC) emissions and ozone. Land use change (LUC), especially change in soil carbon stock, to increase ethanol feedstock supply is an important factor in overall greenhouse gas (GHG) emissions of the first-generation biofuels, contributing about 58 - 60% of the net GHG emissions. In addition, the government is expected to lower the ethanol consumption target under AEDP 2015 (Thailand

Alternative Energy Development Plan 2015) to 2.6 billion litres in 2036, down by 37% from the initial target of 4.1 billion litres, due to the uncertainty over the ability to further increase molasses and cassava supplies, the primary feedstocks for ethanol production.

The United States is the world’s largest producer and consumer of gasohol, and has established a mandatory policy (The Renewable Fuel Standard - RFS) to produce and consume E10 since 2005. This programme assigns to obligated parties (fuel refiners, blenders, and importers) a renewable volume obligation (RVO). The RVO for each party is the volume of renewable fuels it is obligated to sell, based on a percentage of the company’s total fuel sales. However, meeting RVO is not easy, oil refiners bear hundreds of millions of dollars each year to comply with the RFS ethanol blending requirements. Similar to Thailand, in the US, air quality has regularly been a subject of controversy. Through July 2003 in California, which had recently switched to ethanol in gasoline, the ozone exceedances in the South Coast Air Basin were twice the levels of the prior 3 years. Moreover, RFS has resulted in unintended consequences which include higher food prices, a boom-and-bust ethanol industry that is now looking to export its product. As a result, opposition to the RFS and ethanol use in the U.S. has been mounting. Twelve automotive manufacturers have even opposed any further increase above 10 vol.% ethanol in gasoline over concerns about corrosion of automotive components [13].

3. Which direction for gasohol?

It can be seen that after more than 2 decades of bio-gasoline development, the positive side of gasohol development is to reduce the dependence on mineral

gasoline, reduce CO₂ emissions, and open up opportunities for more advanced development in the future. On the other hand, the reality also indicates the limitations that the supply of raw materials is not guaranteed, consuming many fertile lands that should be used to grow food for the world's population.

The planting of crops also requires a lot of water and fertiliser, which can cause chemical residues in the soil and the lack of freshwater for people. According to a 2013 report of the United Nations Food and Agriculture Organisation (FAO), it takes 1,000 - 4,000 litres of water to produce 1 litre of ethanol.

Moreover, although using gasohol emit low CO₂, contributing to reducing climate change, the process of consuming them gives off other harmful gases such as CO, VOC, and NO_x which badly impact human health [13, 14]. It was indicated by the Ministry of Environment in 2014 in Brazil, the 2nd country in the world in terms of gasohol consumption.

Besides, many countries are turning to second- and third-generation development. Second-generation biofuels are derived from cellulose, hemicellulose, lignin or pectin, for example, waste or waste in agriculture-forestry, or plant materials grown not intended for food (short-term plantations, some grasses, etc.). Third-generation biofuels are derived from natural aquatic organisms (algae). These may be research directions for development because the advantages of the next generation biofuels are less usage of agriculture land, exploiting waste and saving farming area while getting higher efficiency: algae can deliver energy efficiency 60 times more than land crops and can grow in brackish water in rural areas or barren villages.

Vietnam will continue to consume gasoline in transportation in the next period, and gasohol is still more environmentally friendly than gasoline which is a type of mineral fuels. Furthermore, the energy picture in the future will be a diversification of environmentally friendly energy/fuel sources. Energy for transportation will focus on biofuel, electrical energy (for electric vehicles-EV) and hydrogen (for fuel cell electric vehicles - FCEV). Specifically, EV and FCEV will be widely developed in the next 10 - 20 years, and biofuels are considered as a transitional step in the gradual transition from mineral fuels to eco-friendly fuels/energy. It is a fact that many countries in the world such as Thailand, the US, and European countries still use E5, E10, and E20 gasoline,

and also promote the development of electric vehicles and hydrogen vehicles. Therefore, in our point of view, for the current E5 production and distribution infrastructure, Vietnam should maintain a proportion of E5 gasohol from 30 - 40% of the total gasoline consumption as at present, stop developing E10 and set a strategy/plan to develop electric and hydrogen vehicles.

To increase the diversification of the energy resource mix for transportation, the government as well as gasohol production and distribution enterprises need to implement synchronous policies and solutions:

For the government:

- Set specific goals and a roadmap for the development and transition to environmentally friendly vehicles, including a clear biofuel development goal and a mandatory roadmap on the minimum blending ratio of biofuels for wholesalers and monitor implementation; consider supporting to develop research and application of the second- and third-generation biofuels.

- In the short-term, regional planning can be considered to meet the amount of raw materials; help farmers increase productivity; create a policy of price difference between traditional gasoline and E5 gasoline large enough to encourage consumers through environmental fees and petroleum stabilisation fund, the difference is about 15 - 20% like Thailand's policy.

- In the long-term, impose environmental taxes (CO₂ taxes) on fossil fuels. The Environmental Law promulgated in 2020 has introduced the law on environmental tax. The implementation roadmap will be applied experimentally from now until the end of 2027 and applied officially from 2028.

For the bioethanol production enterprises:

- Ethanol production enterprises need to closely associate with cassava farmers, negotiate and sign cassava offtake contracts to ensure a stable source of input materials and harmonise the interests of the parties.

For the gasohol production and distribution enterprises:

- The wholesalers need to build a gasohol strategic plan including measures to cut costs; and improve right awareness of consumers about gasohol to promote biofuel consumption.

4. Conclusion

These days, gasohol is used in over 50 countries worldwide. This is considered a solution to help protect the environment and reduce the dependence on fossil fuels. From 1 January 2018, Vietnam has applied the policy that only E5 biofuel and RON 95 would be produced and available for purchase.

However, ethanol production facilities in Vietnam sometimes struggled with a shortage of raw materials because the export price of cassava to China is higher than the domestic purchase price. Besides, the difference of retail price between E5 RON 92 gasoline and traditional gasoline is not attractive enough and people's concerns causes a trending down of the consumption E5 RON 92 gasoline from 40% in 2018 to 32% in 2020.

In our point of view, for the current E5 production and distribution infrastructure, Vietnam should maintain a proportion of E5 gasohol from 30 - 40% of the total gasoline consumption as at present, stop developing E10 and set a strategy/plan to develop electric and hydrogen vehicles. The development of biofuel requires close coordination between businesses and the government while ensuring biodiversity, soil and water quality. In addition, there are some sustainable solutions which should be implemented to reduce carbon in the transportation sector including electric and hydro vehicle conversion.

References

[1] Do Xuan Dong, "The orientation in the production and use of biofuels in Vietnam", The regional workshop on "Sustainable bioenergy production and use in Southeast Asia", Ha Noi, 16 - 17 November, 2017.

[2] General Statistics Office of Vietnam. [Online]. Available: <https://www.gso.gov.vn/default.aspx?tabid=717>.

[3] Tạp chí Công Thương, "Bài toán nguyên liệu cho sản xuất cồn ethanol", 29/3/2017.

[4] Nghiêm Thị Ngoan và nnk, "Nghiên cứu, xây dựng báo cáo định kỳ về tình hình sản xuất và xuất nhập khẩu các sản phẩm xăng, dầu", VPI 2020.

[5] Bộ Tài chính, Thông tư liên tịch số 90/2016/TTLT-BTC-BCT ngày 24/6/2016 sửa đổi, bổ sung một số điều

của Thông tư liên tịch số 39/2014/TTLT-BCT-BTC ngày 29/10/2014 quy định về phương pháp tính giá cơ sở; cơ chế hình thành, quản lý, sử dụng Quỹ bình ổn giá và điều hành giá xăng dầu theo quy định tại Nghị định số 83/2014/NĐ-CP ngày 3/9/2014 của Chính phủ về kinh doanh xăng dầu. 2016.

[6] Mahmood Ebadian, James D. McMillan, Jack (John) N. Saddler, and Susan van Dy, "Implementaation agendas: 2018-2019 update compare and contrast transport biofuels policies", IEA Bioenergy, 2019.

[7] Matthew Fielding and May Thazin Aung, "Bioeconomy in Thailand: A case study", Stockholm Environment Institute, 2018.

[8] Sakchai Preechajarn, Ponnarong Prasertsri, and Maysa Chanikornpradit, "Thailand biofuels annual", United States Department of Agricultural, Foreign Agricultural Service, 15/11/2019.

[9] Narin Tunpalboon, "Thailand industry outlook 2019-21: Ethanol industry", Krungsri Research, 7/2019. [Online]. Available: https://www.krungsri.com/bank/getmedia/0c42d6fd-18d7-41c1-9369-96dded234800/IO_Ethanol_190710_EN_EX.aspx.

[10] Anuman Chanthawong, Shobhakar Dhakal, John K.M. Kuwornu, and Khalid Farooq, "Impact of subsidy and taxation related to biofuels policies on the economy of Thailand: A dynamic CGE modelling approach", *Waste and Biomass Valorization*, Vol. 11, pp. 909 - 929, 2020. DOI: 10.1007/s12649-018-0417-4.

[11] Thailand Board of Investment, "A business guide to Thailand 2019". [Online]. Available: <https://www.boi.go.th/upload/content/A%20Business%20Guide%20to%20thailand%202019.pdf>.

[12] Energy Policy and Planning Office, Ministry of Energy. [Online]. Available: <http://www.eppo.go.th/index.php/en/en-energystatistics/petroleumprice-statistic>.

[13] Asian Clean Fuels Association, "Biofuel experiences in Southeast Asia", 2019.

[14] Larry G. Anderson, "Ethanol fuel use in Brazil: Air quality impacts", *Energy & Environmental Science*, Vol. 2, pp. 1015 - 1037, 2009. DOI: 10.1039/B906057J.

A BREAKTHROUGH IN 3D SEISMIC INTERPRETATION

Nguyen Xuan Thinh¹, Ha Quang Man²

¹Eliis Australia Pty, Ltd.

²Petrovietnam Exploration and Production Corporation (PVEP)

Email: eric.nguyen@eliis.fr

Summary

Accompanying the advancement of computer science and technologies, new techniques have been introduced to optimise the seismic interpretation workflow. In this study, we apply the "Global seismic interpretation method", developed by Pauget et al. [1]. A 3D Relative Geologic Time (RGT) model was obtained directly from the 3D seismic volume which is the outcome of this method. Given the fact that in the 3D RGT model, the geologic time is continuous, a relative geologic age can be interpolated and assigned to every voxel of the seismic volume.

The dataset used in this study is the Maui 3D seismic volume from Taranaki basin, offshore New Zealand. A stack of 400 continuous stratigraphic horizons is produced from the Maui RGT model, even for complex areas where classical methods failed to achieve or would take a long time to complete. Integrated with seismic attribute mappings such as RMS amplitude and/or spectral decomposition, the horizon stack enables to navigate the seismic volume in stratigraphic order. Thus, the result enhances the identification of geological elements, stratigraphic insights, and paleo-depositional environments in greater detail for stratigraphic reservoir detection and characterisation. The novel methodology indicates a new way to conduct seismic interpretation, utilises all the information in the 3D seismic data, hence greatly reduces the exploration time cycle.

Key words: Seismic interpretation, seismic attributes, geologic time model, subsurface imaging, Taranaki basin.

1. Introduction

In the last few decades, seismic interpretation techniques have been rapidly developed for detailed reservoir delineation and characterisation. The traditional approach is generally an intensively time-consuming process that is heavily reliant on manually picking or auto-tracking of single horizons within the seismic volume. The tool allows tracking only one horizon at a time and is limited to areas with clear seismic signals or relatively simple geological structures.

New methods have been introduced to exploit the 3-dimensionality of the data and simultaneously auto-track every horizon throughout the seismic volume [2 - 7]. In 2009, Pauget et al. proposed a global method to build a 3D geological model directly from the 3D seismic volume [1]. This innovative method optimises the seismic

interpretation workflow with greater confidence and accuracy. Continuous chronostratigraphic surfaces can be generated at every sample of the seismic data, enabling to overcome the limitation of seismic polarity changes. In this study, we have applied this advanced seismic interpretation method and its associated attributes for enhancing subsurface imaging, reservoir delineation and characterisation for the Maui 3D seismic volume from Taranaki basin, offshore New Zealand.

2. Regional geological settings

Extending 100,000 km² along the western margin and filled with 10 km thick Cretaceous - Cenozoic sediments, the Taranaki basin is the largest offshore sedimentary basin in New Zealand (Figure 1). Rifting started from the Late Cretaceous and completely ended in the Paleocene, along with a rapid deposition within graben areas accompanied by high heat flow. During the Paleocene - Eocene period, a passive margin developed over the entire sub-continent; a slow subsidence rate allowed sediments to accumulate

across the shelf and coastal plain areas in the Taranaki basin [8]. The Late Eocene-Early Oligocene period marked the starvation of clastic materials [9]. Thereafter, this basin underwent a significant phase of subsidence from the Oligocene to the Early Miocene due to the development

of the Australia-Pacific plate boundary zone in the eastern area. This was followed by the widespread of limestone and marl deposition in the outer shelf to upper bathyal water depths [9]. Increasing sediment loading contributed to the evolution of the shelf-slope system in the Miocene, resulting in the deposition of sandstone, interbedded mud and siltstone in the outboard areas. The plate boundary evolution also caused the basement to overthrust the Taranaki fault in the Early Miocene and the formation of the Tarata thrust zone in the Early Miocene. By the Middle Miocene, the compressional effect on the northern area and its eastern margin had decreased, coinciding with the development of the submarine volcanic arc. During the Pliocene, the volcanic arc moved southeastward onshore and the northern areas of the Taranaki basin started extending, creating accommodation space for the Plio-Pleistocene progradation and aggradation of the Giant Foresets formation in the Northern and Central grabens.

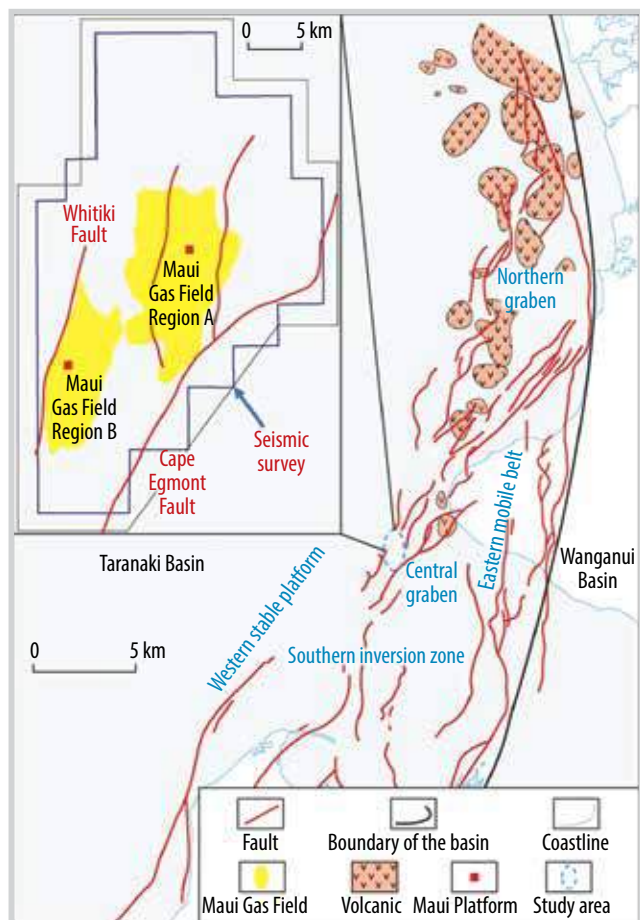


Figure 1. Location map of Maui gas field and Maui 3D seismic survey, Taranaki basin, offshore New Zealand. Modified after King and Thrasher [9], Higgs et al. [10], and Haque et al. [11].

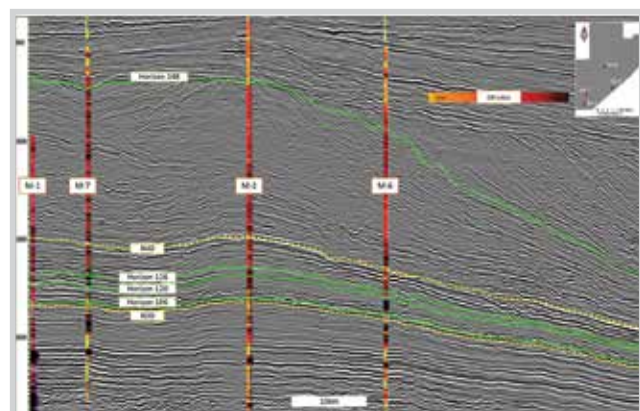


Figure 2. Seismic arbitrary line from the Maui 3D traverses through Maui (M) 1, 7, 2, 6 petroleum wells. Dashed, yellow lines are interpreted horizons N40 and N30 in the Middle Miocene interval from Thrasher et al. [12]. Green lines are horizons 106, 120, 126, and 248 from the Horizon Stack (Figures 5, 6, and 7).

3. Database and workflow

3.1. Subsurface data

The Maui 3D seismic data used in this study is a full offset, post-stack time-migrated volume which covers a surface area of approximately 1,000 km². All seismic data are zero-phase processed where acoustic impedance increases are displayed by positive amplitudes (peak reflections) and decreases in acoustic impedance are indicated by negative amplitudes (trough reflections) on the seismic section (Figure 2). The 3D seismic survey was acquired with 25 × 25 bin size, 1836 samples/trace, 3 ms sample rate and a total record length of 5,600 ms. In this area, the Maui gas field with 17 exploration and production wells is one of the largest gas condensate fields in New Zealand (Figure 1).

3.2. A global seismic interpretation method: From 3D seismic volume to 3D geological model

Building a 3D geological model directly from a 3D seismic cube plays a vital role in reducing the time cycle and enhancing the quality of seismic interpretation. This workflow, based on the cost function minimisation algorithm [1], consists of two steps.

The first step consists of computing a 3D grid of horizon patches, call "3D Model Grid" (Figure 3). Millions of grid points or nodes are distributed in 3D seismic volume, onto every seismic polarity such as peaks, troughs, zero crossings, or inflection point with a constant step of seismic bin size (Figure 3a). Each node is an elementary

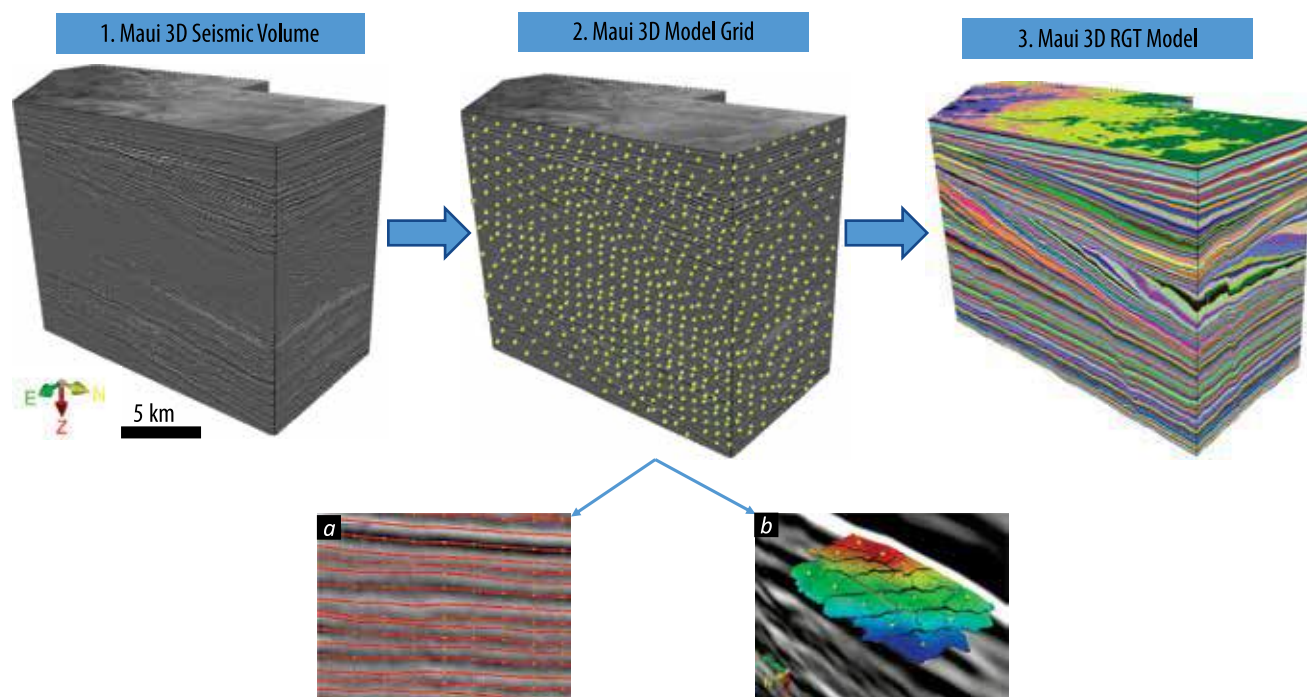


Figure 3. Summary of the workflow: (1) Maui 3D seismic volume, (2) 3D model grid creation. Auto propagation is based on a correlation threshold in the model grid when nodes (yellow points) are connected, showing on both 2D (a) and 3D (b) viewer, (3) Maui 3D geo-model is the result of the model grid interpolation.

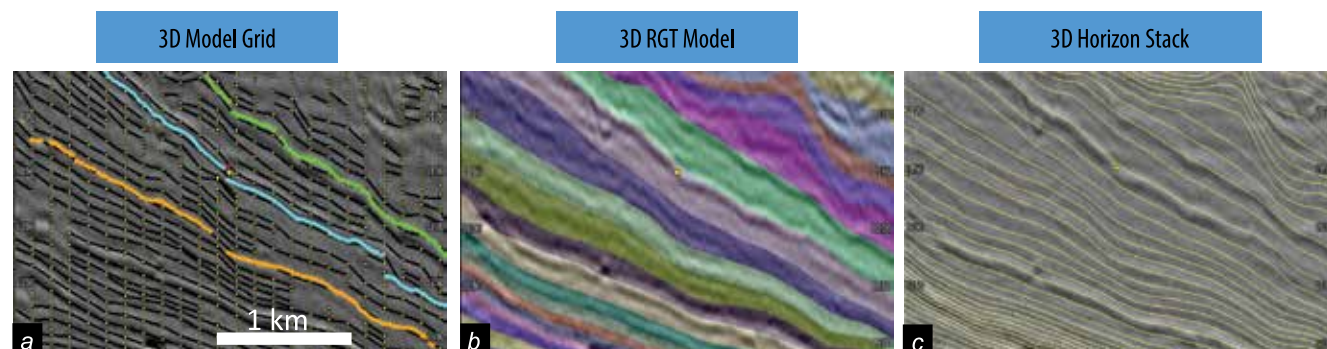


Figure 4. (a) the 3D model grid where key horizon patches can be editable and highlighted in colours, following the interpreter's ideas, (b) 3D RGT model is blended with 3D seismic volume, showing the same geometry. Instead of having seismic amplitudes, there are relative age values assigned to each voxel of the 3D RGT model, (c) The horizon stack comprises dense stratigraphic horizons, representing the geologic time values in the RGT model.

horizon patch in 3D with the seismic bin size square (Figure 3b). Using the afore-mentioned algorithm, all elementary horizon patches are linked based on the similarity of the seismic wavelets and their distance. For example, if two wavelets are 3 seismic bin size apart and 30% similar, the nodes on these wavelets will be linked. As a result of this process, all possible horizons within the seismic volume are auto propagated in one attempt (Figure 3a, 3b), acting as a framework for the 3D geological model. The fact that the same geologic age is assigned to patches connected laterally, so each auto-tracked horizon, having its relative age, is sorted stratigraphically and never crosses each other thanks to this advanced algorithm.

In the second step, the 3D relative geologic time

(RGT) model is computed from the interpolation of the 3D model grid (Figure 3), in which the relative geologic time is obtained for every sample of the seismic volume. The role of the seismic interpreter involves refining the RGT model by modifying and constraining the relationships of the horizon patches in the 3D model grid until an optimal result could be achieved.

3.3. Horizon stack and stratal slicing

From the RGT model, a horizon stack comprising of unlimited chrono-stratigraphic or iso-geological time surfaces can be created for imaging geological elements and thin stratigraphic events even at a sub-seismic scale. Those surfaces are only 5 - 7 ms apart and represent

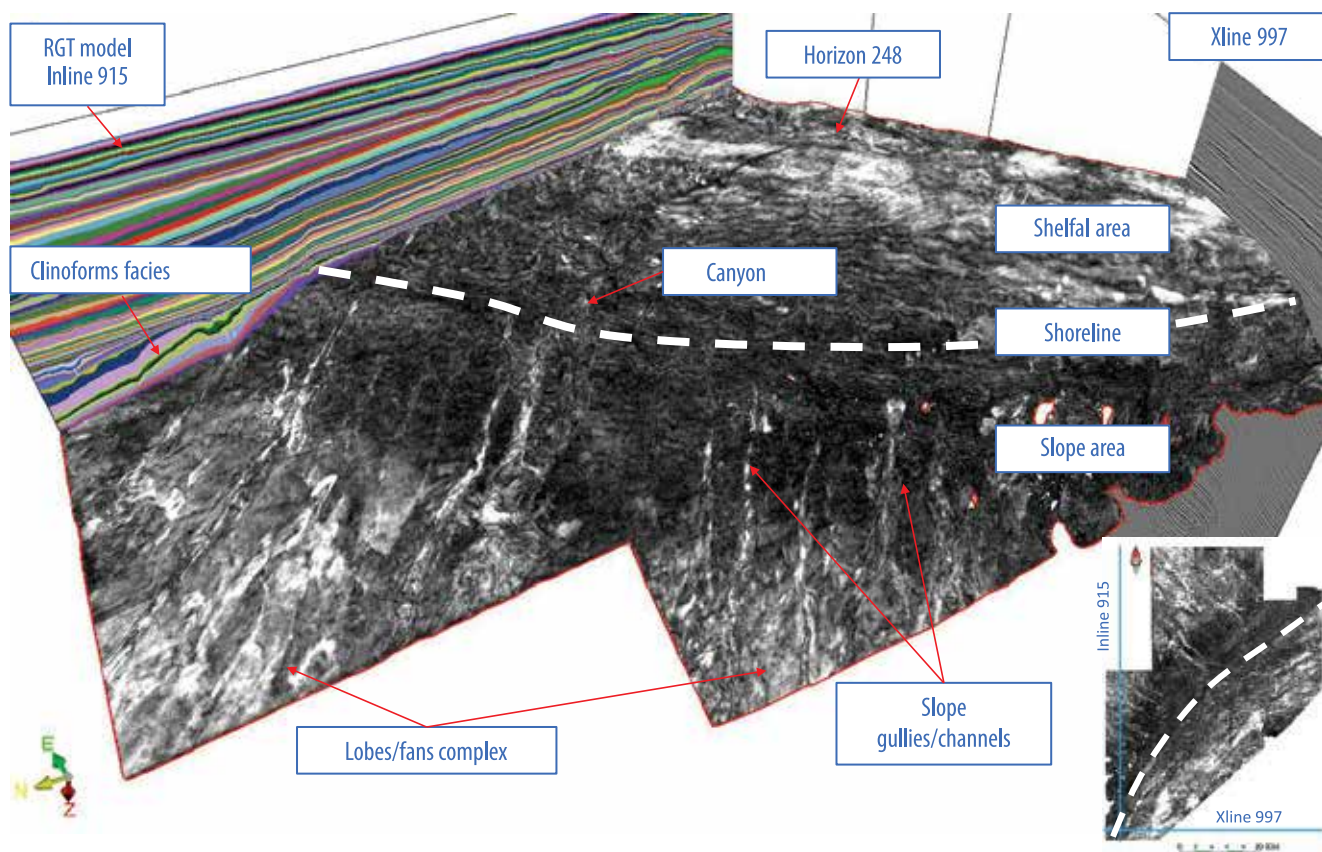


Figure 5. From the RMS amplitude attribute horizon stack, the geological features of the marginal marine depositional environment in the Giant Foresets Formation were highlighted in great detail on horizon 248 (see Figure 2 for a stratigraphic position).

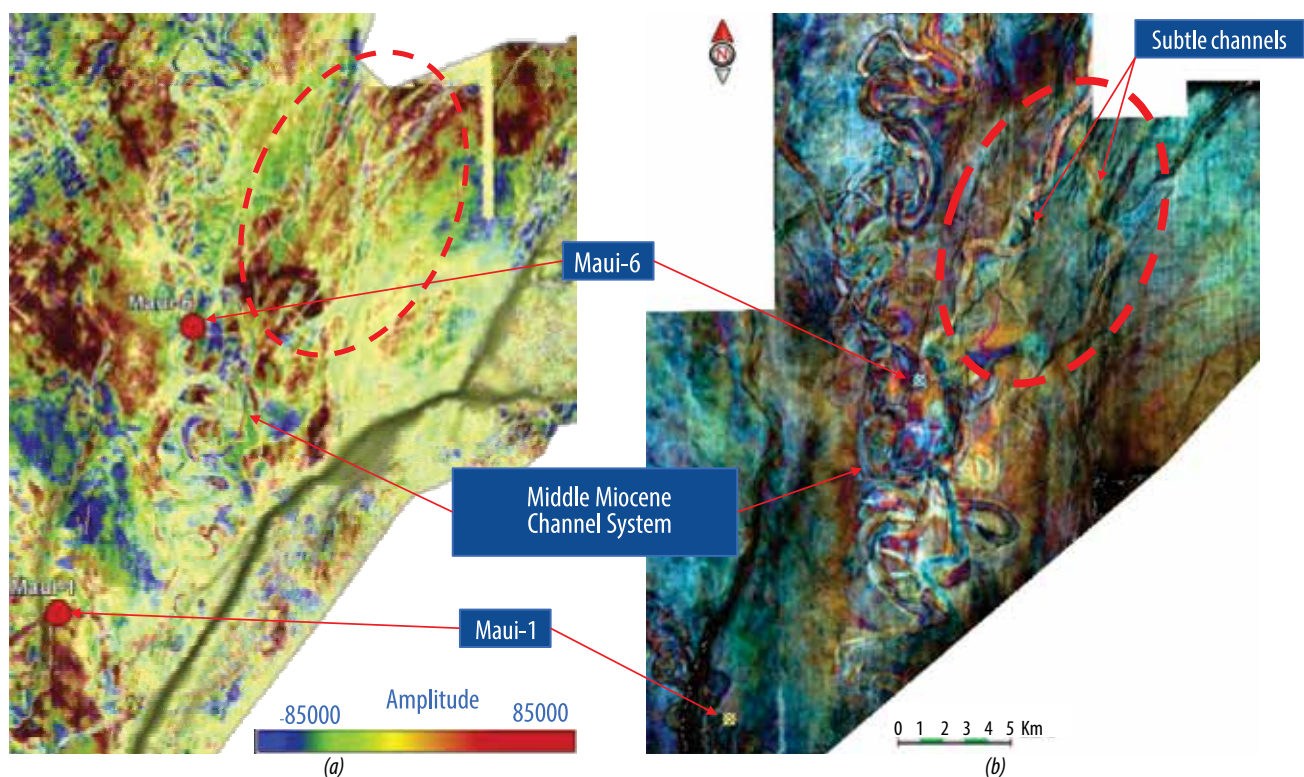
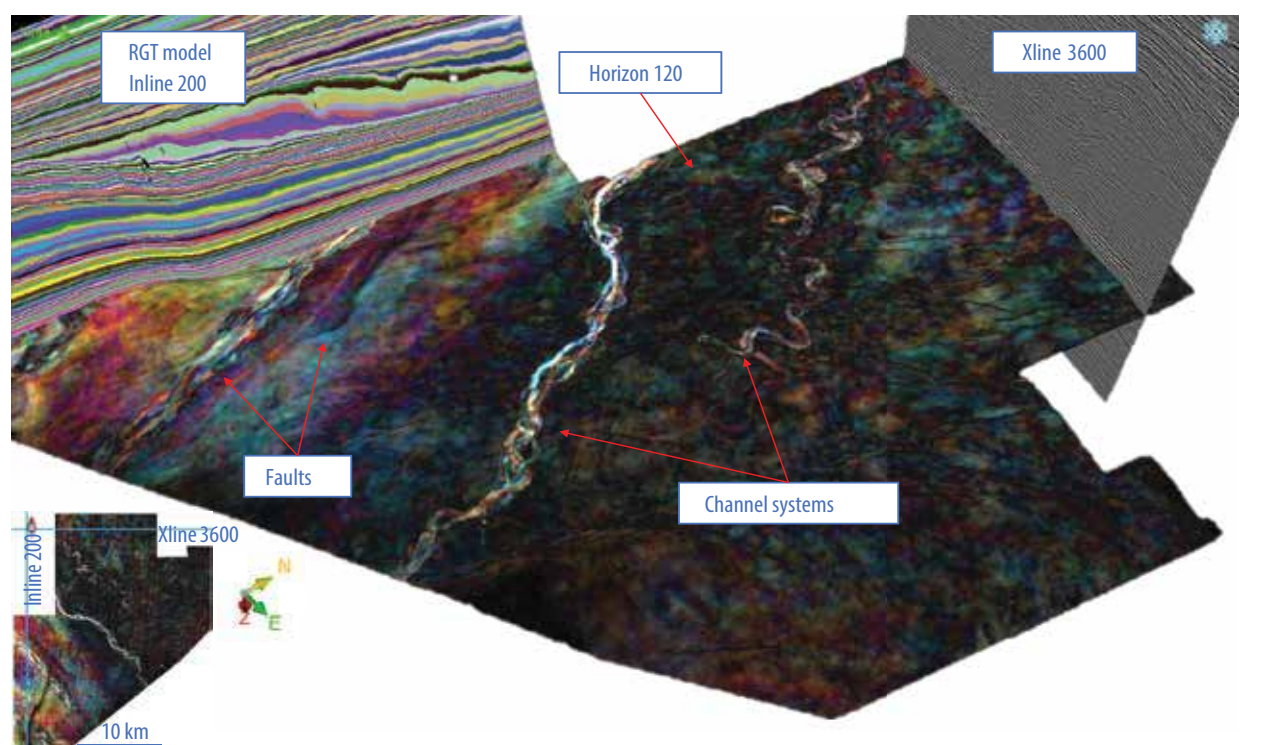
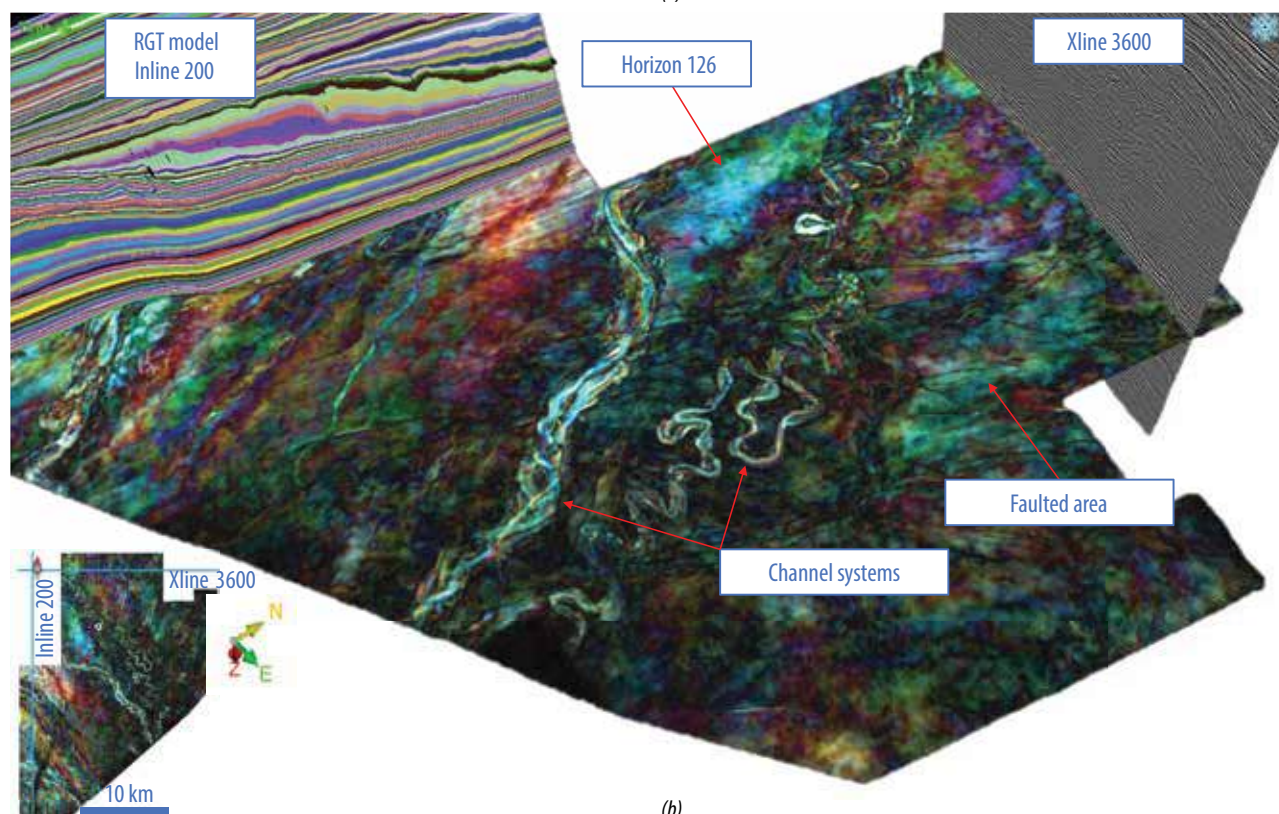


Figure 6. Comparison between (a) horizon from N30-N40 interval using the isoproportional slicing method in Kroeger et al. [17] and (b) horizon 106 from the horizon stack with colour-blended spectral decomposition with three different frequencies (see Figure 2 for a stratigraphic position). Note that on horizon 106 of the horizon stack, the subtle channels in the dash, red circle area, and the overall geometry of the Middle Miocene channel system were revealed more robustly.



(a)



(b)

Figure 7. Using spectral decomposition seismic attribute and the colour blending tool to detect the geological features on horizon 120 (a) and horizon 126 (b) of the horizon stack (horizon 126 is above horizon 120 in stratigraphic order or “younger” in the relative geologic time domain). The evolution of the Middle Miocene, meandering channel system, from horizon 120 to 126 is highlighted in both time and space (see Figure 2 for a stratigraphic position).

stratigraphic horizons (Figure 4), contrary to horizontal slices (i.e. time slices) from the seismic volume. Several seismic attributes can be extracted on those horizons

such as RMS amplitude and colour-blended spectral decomposition attribute. These attributes are calculated from a fixed window size in seismic samples along each

horizon (e.g. a window size of 5 with a vertical sampling of 4 means the time window is 20 ms, the attribute will be mapped from 10 ms above and 10 ms below each horizon). This method has been used successfully on numerous case studies with different basin settings for thin-bed reservoir detection and characterisation, along with enhancing fault and fracture imaging [13 - 16].

4. Results and discussion

Using PaleoScan™ software, all possible horizons in the seismic volume are auto-tracked in one attempt either in peak, trough, and zero-crossing, reducing the time cycle on manually picking and seed-based auto-tracking horizon methods. A 3D RGT model is the outcome obtained directly from the Maui 3D seismic volume. In this process, the interpolation of the 3D model grid plays a key role, assigning relative ages to every voxel of the seismic volume to create both vertical and lateral continuity in the 3D RGT model.

In this study, 400 continuous chronostratigraphic surfaces representing relative geological ages are extracted from the 3D RGT model. This unique technique allows the seismic volume to be navigated stratigraphically, revealing stratigraphic insights at a very high resolution, even with thin-bed events or in complex depositional environments (e.g. shallow or marginal marine, Figure 5) that cannot be shown when using the traditional approach.

In the conventional workflow, seismic attributes are only mapped on manually picked key horizons or their shifted ones, which can be time-consuming and not feasible in complex intervals. Here in the same amount of time, hundreds or thousands of horizons with different seismic attributes can be extracted from the RGT model taking into account all the samples of the seismic volume. Also, different from iso-proportional horizons which are generated in the interval between two specific horizons, the horizon stack provides continuous surfaces inside the complex stratigraphic intervals but still strictly follows the geological events and seismic facies of the data, thus it is better for subsurface imaging in those locations (Figure 6).

This innovative workflow has made seismic interpretation more efficient, delivering to geologists a fully consistent, data-driven geo-model along with high-quality horizons (Figures 6 and 7) and faults for further modelling purposes.

5. Conclusion

In this paper, a new interpretation technique has been presented which utilises 3D seismic data and directly transforms it into a 3D RGT Model. This allows generating a dense library of stratigraphic horizons, even in complex intervals to identify subtle events, unseen from conventional methods, which are based on manually picking and seed-based auto-tracking horizons [18].

From an example of Maui 3D, located offshore Taranaki basin, a 3D RGT model was obtained in a short time frame, producing 400 chrono-stratigraphic surfaces. These surfaces mapped with seismic attributes such as RMS amplitude and spectral decomposition using colour-blended method help the interpreters to build up a geological history of the area. The results suggest that this approach could be applied not only to subsurface imaging, the detection of subtle stratigraphic events, but also for modelling purposes, at both regional and reservoir scales. The new workflow drastically accelerates the entire exploration cycle and shapes a new form of seismic interpretation in the future [18].

Acknowledgment

The case study presented in this paper is achieved with PaleoScan™ software, developed by Eliis (www.eliis.fr). The authors would like to thank the Ministry of Business, Innovation, and Employment (MBIE), New Zealand, for the authorisation to publish the Maui 3D seismic data.

References

- [1] Fabien Pauget, Sébastien Lacaze, and Thomas Valding, "A global approach to seismic interpretation based on cost function and minimization", *SEG Technical Program Expanded Abstracts 2009*. DOI: 10.1190/1.3255384.
- [2] Hilde G. Borgos, Thorleif Skov, Trygve Randen, and Lars Sonneland, "Automated geometry extraction from 3D seismic data", *SEG Technical Program Expanded Abstracts 2003*. DOI: 10.1190/1.1817590.
- [3] Paul de Groot, Arnaud Huck, Geert de Bruin, Nanne Hemstra, and Jonathan Bedford, "The horizon cube: A step change in seismic interpretation", *The Leading Edge*, Vol. 29, No. 9, pp. 1048 - 1055, 2010. DOI: 10.1190/1.3485765.
- [4] H.J. Ligtenberg, G. de Bruin, N. Hemstra, and C. Geel, "Sequence stratigraphic interpretation in the

wheeler transformed (flattened) seismic domain", 68th EAGE Conference and Exhibition Incorporating SPE EUROPEC 2006. DOI: 10.3997/2214-4609.201402337.

[5] Jesse Lomask, Antoine Guitton, Sergey Fomel, Jon Claerbout, and Alejandro A. Valenciano, "Flattening without picking", *Geophysics*, Vol. 71, No. 4, pp. 13 - 20, 2006. DOI: 10.1190/1.2210848.

[6] Xinming Wu and Dave Hale, "Horizon volumes with interpreted constraints", *Geophysics*, Vol. 80, No. 2, 2015. DOI: 10.1190/geo2014-0212.1.

[7] Tracy J. Stark, "Relative geologic time (age) volumes - Relating every seismic sample to a geologically reasonable horizon", *The Leading Edge*, Vol. 23, No. 9, pp. 928 - 932, 2004. DOI: 10.1190/1.1803505.

[8] Peter R. King, "Tectonic reconstructions of New Zealand: 40 Ma to the present", *New Zealand Journal of Geology and Geophysics*, Vol. 43, No. 4, pp. 611 - 638, 2000. DOI: 10.1080/00288306.2000.9514913.

[9] P.R. King and Glenn P. Thrasher, "Cretaceous-Cenozoic geology and petroleum systems of the Taranaki basin, New Zealand", *Institute of Geological and Nuclear Sciences*, Vol. 13, No. 2, 1996.

[10] K.E Higgs, P.R. King, J.I Raine, R. Sykes, G.H Browne, E.M Crouch, J.R Baur, "Sequence stratigraphy and controls on reservoir sandstone distribution in an Eocene marginal marine-coastal plain fairway, Taranaki Basin, New Zealand". *Marine and Petroleum Geology*, Vol. 32, No. 1, pp. 110 - 137, 2012. DOI: 10.1016/j.marpetgeo.2011.12.001.

[11] Eahsanul Haque, Aminul Islam, and Mohamed Ragab Shalaby, "Structural modeling of the Maui gas field, Taranaki basin, New Zealand", *Journal of Petroleum Exploration and Production Technology*, Vol. 43, No. 6, pp. 965 - 975, 2016. DOI: 10.1016/S1876-3804(16)30114-8.

[12] G. Thrasher, H. Seebeck, P. Viskovic, S. Bull, M.

Sarma, and K. Kroeger, "Time structure grids for the greater Maui-Maari-Tui region, Taranaki basin, New Zealand", *GNS Science Data Series*, 2018.

[13] Ingelise Schmidt, Sebastien Lacaze, and Gaynor Paton, "Spectral decomposition and geomodel interpretation - Combining advanced technologies to create new workflows", 75th EAGE Conference & Exhibition Incorporating SPE EUROPEC 2013, London, UK, 10 - 13 June 2013. DOI: 10.3997/2214-4609.20130567.

[14] Marco Fonesu, Denis Palermo, Mauro Galbiati, Marco Marchesini, Enrico Bonamini, and Daniel Bendias, "A new world-class deep-water play-type, deposited by the syndepositional interaction of turbidity flows and bottom currents: The giant Eocene Coral field in northern Mozambique", *Marine and Petroleum Geology*, Vol. 111, pp. 179 - 201, 2020. DOI: 10.1016/j.marpetgeo.2019.07.047.

[15] Tony Marsh and Anne Powell, "Regional stratal slice imaging of the Northern Carnarvon basin, Western Australia", *ASEG Extended Abstracts*, 2019. DOI: 10.1080/22020586.2019.12073062.

[16] Lia Turrini, Christopher A-L. Jackson, and Philip Thompson, "Seal rock deformation by polygonal faulting, offshore Uruguay", *Marine and Petroleum Geology*, Vol. 86, pp. 892 - 907, 2017. DOI: 10.1016/j.marpetgeo.2017.06.038.

[17] Karsten F. Kroeger, Glenn P. Thrasher, and Monmoyuri Sarma, "The evolution of a Middle Miocene deep-water sedimentary system in northwestern New Zealand (Taranaki basin): Depositional controls and mechanisms", *Marine and Petroleum Geology*, Vol. 101, pp. 355 - 372, 2019. DOI: 10.1016/j.marpetgeo.2018.11.052.

[18] Nguyễn Xuân Thịnh và Hà Quang Mẫn, "Đột phá trong minh giải tài liệu địa chấn 3D để phát hiện các bẫy chứa địa tầng", *Tạp chí Dầu khí*, Số 3, trang 45 - 51, 2021. DOI: 10.47800/PVJ.2021.03-06.



8% INCREASE IN UPSTREAM SPENDING IN 2021

In “World energy investment 2021” report by the International Energy Agency (IEA) (1), upstream spending is expected to rise 8% in 2021, taking the total spending to over USD 350 billion, but the oil and gas industry remains under strong pressure from the Covid-19 pandemic and energy transitions.



Source: Shutterstock

According to the IEA, oil and gas company spending plans show an 8% increase in upstream spending in 2021, taking the total spending to over USD 350 billion, but this remains well below 2019 levels.

There are variations among companies but, in aggregate, the majors are holding a conservative line on upstream capital spending plans: these are essentially flat compared with 2020 (-2%). Continued investor pressure to diversify into low-carbon energy underpins more modest spending programmes, which are also aimed at reducing debt and supporting dividend payments.

The shale sector is another crucial bellwether for investment trends and market balances. After another round of belt-tightening in 2020, shale players face the unfamiliar prospect of generating significant free cash flow in 2021. For the moment, the industry is using the influx of cash to pay down debt and return money to shareholders, rather than increase output. Investors have welcomed this commitment to capital discipline. However, if or when a leaner and more profitable sector starts to regain the confidence of capital markets, priorities could swing again back towards growth.

Caution remains the watchword also for the exploration sector, which slumped already in the 2010s as companies turned to shale (which does not require exploration in the usual sense). Exploration activity is sharply down in most parts of the world, with the main pocket of activity outside of the Middle East being in offshore Brazil, Guyana and Suriname.

The overall expectation is that upstream investment by national oil

Prices and revenues have been higher in the Q1/2021, but it is far from certain that this will trigger additional upstream spending. Companies face multiple dilemmas as they put together their spending plans. Demand

uncertainties related to the pandemic and the speed of energy transitions are accompanied on the supply side by the large spare capacity held by countries in the OPEC+ grouping, and questions over the pace at which OPEC+ supply cuts will be unwound.

companies (NOCs) increases by around 10% in 2021, but this average figure masks a range of spending plans, strategies, and financial pressures. While many NOCs still face severe revenue and spending constraints, some are stepping up countercyclical investments. PetroChina, CNOOC and Sinopec have announced large capital budgets for 2021, with PetroChina having the largest upstream programme of any company.

Some large players in the Middle East are also in expansion mode, with Saudi Aramco and Abu Dhabi National Oil Company (ADNOC) both charged with increasing production capacity by around 1 million barrels per day in the

coming years. ADNOC announced a USD 120 billion spending programme for 2021 - 2025. Saudi Aramco plans total capital expenditures of USD 35 billion in 2021 (versus USD 27 billion in 2020) although the need to keep revenue flowing to the state during the crisis has pushed up the company's borrowing, taking on an extra USD 90 billion in debt in 2020 [1].

According to Rystad Energy report [2], the toll of the Covid-19 pandemic on upstream investments in the first 2 years of the downturn is estimated at a whopping USD 285 billion. Although spending will slowly start to rise from 2022, it will not reach pre-crisis levels in the coming period. The shale sector has been the most affected, with conventional exploration and investments in mature assets suffering the least thus far.

Before Covid-19 started impacting the global energy system, Rystad Energy estimated global upstream investments for the year would end up at around USD 530 billion, almost at the same level as in 2019. Rystad Energy forecasts at the time suggested 2021 investments would remain in line with the previous year's level.

However, as the Covid-19 pandemic triggered a collapse in oil prices during the early part of the second quarter last year, E&P companies slashed investment budgets to protect cash flow. This spending trend was not reversed in 2021, when prices rose. Compared to pre-pandemic estimates for 2020 and 2021, it is observed that spending fell by around USD 145 billion last year and will end up losing USD 140 billion by the end of

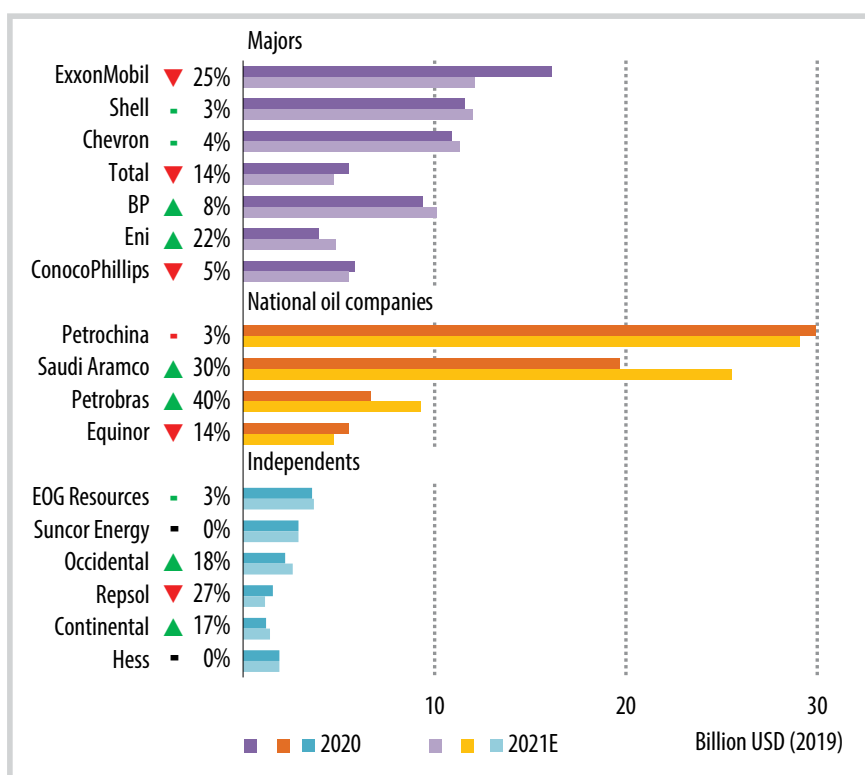


Figure 1. Upstream spending by selected company, 2020-2021E [1].

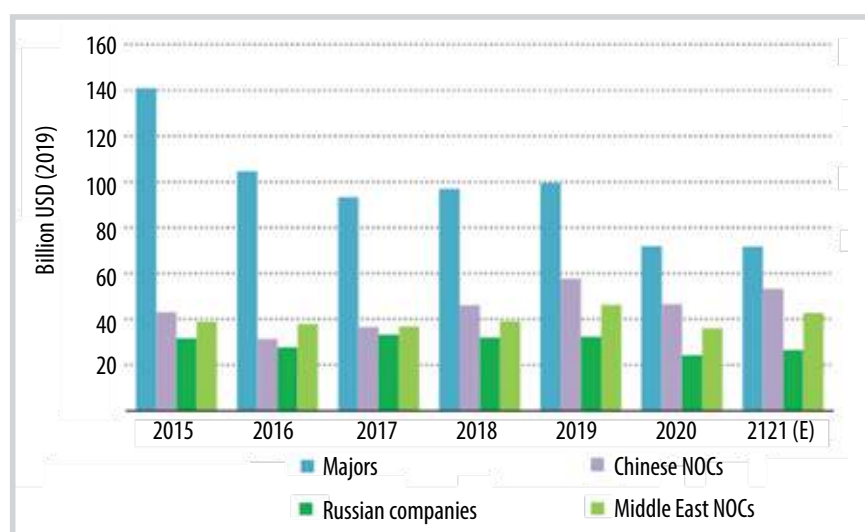


Figure 2. Upstream spending by selected company types [1].

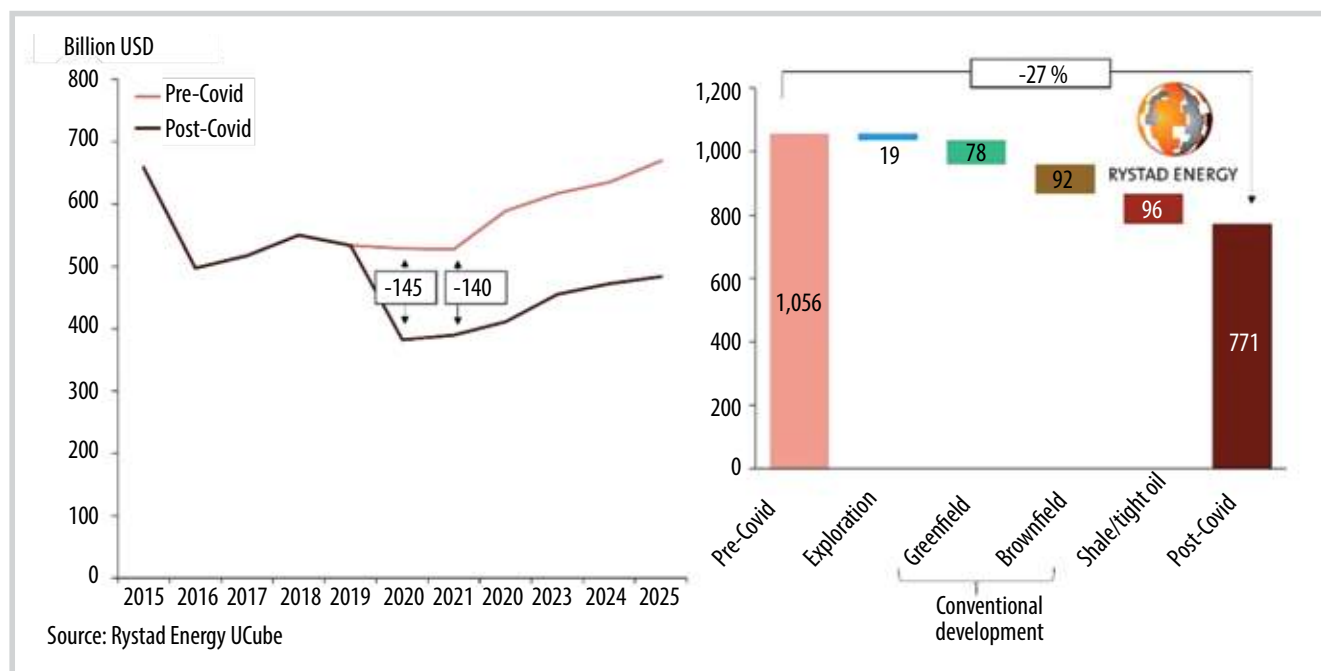


Figure 3. Global upstream investment forecast to 2025 [2].

this year. This implies Covid-19 removed 27% of planned investments.

Upstream spending was limited to USD 382 billion in 2020 and is forecast to marginally grow to USD 390 billion this year. Rystad Energy expects the effect of the pandemic to be a lasting one as - even though spending will start growing from 2022 - it will not return to the pre-pandemic level of USD 530 billion. Growth will be limited, and investments will only inch up annually, rising to just over USD 480 billion in 2025, when Rystad Energy report’s forecast ends.

Over the 2-year period between 2020 and 2021, shale/tight oil investments are the ones most affected in both absolute and percentage terms, losing USD 96 billion of the previously expected spending, or 39% for the sector. Exploration spending is expected to drop by USD 19 billion, or 22%, compared to what was previously forecast. Greenfield investment in new conventional projects will suffer a USD 78 billion loss, or 28%, while brownfield investment in existing such projects will fall by USD 92 billion, or 20%.

“Since shale/tight oil is both the segment with the highest decline in activity and the supply source in greatest need of continuous reinvestment to keep production growing, the immediate impact on output from this sector has been significant”, says Espen Erlingsen, Head of Upstream Research at Rystad Energy [2].

The proven oil and gas reserves of the group of major companies called “big oil” (ExxonMobil, BP, Shell, Chevron, Total and Eni) are falling at an alarming rate, as produced volumes are not being fully replaced with new discoveries. A Rystad Energy analysis shows that “big oil” lost 15% of its stock levels in the ground last year and as its currently estimated remaining reserves are set to be produced in less than 15 years, the group needs to add proven volumes by new commercial discoveries - or revisions of existing ones - to keep a balance [3].

The task is becoming more and more challenging as investments in exploration shrink and success rates slump. The declining proven reserves could create serious challenges for big oil to maintain stable production levels in coming years. This would in turn cause revenue to dwindle and pose a major threat to the financing of the group’s energy transition plans.

Big oil saw its proven reserves drop by 13 billion barrels of oil equivalent in 2020 as the companies took large impairment charges, and this year’s exploration has not come off to a great start either. The industry’s global first quarter discovered volumes totalled 1.2 billion barrels of oil equivalent, the lowest in seven years, as high-ranked prospects failed to deliver, and successful wildcats only yielded modest-sized finds.

The collapse in crude oil demand and prices due to the Covid-19 pandemic and an increased focus on capital

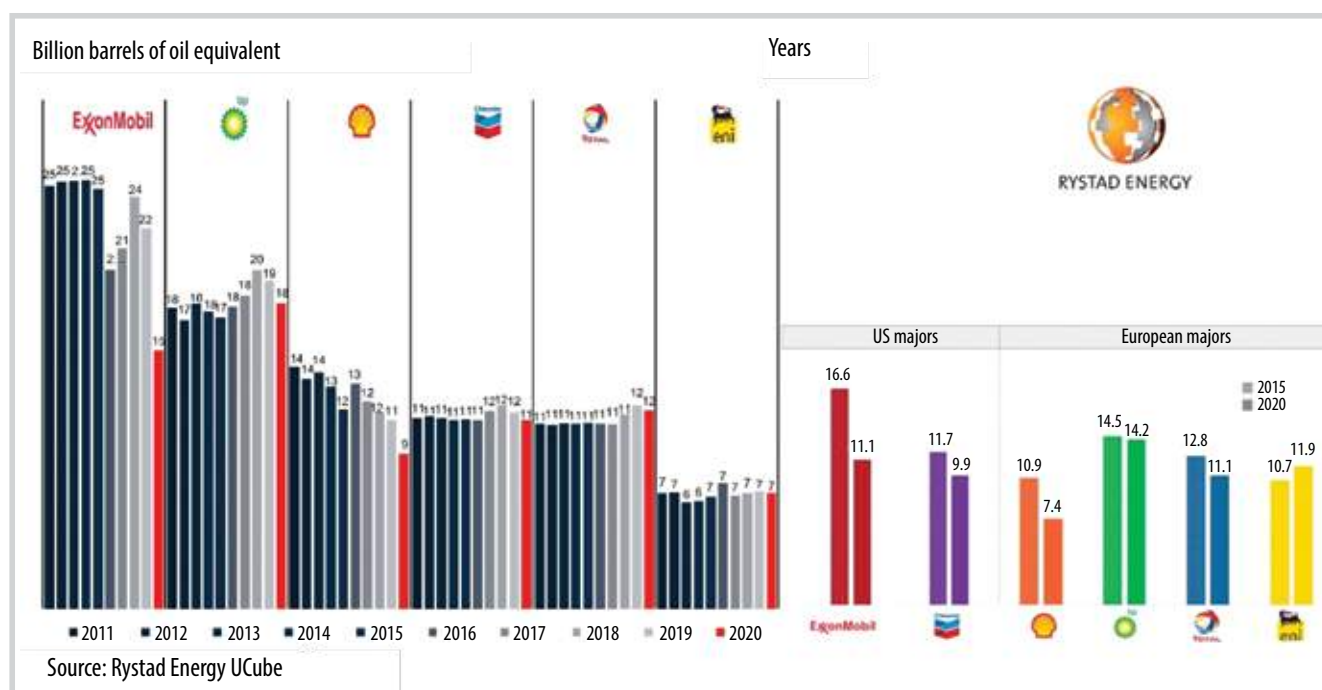


Figure 4. Proven reserves for big oil between 2011 and 2020, reserves to production ratio [3].

discipline has led to investment cuts that could aggravate the challenge of many major operators as they strive to boost their proven reserves. Even for European majors, which are increasingly focusing on the energy transition, business models will continue to be dominated by the sale of oil and gas.

“The ability of big oil to generate future revenues will continue to depend on the volume of oil and gas the companies have at their disposal to sell. If reserves are not high enough to sustain production levels, companies will find it difficult to fund expensive energy transition projects, resulting in a slowdown of their clean energy plans” says Parul Chopra, Vice President of upstream research at Rystad Energy.

ExxonMobil’s proven reserves shrank by 7 billion barrels of oil equivalent in 2020, or 30%, from 2019 levels. This was mainly due to reductions in Canadian oil sands and US shale gas properties. ExxonMobil’s proven reserves of liquids in Canada were revised from 4.8 billion barrels of oil to less than 900 million barrels, while bitumen-related reserves for the Kearl and Cold Lake oil sands projects were slashed from 3.8 billion barrels to less than 100 million barrels. In addition, liquid reserves related to some US shale plays have been reduced by 1 billion barrels.

Also, ExxonMobil’s proven gas reserves dropped last year by 9 trillion cubic feet, mostly in the US. The revisions

were primarily linked to the gas assets ExxonMobil bought from XTO in 2009.

Shell, meanwhile, saw its proven reserves fall by 20% to 9 billion barrels of oil equivalent last year. Liquid reserves accounted for one-third of total reductions and were mostly down to US and South American projects, and a lack of new discoveries elsewhere. Gas reserves accounted for two-thirds of the reductions, led by a 600 million barrels of oil equivalent revision in Australian projects.

Chevron also suffered reserve losses due to impairments, despite the addition of around 2 billion barrels of oil equivalent of proven reserves to its inventory through the acquisition of Noble Energy. Similarly, BP saw its total proven reserves drop from 19 billion barrels of oil equivalent in 2019 to 18 billion barrels of oil equivalent in 2020, mainly due to the sale of existing assets and a lack of major new discoveries. Total and Eni, however, have been able to avoid any reduction in proven reserves over the past decade.

Amid the proven reserve reductions - due to impairments and a lack of new discoveries - companies are seeing a negative impact on their ratio of proven reserves to production. When assessing the development of this ratio for the period from 2015 through 2020, ExxonMobil, Chevron and Shell show the highest decline.

For ExxonMobil, for instance, the proven-reserves-to-production ratio has not fallen below 13 years for the past 2 decades, but the 15 billion barrels of oil equivalent of reserves declared in 2020 means its volumes would run out in just over 11 years, compared to the previous expectation that these would last for more than 16 years. The reserves to production ratio for Shell, meanwhile, fell dramatically to 7.4 years in 2020 - the lowest level among all majors. The company has already reported its oil production peaked in 2019 and it expects an annual decline in output of between 1% and 2% until 2030.

New discovered volumes - a measurement of a company's exploration performance - illustrates

the daunting challenge faced by oil majors to maintain their reserves base and supply existing customers. Over the past 5 years, the 6 majors have replaced only 45% of their production through reserves from new discoveries. ExxonMobil fared better than its peers, adding more than 70% of the produced reserves thanks to 9 billion barrels of oil equivalent of discovered volumes in the offshore Stabroek Block in Guyana.

Total also enjoyed significant exploration success last year in the Guyana-Suriname basin, while Eni did well thanks to success in Africa. Chevron and Shell, on the other hand, have struggled to register new discovered volumes. Chevron managed to replace only 15% of

its produced volumes from 2016 through 2020, while Shell replaced 27% [3].

References

[1] IEA, "World energy investment 2021", 6/2021.

[2] Rystad Energy, "Upstream spending cut by \$285 billion in two years will struggle to recover to pre-pandemic levels", 12/5/2021.

[3] Rystad Energy, "Big oil faces major reserves challenge as new discoveries fail to replace production", 5/5/2021.

Reported by **Hanh Nguyen**